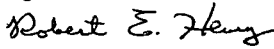
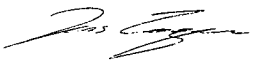
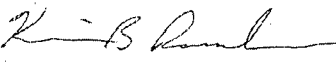
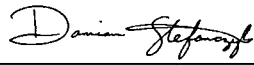

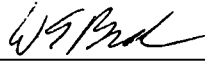



FAUSKE & ASSOCIATES, INC.
CALCULATION NOTE COVER SHEET

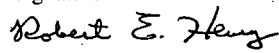
SECTION TO BE COMPLETED BY AUTHOR(S):

Calc-Note Number	FAI/08-70	Revision Number	1
Title	Gas-Voids Pressure Pulsations Program		
Project	Investigate the Waterhammer Pressures and Axial Forces for Different Length High Points		Project Number or Shop Order WE-198
Purpose:	This activity measures the waterhammer pressures and axial force imbalances as a function of the piping highpoint length and the void fraction of the accumulated gas volume		
Results Summary:	The results of this experimental program show that : (1) a Froude number in the piping highpoint of 0.54 is sufficient to sweepout an accumulated gas volume, (2) the gas void fraction for the initial stratified gas-water configuration is essentially preserved during the waterhammer event, (3) the peak waterhammer pressure is determined by the initial gas pressure and volume, the pump shutoff head and whether the system is flushed before the test conditions are established, (4) the peak force generated by the gas-water waterhammer event is determined by the peak pressure and the rate of rise of the waterhammer pressurization, (5) if the system piping includes a swinging check valve, the closure induced by the waterhammer event can cause subsequent forces, in both axial directions (upstream and downstream), that are larger than the waterhammer induced force and (6) the peak forces are a function of both the piping configuration and the initial gas volume.		
References of Resulting reports, Letters, or Memoranda (Optional)			
Author(s): Name (Print or Type)	Signature	Completion Date	
Robert E. Henry		August 20, 2008	
Jens Conzen		August 20, 2008	
Kevin Ramsden		August 20, 2008	
Damian Stefanczyk		August 20, 2008	
Karim Dhanji		August 20, 2008	

SECTION TO BE COMPLETED BY VERIFIER(S):

Verifier(s): Name (Print or Type)	Signature	Completion Date
William E. Berger		September 3, 2008
Christopher E. Henry		September 3, 2008
Method of Verification: Design Review _____, Alternate Calculations <input checked="" type="checkbox"/> _____, Testing _____ Other (specify) _____		

SECTION TO BE COMPLETED BY MANAGER:

Responsible Manager: Name (Print or Type)	Signature	Approval Date
Robert E. Henry		September 3, 2008

CALC NOTE NUMBER FAI/08-70 PAGE 2

CALCULATION NOTE METHODOLOGY CHECKLIST

CHECKLIST TO BE COMPLETED BY AUTHOR(S) (CIRCLE APPROPRIATE RESPONSE)

1. Is the subject and/or the purpose of the design analysis clearly stated?..... ☒ YES NO
2. Are the required inputs and their sources provided? ☒ YES NO N/A
3. Are the assumptions clearly identified and justified? ☒ YES NO N/A
4. Are the methods and units clearly identified? ☒ YES NO N/A
5. Have the limits of applicability been identified? ☒ YES NO N/A
(Is the analysis for a 3 or 4 loop plant or for a single application.)
6. Are the results of literature searches, if conducted, or other background data provided? YES NO ☒ N/A
7. Are all the pages sequentially numbered and identified by the calculation note number?.. ☒ YES NO
8. Is the project or shop order clearly identified?..... ☒ YES NO
9. Has the required computer calculation information been provided? YES NO ☒ N/A
10. Were the computer codes used under configuration control?..... YES NO ☒ N/A
11. Was the computer code(s) used applicable for modeling the physical and/or computational problems identified? ... YES NO ☒ N/A
(i.e., Is the correct computer code being used for the intended purpose.)
12. Are the results and conclusions clearly stated?..... ☒ YES NO
13. Are Open Items properly identified YES NO ☒ N/A
14. Were approved Design Control practices followed without exception? YES NO ☒ N/A
(Approved Design Control practices refers to guidance documents within Nuclear Services that state how the work is to be performed, such as how to perform a LOCA analysis.)
15. Have all related contract requirements been met? ☒ YES NO N/A

NOTE: If NO to any of the above, Page Number containing justification _____

FAI/08-70, REV. 1

***GAS-VOIDS PRESSURE
PULSATIONS PROGRAM***

Prepared For:

***Pressurized Water Reactor Owners' Group
(PWROG)***

Prepared By:

Fauske & Associates, LLC

16W070 West 83rd Street

Burr Ridge, Illinois 60527

TEL: (630) 323-8750

FAX: (630) 986-5481

September, 2008

ABSTRACT

This report documents the experimental data taken to aid the nuclear power plant operators in their evaluation of the noncondensable gas-water waterhammer issues identified in NRC Generic Letter 08-01.

TABLE OF CONTENTS

	<u>Page</u>
CALCULATION NOTE COVER SHEET	1
CALCULATION NOTE METHODOLOGY CHECKLIST	2
TITLE PAGE	3
ABSTRACT.....	4
TABLE OF CONTENTS.....	5
LIST OF FIGURES	8
LIST OF TABLES	12
1.0 INTRODUCTION.....	13
2.0 ANALYTICAL CONSIDERATIONS.....	16
2.1 Approach to Develop a Bubble Model of Non-Condensable Gas in the High Point	16
2.2 Acceleration Phase.....	19
2.3 Deceleration Phase (Waterhammer Transient)	23
3.0 THE EXPERIMENTAL APPARATUS	26
3.1 The Test Configuration	26
3.2 Highpoint Test Sections.....	29
3.3 Test Procedures.....	33
3.4 Mini Flow Line	37
3.5 Multiple High Points.....	37
4.0 EXPERIMENTAL CONDITIONS.....	40
4.1 Initial Conditions and Test Matrix.....	40

4.2	Data Reduction and Interpretation	50
4.2.1	Pressure Plots	50
4.2.2	Force Plots	55
4.2.3	Flow Rate Plots	60
5.0	TEST RESULTS	65
5.1	The Transparent Test Section	65
5.1.1	“Washout” Water Velocity	65
5.1.2	Gas-Water Flow Pattern for the Waterhammer Event	71
5.2	Measured Air-Water Waterhammer Pressures	76
5.2.1	Influence of “Flushing” on the Peak Waterhammer Pressure	76
5.2.2	Influence of the Check Valve on the Peak Waterhammer Pressure	81
5.2.3	Influence of the Mini Flow Line on the Peak Waterhammer Pressure	90
5.3	Axial Forces Generated on the Piping by the Waterhammer Event	92
5.4	Axial Forces Generated on the Piping by the Check Valve Slam	99
5.5	Influence of Mini Flow Line on Axial Forces	101
5.6	Multiple Bubble Tests	106
6.0	APPLICATIONS TO PLANT EVALUATIONS	109
6.1	Cautions and Limitations in Plant Applications	109
6.2	Evaluation of Sufficient Conditions to “Washout” a Gas Volume	110
6.3	Gas-Water Waterhammer Pressures	111
6.4	Force Imbalances Developed by the Gas-Water Waterhammer Event	114
6.4.1	Force Imbalances Developed by a Check Valve Closure Induced by a Gas-Water Waterhammer Event	116

7.0	CONCLUSIONS.....	118
8.0	REFERENCES	120
APPENDIX A: Sensitivity of Force Measurements to System Structural Characteristics.....		121
APPENDIX B: Application of Analytical Consideration to Air-Water Waterhammer Data..		160
APPENDIX C: Sample Problems for Estimating Air-Water Waterhammer Consequences...		164

LIST OF FIGURES

		<u>Page</u>
Figure 2-1	Example configuration for a pump start with a noncondensable gas volume in the discharge piping.....	17
Figure 2-2	Local pressure profile.....	18
Figure 2-3	Simplified view of the gas compression by a water column.....	21
Figure 3-1	Schematic - experimental setup without the mini-flow line represented.....	26
Figure 3-2	Schematic of the various highpoint lengths to be studied.....	30
Figure 3-3	Photograph of the transparent highpoint test section used to assess the Froude flush criterion.....	31
Figure 3-4	Schematic - experimental setup, including mini flow line	38
Figure 3-5	Schematic of the test apparatus with two highpoint and two accumulated gas volumes.....	39
Figure 4-1a	Sample pressure vs. time data plot with a flushed system and no check valve.....	51
Figure 4-1b	Sample pressure vs. time data plot with a flushed system and check valve included	52
Figure 4-1c	Sample pressure vs. time data plot with a non-flushed system.....	53
Figure 4-1d	Sample pressure vs. time data plot with a flushed system, check valve included, and the initial pressure in the bubble equal to -15 in Hg.....	54
Figure 4-2a	Sample load (force) vs. time data plot with a flushed system and no check valve included.....	56
Figure 4-2b	Sample load (force) vs. time data plot with a flushed system and the check valve included.....	57
Figure 4-2c	Sample load (force) vs. time data plot with a non-flushed system	58
Figure 4-2d	Sample force vs. time data plot with a flushed system, check valve included, and the initial pressure in the bubble equal to -15 in Hg.....	59

Figure 4-3a	Sample flow rate vs. time data plot with a flushed system and no check valve included	61
Figure 4-3b	Sample flow rate vs. time data plot with a non-flushed system and check valve not included	62
Figure 4-3c	Sample flow rate vs. time data plot with a non-flushed system and check valve not included	63
Figure 4-3d	Sample flow rate vs. time data plot with a flushed system, check valve included, and the initial pressure in the bubble equal to -15 in Hg.....	64
Figure 5-1	Stratified air-water configuration observed for a suction Froude number of 0.18	67
Figure 5-2	Stratified air-water configuration observed for a suction Froude number of 0.28	68
Figure 5-3	Stratified air-water configuration observed for a suction Froude number of 0.41	69
Figure 5-4	Air-water flow pattern observed for a suction Froude number of 0.45	70
Figure 5-5	Terminal velocity of air bubbles in filtered or distilled water as function of bubble size (taken from Wallis, 1969)	72
Figure 5-6	Sequential pictures of the two-phase flow pattern for water compressing a gas volume with the initial conditions of -24 inches of Hg (2.5 psia) and 1.5 liters of water drained (initial void fraction = 0.25)	73
Figure 5-7	Comparison of the measured peak gas-water waterhammer event pressures for the three highpoint lengths tested with controlled initial conditions	78
Figure 5-8	The measured peak waterhammer pressures for the full length highpoint with (a) larger volumes of water drained, (b) an initial gas volume pressures of -24 and -15 inches Hg and (c) the test section flushed to establish the initial condition	80
Figure 5-9	Comparison of peak gas-water waterhammer pressures for flushed and non-flushed systems	82
Figure 5-10	Response of a check valve to a downstream gas-water waterhammer event	83

Figure 5-11	Response of a check valve to a downstream gas-water waterhammer event	84
Figure 5-12	Response of a check valve to a downstream gas-water waterhammer event	85
Figure 5-13	Comparisons of the measured water flow rates for the tests in the full length highpoint with (blue), and without (red), a swing check valve installed	86
Figure 5-14	Comparisons of the measured air-water pressure histories for the tests in the full length highpoint with (blue), and without (red), a swing check valve installed	87
Figure 5-15	Comparisons of the measured peak waterhammer pressure for the 51" long highpoint as a function of whether the test apparatus includes a swing check valve	89
Figure 5-16	Pressure versus time - comparison for mini flow line tests	91
Figure 5-17	Comparison of the measured axial forces histories for the 102" length highpoint with, and without a swing check valve installed	93
Figure 5-18	Comparison of the calculated reference pressurization rates for the full and half length highpoint segments with an initial gas pressure of -15 inches Hg	96
Figure 5-19	Comparison of the calculated reference pressurization rates for the full and half length highpoint segments with an initial gas pressure of -20 inches Hg	97
Figure 5-20	Comparison of the calculated reference pressurization rates for the full and half length highpoint segments with an initial gas pressure of -24 inches Hg	98
Figure 5-21	Comparison of the highpoint force imbalance measured for a 2 Liter gas volume with and without a mini-flow line	102
Figure 5-22	Comparison of the highpoint force imbalance measured for a 1 Liter gas volume with and without a mini-flow line	103
Figure 5-23	Force comparison for mini-flow line tests	104
Figure 5-24	Force comparison for mini-flow line tests	105

Figure 5-25 Comparison of the single and multiple highpoint measurements of the
peak gas-water waterhammer pressure as a function of the gas volume
distribution 107

Figure 5-26 Comparison of the single and multiple highpoint measurements of the
maximum compressive force as a function of the gas volume distribution..... 108

LIST OF TABLES

	<u>Page</u>
Table 3-1 Instrumentation for Waterhammer Testing.....	32
Table 3-2 Checklist for the Performance of the Experiment.....	36
Table 4-1 Test Matrix (Experimental Planning)	41
Table 5-1	66

1.0 INTRODUCTION

A significant flow transient can result when a water mass is accelerated into a noncondensable gas volume as the result of a pump start or the opening of a valve. This acceleration is due to a pressure difference acting on the available water mass with the subsequent motion compressing the gas volume thereby increasing the pressure. Eventually, the gas volume pressure exceeds the pump shutoff head pressure or the stagnation pressure of the water upstream of the valve and the water begins to decelerate. If this deceleration process occurs faster than the resulting compression pressure waves caused by the continued compression of the gas volume, the hydrodynamic process is essentially governed by the acoustic transmission of these pressure waves through the water in the piping. Consequently, this evolves into a gas-water waterhammer event and the accompanying force imbalances on the piping segments can be sufficient to challenge the piping supports and restraints.

EPRI has compiled numerous plant waterhammer experiences into a handbook for plant engineers (Van Duyne and Merilo, 1996) that is appropriately focused on steam-water waterhammer causes and prevention, since both the frequency of occurrence and the piping loads are substantially greater for the steam-water conditions. Nonetheless, the list of seven mechanisms considered as capable of generating a waterhammer, those associated with "Rapid Valve Action (Valve Slam)" and "Filling of a Voided Line (Column Rejoining)" are relevant, in several respects, to the waterhammer events that can occur with the rapid compression of a noncondensable gas. Therefore, references are made to the EPRI Handbook when the discussions have common features with the mechanisms presented in the EPRI document. One of the specific differences of note is that the EPRI Handbook considers the piping loads due to the steam-water events as the product of the axial pressure difference and the flow area where the pressure difference is calculated by the Joukowsky-Frizell equation ($\Delta P = \rho C_w U$) (Joukowsky, 1898 and Frizell, 1898). (This is also commonly referred to as the waterhammer equation and the variables are defined as: ρ is the density of water, C_w is the speed of sound in water and U is the water velocity immediately prior to the waterhammer.) Such a modeling approach is appropriate for steam-water events because the steam volume is condensed as the cold water advances and the rate of rise of the waterhammer pressurization is very fast. As is discussed and shown by the data in this report, the rate of rise for noncondensable gas-water

waterhammer events are an order of magnitude longer than those for steam-water events. Consequently, this modeling approach for the axial forces on the piping is overly conservative for gas-water events. One of the specific areas of interest for the experimental data reported herein is to provide a means to better estimate the rates of rise for noncondensable gas-water events and to therefore better characterize the axial forces imposed on the piping. When considering an existing design, this is more appropriately described as; given the design rating of the existing axial restraints/supports, what gas volume can be tolerated as the source of a noncondensable gas-water event? Once this value is quantified, operational strategies, such as surveillance, can be implemented to ensure that the piping highpoints do not experience gas accumulations to this extent.

Another important facet to note is that the waterhammer pressures developed by noncondensable gas-water waterhammer events are generally much less than those developed in steam-water events. Principally, this is due to the continued compression of a noncondensable gas volume that occurs over hundreds of milliseconds compared to the continued condensation of a steam volume that essentially experiences no pressure increase until the water impacts a solid boundary or another fluid interface as in column rejoining as discussed in the EPRI Handbook. As a result, the pressure in the gas volume is always increasing whereas the pressure in a steam volume typically remains constant, or can even decrease, as the water is accelerated. Because the gas volume compression occurs over a much longer interval and the resulting compression waves propagate upstream and thereby influence (limit) the water flow rate, the resulting waterhammer is limited (somewhat cushioned). These events are further limited, compared to steam-water events, through the lower pump shutoff heads and the initial pressure within the gas volume. As a result, the noncondensable gas-water waterhammer pressure increases are generally not of sufficient magnitude to challenge the pipe wall integrity. On the other hand, these dynamic pressurization events can be sufficient to cause relief valves to lift and stick open. Moreover, the axial forces on the piping can be sufficient to damage the piping restraints/supports. Consequently, challenges to the system relief valves and the piping restraints and supports are the features to be evaluated in response to the NRC Generic Letter 08-01 and are addressed by the experiments discussed in this report.

This report is organized in the following manner:

- Section 1 is this introductory section.
- Section 2 outlines the analytical considerations for gas-water waterhammer events and the manner in which these influence the axial loads on the piping. Since this is an experimental activity, these are only presented in the general sense to illustrate those considerations that are important to the use of the results.
- Section 3 describes the experimental apparatus, the specific test sections utilized and the manner in which the tests were conducted.
- Section 4 presents the initial conditions of interest to these experiments and the test matrix and how the data was analyzed.
- Section 5 discusses the test results with respect to the major observations regarding “bubble washout”, the two-phase flow pattern immediately prior to the waterhammer event, the measured waterhammer pressures and the axial force imbalances observed during the tests.
- Section 6 presents the manner in which these results are recommended to be used in supporting plant specific evaluations.
- Section 7 lists the conclusions developed as a result of these experiments.
- Section 8 documents the references used in performing and interpreting the experimental program.

2.0 ANALYTICAL CONSIDERATIONS

2.1 Approach to Develop a Bubble Model of Non-Condensable Gas in the High Point

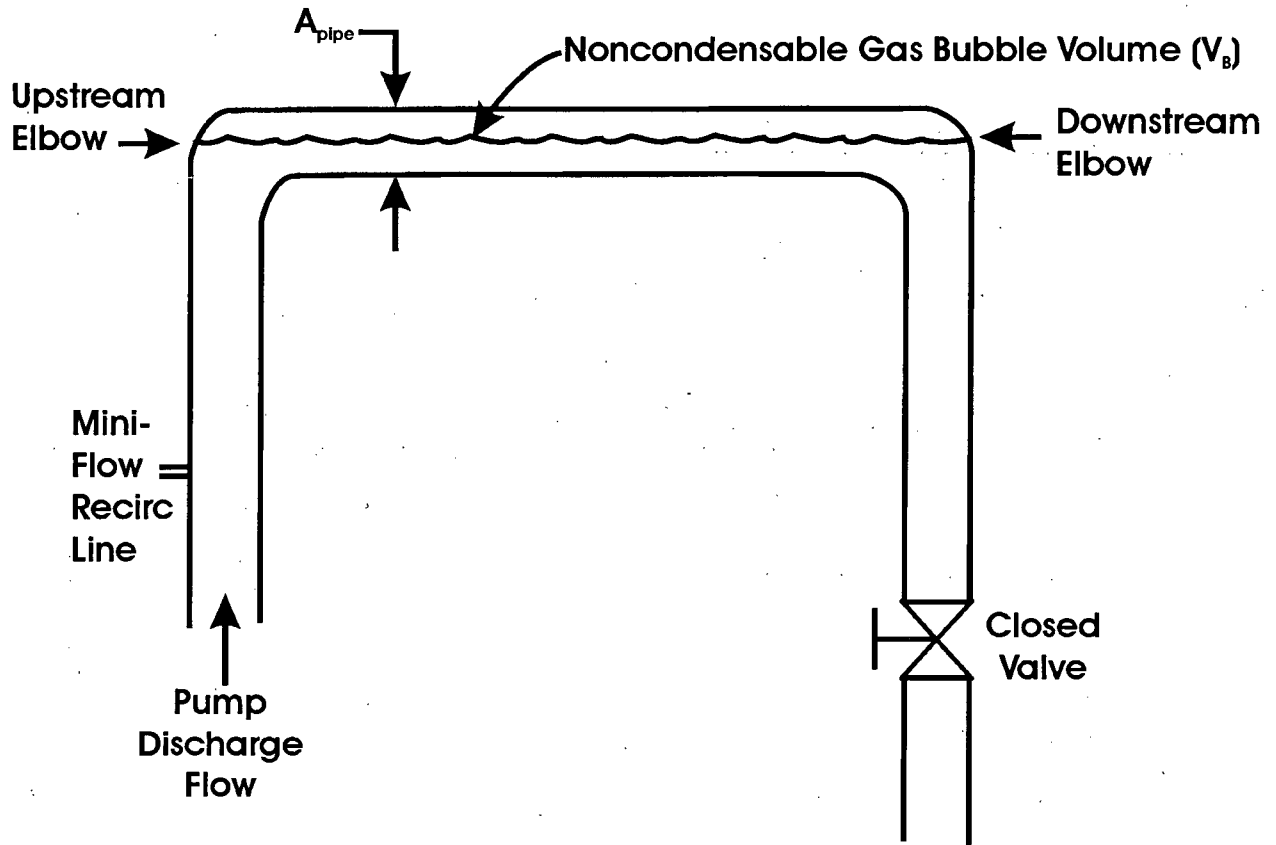
This section describes a methodology to model the acoustic response of a noncondensable gas volume that is accumulated in a piping high point and pressurized as a result of a pump start up. The equations of the model have been validated against experimental data and the model conservatively bounds the data. Therefore, the model can be used to (a) derive a force loading profile knowing the non-condensable gas volume or (b) estimate the maximum allowable gas volume knowing the maximum allowable force.

Derivation of the model is straightforward, but it's important to note the assumptions that are made throughout the process:

- a) pump run-up (increase in the volumetric flow rate) varies linearly with time until the pump operating point is reached,
- b) initially the bubble resides at the top of the designated high point with its length equal to that of the high point (see Figure 2-1),
- c) The noncondensable gas can be represented as an ideal gas and in the early acceleration phase follows a polytropic path, i.e. $PV^n = \text{constant}$, where n is a semi-empirical coefficient based on experimental data,
- d) maximum bubble pressure at the end of the acceleration phase is equal to a pressure that is larger than the pump shut-off pressure and less than the waterhammer pressure,
- e) maximum water flow rate is equal to the pump discharge flow rate, and
- f) water sonic velocity is constant throughout the piping configuration being analyzed.

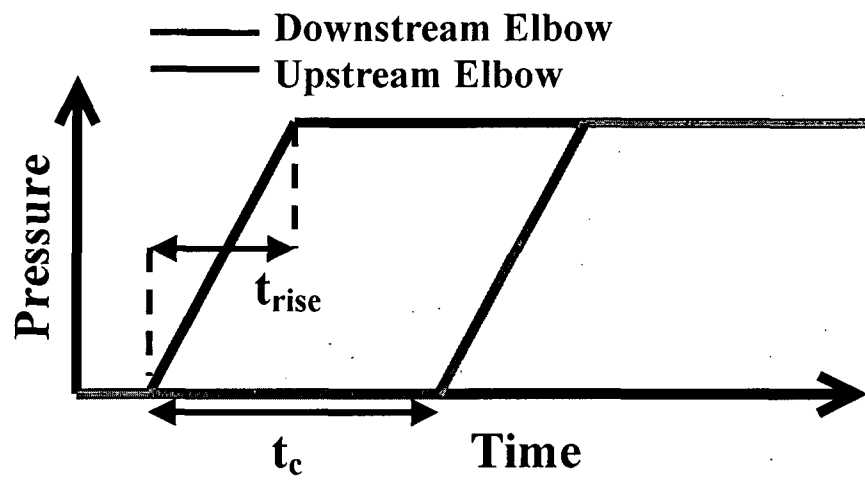
Consider the generic elevated piping configuration shown in Figure 2-1. As a result of a pump start, the early phase consists of the water acceleration followed by the rapid deceleration that causes the waterhammer event. The resulting local transient pressure histories imposed on the upstream and downstream piping high points are illustrated in Figure 2-2. A linear pressure rise is

Figure 2-1: Example configuration for a pump start with a noncondensable gas volume in the discharge piping.



20060609-1REH

Figure 2-2: Local pressure profile.



20060907-11DS

assumed for the decelerating pressurization transient (waterhammer) at the downstream elbow with this transient being propagated upstream and downstream through the water at the water sonic velocity. Since the water in the pipe would be essentially at the same temperature, the water sonic velocity would be constant and the pressurization transient would impose the same linear rate of rise when it reaches the upstream elbow. The propagation time (t_c) can be represented as:

$$t_c = \frac{L}{c_w} \quad (2-1)$$

In this equation, the variables are:

L = length between the elbows, and

c_w = water sonic velocity.

In the following description, we focus our discussion of the hydrodynamic transient in terms of (a) the early phase (fluid acceleration), and (b) the deceleration phase (waterhammer). The phase of propagation and reflection of the sonic wave is discussed in the section 2.3.

2.2 Acceleration Phase

During the acceleration interval the water is accelerated as characterized by the assumed pump run-up behavior and a polytropic thermodynamic path, $PV^n = \text{constant}$. As shown in Figure 2-3, the simplified methodology considers a gas bubble configuration accumulated at the top of the high point with the bubble length equal to the length of the high point. Following the pump start, the water column compresses the bubble as the water moves toward the downstream elbow. During this phase, the bubble is compressed from an initial system pressure to a maximum pressure equal to a pressure that is larger than the pump shut-off pressure but less than the waterhammer pressure. At the end of this early phase, the gas volume has been compressed to a final length defined in Equation (2-2).

$$PV_g^n = \text{Constant} \Rightarrow P_i \cdot L_i^n = P_f \cdot L_f^n \Rightarrow L_f = \left(\frac{P_i}{P_f} \right)^{1/n} \cdot L_i = \left(\frac{P_i}{P_f} \right)^{1/n} \cdot L_{HP} \quad (2-2)$$

In this equation, the variables are:

P = pressure,

V_g = gas volume,

P_i = initial bubble pressure (initial system pressure) at the piping high point,

L_i = initial bubble length as defined in Figure 2-3,

L_f = bubble length at the end of the acceleration phase as defined in Figure 2-3,

P_{so} = bubble pressure (taken to be a pressure that is larger than the pump shut-off pressure but lower than the waterhammer pressure), and

n = semi-empirical coefficient derived from experimental data (more discussion provided in Appendix B).

Hence, for a specified pressure the gas bubble length is minimized by the polytropic path assumption. For convenience, we also define the average high point void fraction at this condition as

$$\bar{\alpha}_f = \frac{V_f}{V_{HP}} = \frac{\alpha_i \cdot A \cdot L_f}{A \cdot L_{HP}} = \alpha_i \left(\frac{P_i}{P_{so}} \right)^{1/n} \quad (2-3)$$

In this equation the variables are:

$\bar{\alpha}_f$ = the average high point void fraction at P_{so} (the pressure at the end of the acceleration interval)

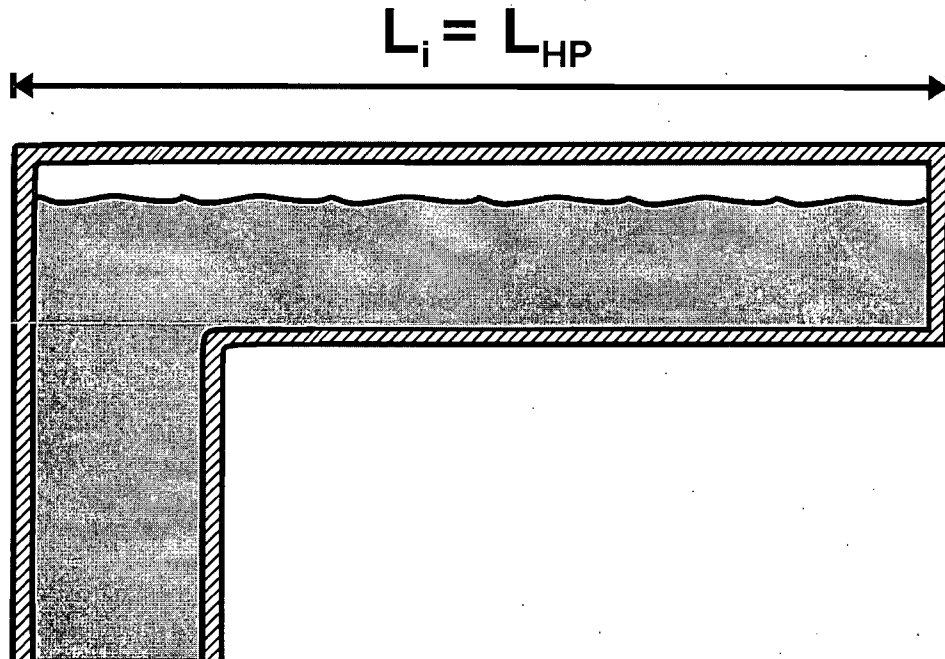
α_i = initial high point void fraction,

V_f = bubble volume at P_{so} , and

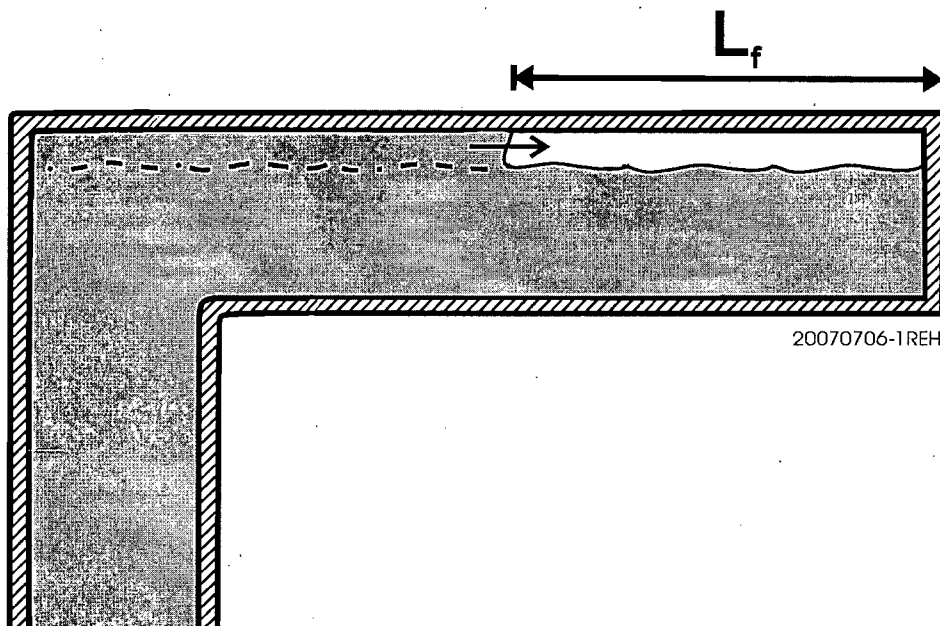
V_{HP} = high point volume.

As expected, the maximum water addition rate (volumetric flow rate) occurs at the end of this acceleration phase. The flow rate can be estimated from the pump discharge flow rate at fully run-up

Figure 2-3: Simplified view of the gas compression by a water column.



(a) *Assumed Initial Configuration*



(b) *Assumed Configuration During the Transient*

condition and the run-up time. As noted previously, the pump is assumed to run-up linearly in time, i.e.

$$Q_{\text{pump}}(t) = Q \cdot \text{MIN}(1, (t/t_{\text{run-up}})) \quad (2-4)$$

where Q_{pump} is the time-dependent pump discharge flow, Q is the pump discharge flow at fully run-up condition, and $t_{\text{run-up}}$ is the run-up time. The volume the pump discharges during the run-up interval is given by:

$$V_{\text{run-up}} = \int_0^{t_{\text{run-up}}} Q_{\text{pump}}(t) dt = \frac{1}{2} Q t_{\text{run-up}} \quad (2-5)$$

As an additional conservatism and a further simplification of the model, t_{WH} , the end time of the acceleration phase can be approximated by the time when the pump discharge volume is equal to the volume of the bubble. This leads to

$$V_i = \int_0^{t_{\text{WH}}} Q_{\text{pump}}(t) dt \quad (2-6)$$

where $V_i = \alpha_i L_{\text{HP}} A$ is the initial volume of the bubble. If V_i is less than $V_{\text{run-up}}$, solution of (2-6) for t_{WH} indicates

$$t_{\text{WH}} = t_{\text{run-up}} (V_i/V_{\text{run-up}})^{1/2} \quad (2-7)$$

Since the maximum pump discharge flow occurs at the end of the acceleration phase, it is given by

$$Q_{\text{max}} = Q \cdot \text{MIN}(1, (V_i/V_{\text{run-up}})^{1/2}) \quad (2-8)$$

With this pump run-up characteristic, the maximum pump discharge flow rate is proportional to the square root of the volume ratio.

2.3 Deceleration Phase (Waterhammer Transient)

Given the water acceleration to a velocity \bar{U} which is defined later, the deceleration results from rapid compression of the gas combined with the impact of the water on the end of the pipe. As a result of this impact and the consequential pressurization, the water is brought to rest by a single wave compression that has the magnitude of

$$\Delta P = \frac{1}{2} \rho c \bar{U} \cdot \alpha_i \quad (2-9)$$

The void fraction term, α_i , is included since the waterhammer pressure is calculated based on an average flow velocity (superficial velocity that assumes the liquid and gas are moving at the same rate), and \bar{U} (as shown below) is the velocity of the water front at the top of the voided section. Additionally, since the actual deceleration in a high point also usually collides with the stagnant water column in the downcomer from the high point, we use the value of $1/2$ which is typical of a water-water impact. The interval over which the pressure increases to this ΔP value (t_{rise}) determines the net force on the piping high point.

Logically, the deceleration phase (waterhammer pressure rise) would occur during the interval defined by the water column traveling to the wall, which is the length L_f . Here we define this interval as

$$t_{rise} = \frac{L_f}{\bar{U}} = \frac{L_{HP}}{\bar{U}} \cdot \left(\frac{P_i}{P_{so}} \right)^{1/n} \quad (2-10)$$

where \bar{U} is the average water transport velocity during the rise interval.

The velocity for the fluid moving at the high point is estimated using the superficial velocity that is defined as ($U_s = Q_{\max}/A$). It is important to note that the area used to calculate the superficial velocity is equal to the total cross-sectional flow area of the piping highpoint. This velocity is used to estimate the pressure rise time (equation 2-10) during the final stages of the pressurization as discussed further in Section 6 in terms of the application for plant analyses. Since the local one-dimensional water velocity \bar{U} is the superficial velocity divided by the initial void fraction α_i , the above expression for the gas-water waterhammer pressure can be put in the form of the superficial velocity and the expression becomes simply:

$$\Delta P = \frac{1}{2} \rho c \bar{U} \cdot \alpha_i \quad (2-11)$$

The last step of the analysis is to estimate a force loading on the piping high point based on the waterhammer pressure, pressure rise time calculated above and the idealization of the pressure signal as presented in Figure 2-2. The local dynamic force based on the waterhammer pressure on either of the elbows is calculated by multiplying the local pressure and the cross-sectional flow area of the pipe. However, the force imbalance, not the local force, is of interest since it is this imbalance of forces that acts to move the piping highpoint and exert a force on the supports. Therefore, the force imbalance is calculated by taking a difference between the downstream elbow force and the upstream elbow force. Similar to the pressure profile shown in Figure 2-2, the force on the upstream elbow is assumed to be equal to the downstream elbow force delayed by the propagation time (equation 2-1). The final equation that estimates the peak force imbalance on the high point is shown in equation 2-12. Even though it was stated that the equation is used to estimate the peak force on a piping high point, the equation could be extended to include any length of piping as long as the proper value of L is used.

$$F = A \frac{dP}{dt} \frac{L}{c_w} = A \frac{P_{WH}}{t_{rise}} \left(\frac{L}{c_w} \right) \quad (2-12)$$

where, F = peak force imbalance on a section of piping,

A = cross-sectional area of the pipe,

P_{WH} = waterhammer pressure = ΔP ,

P_{so} = bubble pressure (taken to be a pressure that is larger than the pump shut-off pressure but lower than the waterhammer pressure),

t_{rise} = pressure rise time,

L = length of piping on which the force imbalance is being calculated (i.e. $L=L_{HP}$ if the high point is being considered), and

c_w = water sonic velocity.

Concluding, it is important to note that this model is a simple, first step, approach into analyzing a load that a system could undergo due to a waterhammer event. The model is semi-empirical, where some of the parameters (such as n or P_{so}) are derived based on experimental data. The results generated by the model have been shown to be conservative (see Appendix B), thus if an analysis is required to reduce conservatism in the results, a more detailed model needs to be used.

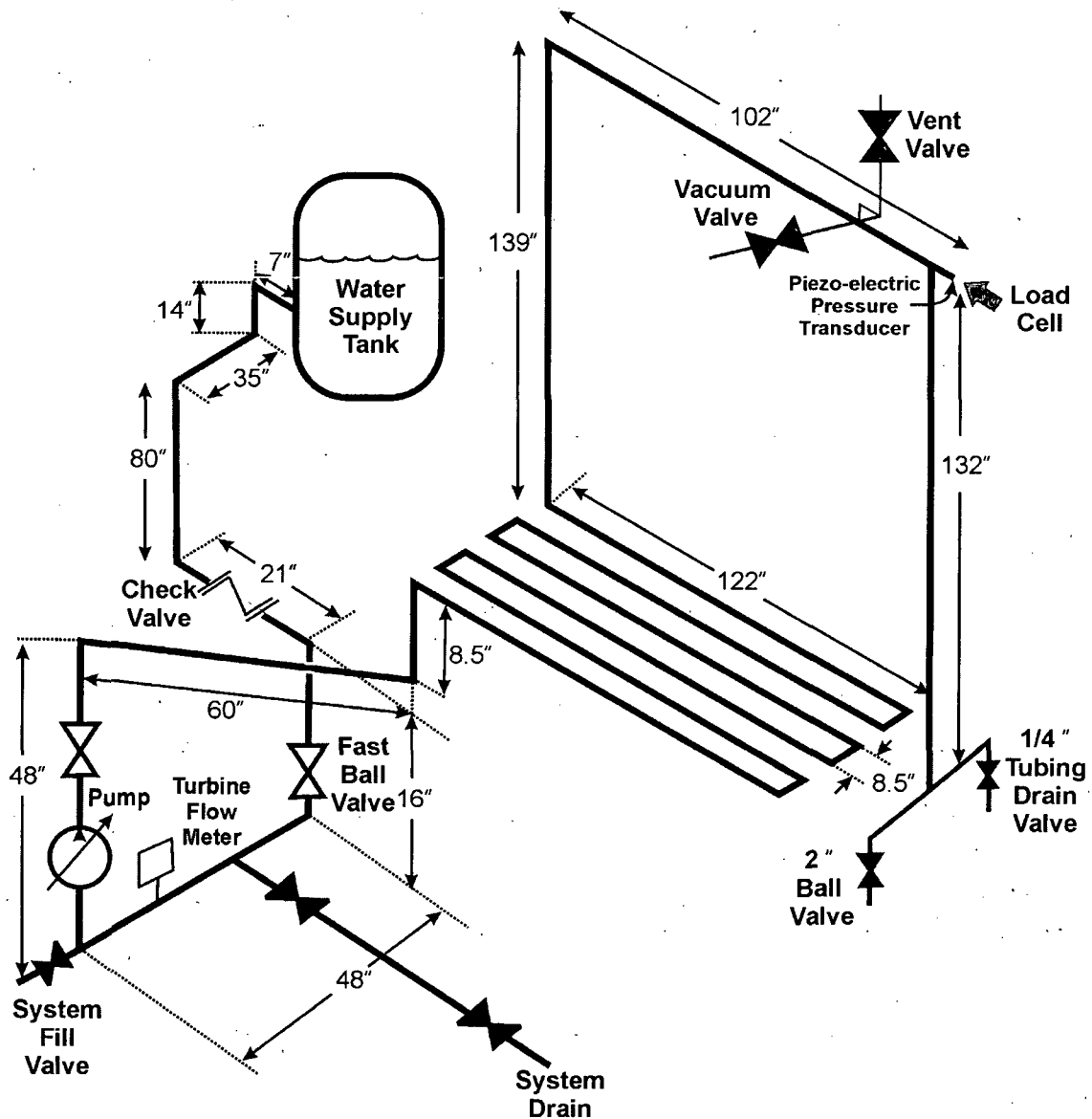
3.0 THE EXPERIMENTAL APPARATUS

3.1 The Test Configuration

The FAI experimental test apparatus consists of approximately 120 feet of 2 inch diameter steel piping as shown schematically in Figure 3-1. This includes the cylindrical storage vessel (Water Storage Tank) that is located about 10 feet above the pump (ground level). To test for noncondensable gas-water waterhammer conditions, it is important that the flow path is sufficiently long so that the accelerated water mass can not be slowed as an inertial water slug. This requires that the length of the water "column" being accelerated is comparable to, or longer than, the distance traveled by a pressure wave traveling at the sonic velocity during the most rapid part of the pressurization transient. When this is satisfied, part (or all) of the water column momentum must be stopped by a compression wave (increasing pressure) traveling at the sonic velocity, i.e. a gas-water waterhammer transient. When this occurs, the piping configuration can be subjected to an imbalance of forces along the axial length that will load the piping support/restraints.

Downstream of the pump, the water flows through six 10 foot long pipe segments, oriented in alternating directions, before it ascends in the riser to the highpoint which is approximately 17 feet above the pump. Each of these piping segments was oriented with a slight uphill orientation to encourage any encapsulated air volume(s) to move toward the vertical riser and thus to the horizontal highpoint segment. The highpoint is the section of main interest, because it contains the gas volume as well as the instrumentation for the measurement of the pressure and axial force histories imposed on the highpoint by the waterhammer event. Additionally, the highpoint configuration includes a downcomer pipe that descends to a 2 inch ball valve followed by a tee and valve combination that enables either (1) a steady-state flow to be developed through the apparatus or (2) the test piping to be filled with water at an elevated pressure and then drained to atmospheric pressure. As is discussed later, this provides a means for the steel piping between the pump and the drain to be tested with respect to the completeness of being "water filled".

Figure 3-1: Schematic - experimental setup without the mini-flow line represented.



NOT DRAWN TO SCALE

20080512-1JC

Typical plant piping arrangements have one, or more, check valve(s) to prevent unwanted reverse flow during normal operating hydraulic flow transients such as single pump operation in a system where multiple pumps discharge into a manifold. To assess the influence of a check-valve in the piping during a gas-water waterhammer acoustic event, some of the tests were performed with a swing check valve between the tank and the pump that permits flow in only one direction, i.e. it will close if the flow attempts to reverse directions. As part of the test matrix, this component is installed for some tests and removed for others (the length of the system remains constant in both cases).

A fast acting pneumatic ball valve is positioned between the check-valve and the pump such that the water source in the Water Supply Tank can be isolated when needed. Activation of this valve opens the flow path to the pump and both of these are activated at the same time. It is important to note that both the pump and valve are activated manually by the experimenter, thus there could be some delay between those two systems. Depending on the initial gas volume generated in the piping high point, the pump discharge flow rate pressurizes the gas volume and induces a waterhammer approximately one second later (varies with the specific test conditions).

The pump discharge is nominally 34 psig (pump head plus the hydrostatic head of the tank) and the pump run-up time is slightly higher than one second. Thus, for a conservative analysis the pump run-up can be represented as 1.0 seconds. The waterhammer transients are achieved by opening the fast acting pneumatic ball valve and concurrently starting the pump. With the pump start, high pressure water is discharged toward the piping high point where accumulated gas is compressed resulting in a waterhammer that stagnates the water flow. The shut-off head at the high point is nominally 27 psig. A turbine flow meter located upstream of the pump measures the transient volumetric flow rate following the pump start. This is an essential measurement to record the maximum velocity of the water "column" that needs to be arrested by the pressurization transient. Since this is a turbine flow meter that counts the magnetic pulses as the turbine blades pass a sensor, it inherently integrates these counts to produce an output of the water flow rate. For this reason, this can not follow the rapid transient that is produced by the waterhammer. Consequently, this signal is only used to measure the flow rate that the pump produces prior to the occurrence of the waterhammer. This flow meter was calibrated with a similar flow meter with a current certified calibration from a qualified laboratory. The calibration record can be found in the Test Plan for these tests (FAI, 2008).

3.2 Highpoint Test Sections

Of particular interest in these experiments is the influence of the highpoint length on the resulting pressure transient and axial force imbalance on the pipe itself. Figure 3-2 illustrates the different lengths of highpoint piping investigated in these tests as well as the instrumentation for measuring the rapid pressure transient at the downstream location of the highpoint.

A load cell is mounted in the axial direction at the downstream end of the piping highpoint and records the force imbalance imposed on the highpoint by the initial noncondensable gas-water waterhammer event as well as the subsequent loadings caused by the acoustic waves traveling through the piping. Since the reverberating compression and rarefaction pressure waves in the test apparatus piping can cause the force on the highpoint to act toward the upstream end and sometimes toward the downstream at others, the load cell was mounted with a bias, i.e. the highpoint was pulled against the load cell with a force considerably greater than those expected during the tests. Through this preloading technique we could ensure that the highpoint never pulled away from the load cell. Consequently, the measured loads are with respect to this imposed bias.

A battery powered vacuum gage was used to set the initial gas pressure at the high point and a second digital pressure gage was installed immediately downstream of the pump discharge. These enabled similar conditions to be developed with the initial gas volume for the different highpoint lengths tested.

During the experiment, the initial value parameters were recorded on test data sheets and the dynamic variables of interest are recorded by a computer controlled data acquisition system. These dynamic variables include the outputs of the turbine flow meter, the piezoelectric pressure transducer and the load cell. Additionally, the maximum pressure recorded by the piezoelectric transducer is recorded.

In addition to the steel piping highpoints shown in Figure 3-2, tests were also performed for the longest highpoint (102") using a transparent PVC pipe (see Figure 3-3). This figure illustrates where the flow regime pictures shown in Figures 5-1 through 5-4 were taken. The objectives of the

Figure 3-2: Schematic of the various highpoint lengths to be studied.
Note that the pictures are included for demonstration purposes and actual high point geometry might vary slightly.

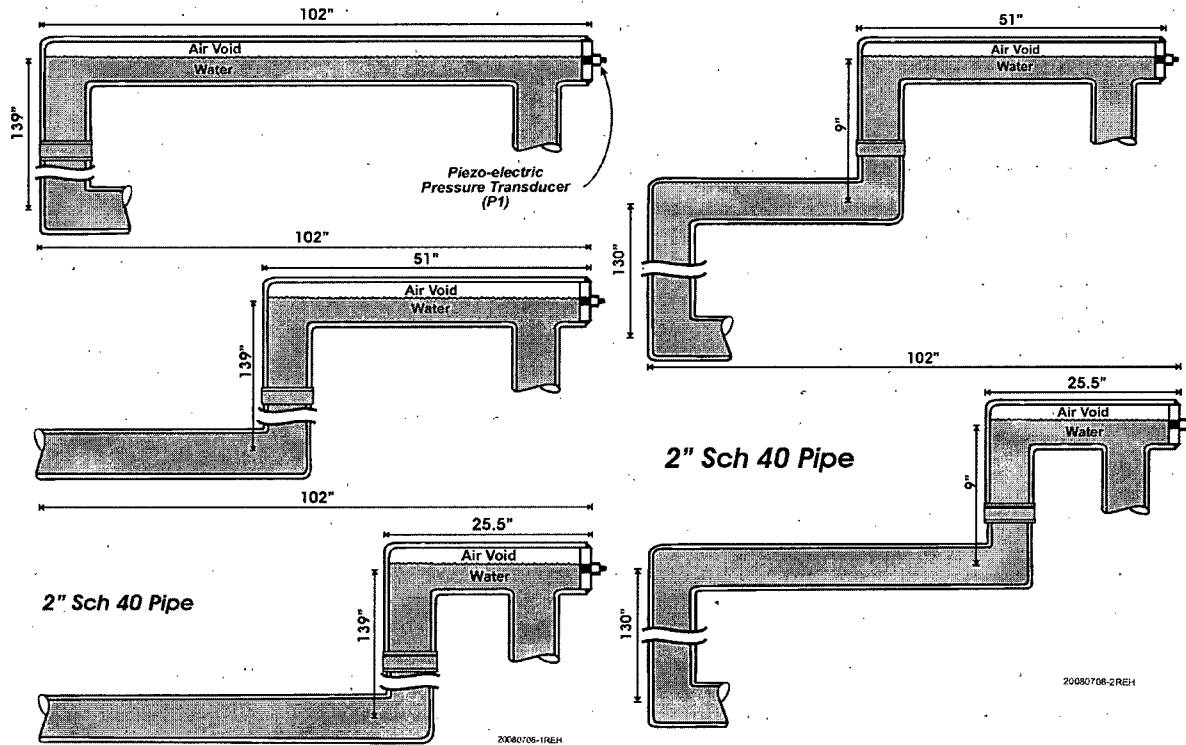
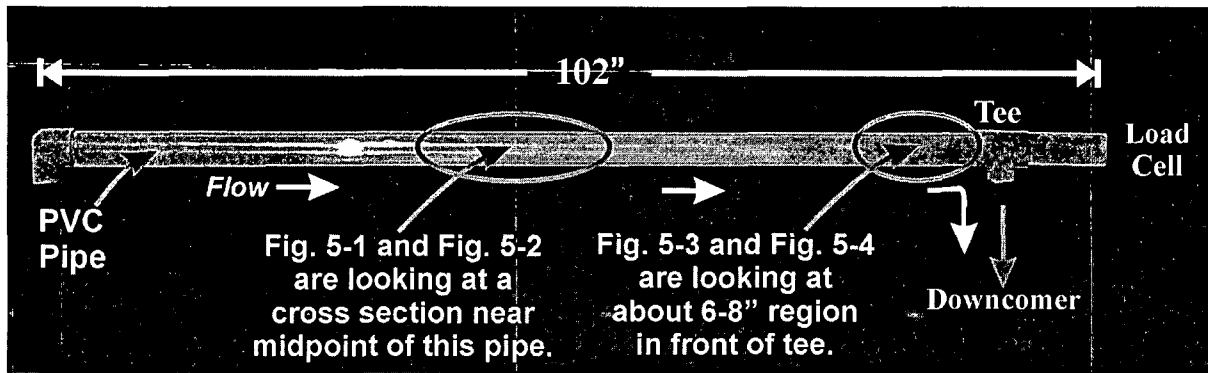


Figure 3-3

**Photograph of the Transparent Highpoint Test Section
Used to Assess the Froude Flush Criterion**



20080703-2KBR

transparent test section were to provide insights related to: (a) the purging flow that is sufficient to “washout” gas accumulations and (b) the two-phase flow pattern as the gas bubble is compressed. Because the softer PVC material influences the waterhammer pressure, this test section did not include the piezoelectric pressure transducer. However, it did include the load cell measurement to provide an indication of the strength of the events measured with the PVC piping. Digital video cameras were used to record the transient two-phase behavior during the gas volume compression and rebound phases of the waterhammer event. As noted above, the compliance of the PVC pipe influences the pressure wave propagation speed and therefore the measurements of the force imbalance are not directly relatable to the steel pipe conditions. Nonetheless, the observations of the two-phase flow patterns as the noncondensable gas volumes were compressed are also those that occurred with the steel pipe in place. These are of particular importance when evaluating the water velocity that impacts the downstream end of the highpoint and the cross-sectional area of the impact. The results of these tests are presented along with the steel pipe tests later in this report.

Table 3-1
Instrumentation For Waterhammer Testing

Instrument Type	Instrument Serial Numbers	Range	Accuracy	Parameter Measured
Flow Meter (Sponsler)	229702 (22947) ¹	8-130 gpm	2% ² (0.47%) ²	Water flow rate.
Load Cell (Himmelstein)	111792	0-10,000 lbf	± 0.02% ³	Axial force at highpoint.
Piezoelectric Pressure Transducer (Kistler)	C120774 (929305) ¹	0-3,000 psi	< ± 1% ⁴	Pressure at highpoint.
Vacuum Gages Supco DPG25V	409-050-0103, 409-500-0074	-30 to 0 InHg (-14.7 to 0 psig)	0.5% ³	Vacuum at highpoints.
Pressure Gage (Cecomp Electronics)	1124201004	0-1000 psig	0.25% ³	Pressure at pump.
Fast Ball Valve (Neles-Jamebury)	F05-S-14	80-125 psig (for activation)	n/a	Open/close

1) Electronics, 2) -Average Value, 3) Manufacturer Information, 4) In-house Calibration (FAI-TC 4.3)

3.3 Test Procedures

To establish the test conditions with an air volume in the highpoint, the piping system was filled with tap water through the filling branch using a water hose connected to the city tap water, which has a water stagnation pressure of approximately 50 psig. During the filling process, the drain line off of the top of the downstream end of the highpoint (see Figure 3-1) was open until water was observed to be continuously discharged from this drain whereupon it was closed. Once the transparent tubing drain line was observed to be flowing only water (no air), one of two different setup conditions were used to develop the initial gas volume in the test apparatus. For one of the initial conditions, the state at the end of the filling process was used directly; this state is designated as being "unflushed". The other set of initial conditions was developed by "flushing" the piping downstream of the pump by opening the 2 inch discharge to the atmosphere and establishing full pump flow through the piping system. Typically, this resulted in a Froude number for water flow through the 2 inch Schedule 40 piping of about 4, which is well above the value of 0.54 (Wallis et al, 1978) that is indicative of the necessary flow for the pipe to run full of water. This flushing process acted to remove any gas volumes trapped in the pipe fittings or the piping surface along the length of the test apparatus. Once this purging flow was established, the 2 inch ball valve was closed and the piping was pressurized to the shutoff head of the pump and the pneumatic ball valve was closed. Both of these setup conditions ended with the piping configuration filled with pressurized water. By measuring the volume of water that was drained during the depressurization to atmospheric conditions, the extent to which the piping was truly water filled could be determined as explained below.

For a completely water filled system, the water mass/volume drained during a depressurization can be calculated by equating the pressure change to the mass change using the definition of the sonic velocity as given by:

$$\Delta P = \frac{C_w^2 \Delta m}{V}$$

where:

- C_w is the sonic velocity of water,
- Δm is the mass of water drained in the depressurization,
- ΔP is the pressure decrease and
- V is the total fluid volume that was depressurized.

Two inch Schedule 40 pipe has a cross-sectional flow area of 0.02330 ft^2 (Crane, 1976), which is 0.002167 m^2 . The piping length that was pressurized by the water supply includes the pump and the piping length to the fast acting ball valve and is approximately 106 ft (32.3 m) long which gives a volume of 2.47 ft^3 (0.070 m^3). At room temperature the velocity of sound for water is approximately 4500 ft/sec (1373 m/sec) such that with a pressure decrease of about 50 psig (3.45 bars), the calculated mass of water drained in the depressurization is 0.0128 kg (12.8 g or 12.8 ml). Given that water is essentially incompressible when compared to the behavior of a gas volume, any measured drainage volume approaching this value is indicative of the piping being essentially water filled.

Typically, when the dynamic flushing process was implemented, the water mass drained was in the range of 25 to 50 ml and when this preconditioning was not used, water drainage volumes in the range of 300 ml to 500 ml were observed. Therefore, the dynamic flushing/purging process in the setup for a given experiment provided an initial condition that was essentially water-filled. In this regard, it is important to note that the conditions that could persist in plant piping could be similar to either of these states since noncondensable gas exiting solution could reside in multiple high points and could also be held-up in any of the horizontal pipes that are not high points but are not exactly horizontal or even as distributed gas bubbles depending on the local conditions causing the gas to exit solution. Alternatively, if the gas was exposed to local flow conditions with a Froude number of approximately one or greater, the gas would be swept out of the other areas and may be re-established in the highpoint depending on the conditions causing the gas volume to form.

These measurements also provide us with an assessment of the average void fraction in the piping configuration before the gas volume in the highpoint is developed by draining from the downcomer with the highpoint vent open. For example, a drained volume of 50 ml represents an

average void fraction throughout the piping configuration of 7.1 E-4 while a drainage volume of 500 ml produces a void fraction 10 times larger. From these averages we can estimate the average pressure wave propagation velocity through the piping of the test apparatus (Henry et al, 1971). These translate into velocities that are less than the all water velocity but with the lowest average void fraction this velocity is only slightly less than the water velocity. With the limited gas volume, the propagation is the most rapid but this may not be the condition that causes the largest axial loadings on the piping. This is discussed in more detail when evaluating the experimental data.

Once the piping "water filled" initial condition was established, the highpoint drain was closed and the water supply was isolated. The drain line at the bottom of the downcomer was opened and the highpoint vent was opened to enable the drainage necessary to produce the desired gas volume in the highpoint piping. Depending on the experiment, the total water volume drained from the downcomer, including that associated with the depressurization to one atmosphere, was varied from 0.5 to 2 liters of water (a few tests were also conducted for voids up to 5L big). After this was done, both the drain and vent valves were closed. A vacuum pump was used to remove the remaining gas in the highpoint volume to produce the specific test conditions to be examined. The vacuum pump is located at ground level and connected by a 1/4" plastic line to the highpoint. This low pressure flow is pumped through a separation chamber that prevents any water carryover from being pulled into the pump suction.

The total volume of the longest highpoint is approximately 6 liters, so drainage of 1 liter induces a 17% gas void. It is important to note that the initial volume drained is considered to be part of this gas volume, i.e. after the initial drainage volume of e.g. 50 ml, and additional volume of 950 ml was drained to establish a test condition of 1 liter drained. For both the tests performed in this program and the conditions of interest for a plant, the pump discharge produces a meaningful compression of the gas volume and therefore is a contribution of the gas-water waterhammer as determined by the ratio of the pump shutoff head to the initial gas volume pressure. Since the pump available for this experiment has a considerably smaller shutoff head than those typical of a plant, to represent the ratios of interest for the plant designs, the initial gas volume pressure in the test apparatus needed to be less than atmospheric pressure.

The water supply tank was filled separately because the check-valve did not allow flow from the fill location to the tank. This was performed periodically during the test program depending on the water demands associated with the initial conditions related to flushing the piping.

Once all of the parameters were at the desired conditions for a given test, the pump was started and the fast-acting pneumatic valve was opened concurrently. The pneumatic ball valve opens in about 100 milliseconds and the pump run-up occurred over several hundred milliseconds. This combination had the effect of increasing the pump discharge pressure as the gas compression began. The pressure difference between the pump discharge and the gas volume accelerated the water mass toward the downstream end of the highpoint. Once the gas volume pressure approached the pump shutoff pressure, the water column began to decelerate with the waterhammer event providing the pressurization that stagnated the water mass. The noncondensable gas-water waterhammer event that occurred in some cases was sufficient to shake the entire structure. Each test was considered to be completed when the pipeline and fluid had come to rest.

Table 3-2 was used as a checklist for performing the experiment. A test data sheet was also filled out by the Test Engineer for each test.

Table 3-2
Checklist for the Performance of the Experiment

Step	Task	Check Box
1	Filling of the pipeline with water (process varies between flushed and non-flushed systems).	
2	Measure the drainage volume necessary to depressurize the test apparatus to one atmosphere.	
3	Drain the specified water volume for the given test.	
4	Pull the specified vacuum for the given test	
5	Start data acquisition.	
6	Open pneumatic valve and start pump concurrently.	
7	Stop data acquisition after test.	
8	Recover data file.	

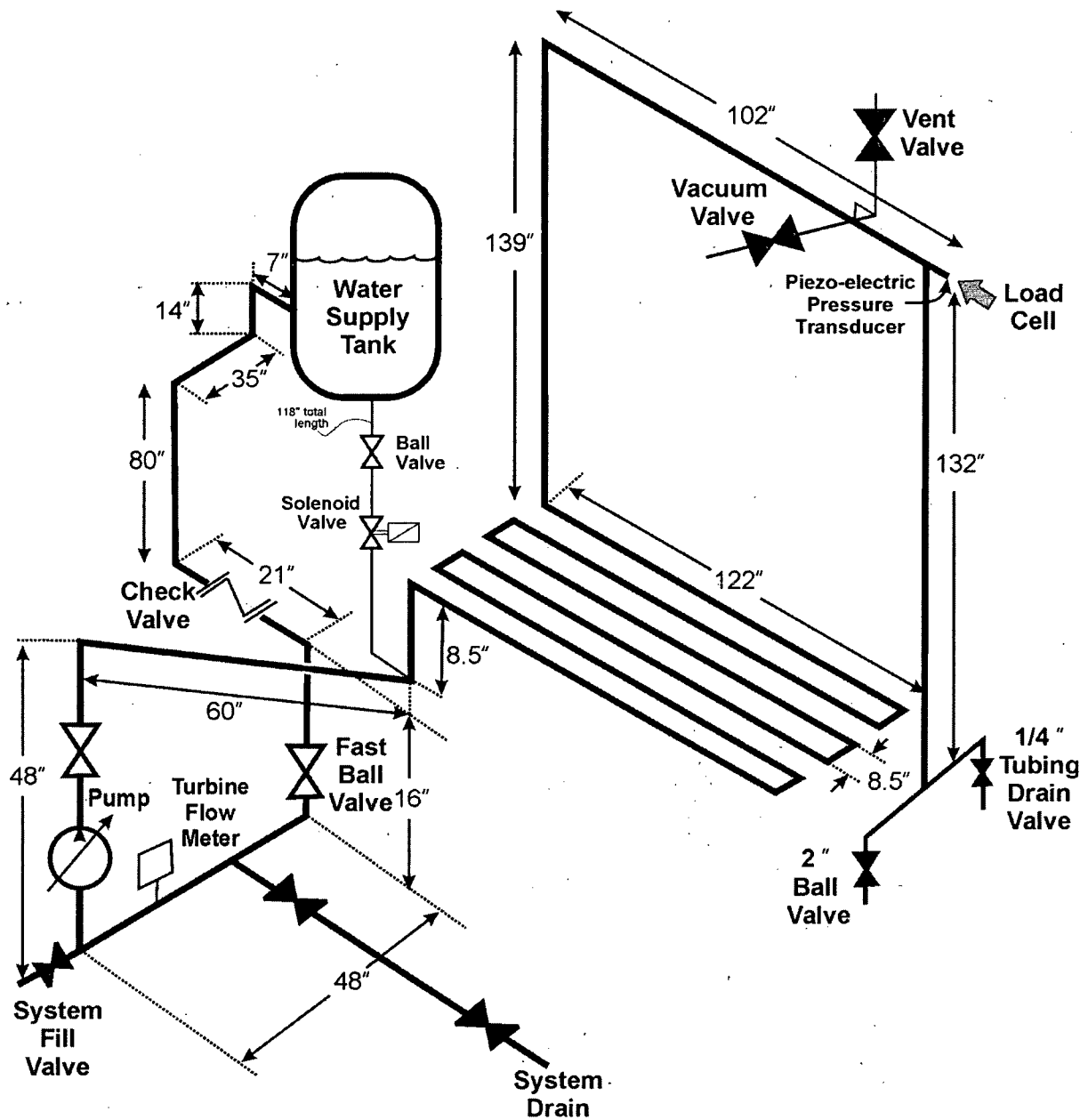
3.4 Mini Flow Line

Later in the experiment a mini flow line was installed to examine its effect on the waterhammer strength. The mini flow line was placed downstream of the pump and the water flow was re-circulated to the bottom of the reservoir as shown in Figure 3-4. A 3/8" diameter Schedule 40 pipe was used and the length of the line was 118". Two valves were mounted in series at the mini flow line. A manual ball valve which could be used as a throttle valve or manual isolation valve and a solenoid valve which opened on the same signal as the fast ball valve (pump start). The flow path through the solenoid valve was 1/2" in diameter so that the pipeline needed to be reduced at that location. The volumetric flow rate through the mini flow line was 5gpm.

3.5 Multiple High Points

At the completion of the test program several tests were performed with two piping highpoints at the same elevation and with separated gas volumes in each highpoint. This test configuration (see Figure 3-5) was produced in the same facility used for the single gas volume tests with the riser to the highpoint location followed by a quarter length (25.5 inches) highpoint, a downcomer to essential the elevation of the switchback piping, a horizontal pipe with a length equal to a quarter length highpoint (25.5 inches), a riser to the highpoint elevation and a half length highpoint (51 inches) to the measurement location with the piezoelectric pressure transducer and the load cell. As part of this experimental configuration, each of the two highpoints had a connection to the vacuum system and a water drain to facilitate the establishment of an initial void fraction with a stratified flow pattern at each location. This enabled the size of the two gas volumes to be set individually with the initial gas volume pressures being equal. Of particular interest are the comparisons between the measured gas-water waterhammer pressures and force imbalances for distributed gas volumes and a single gas volume equal in size to the sum of the two separate volumes. These results are presented in Section 5.

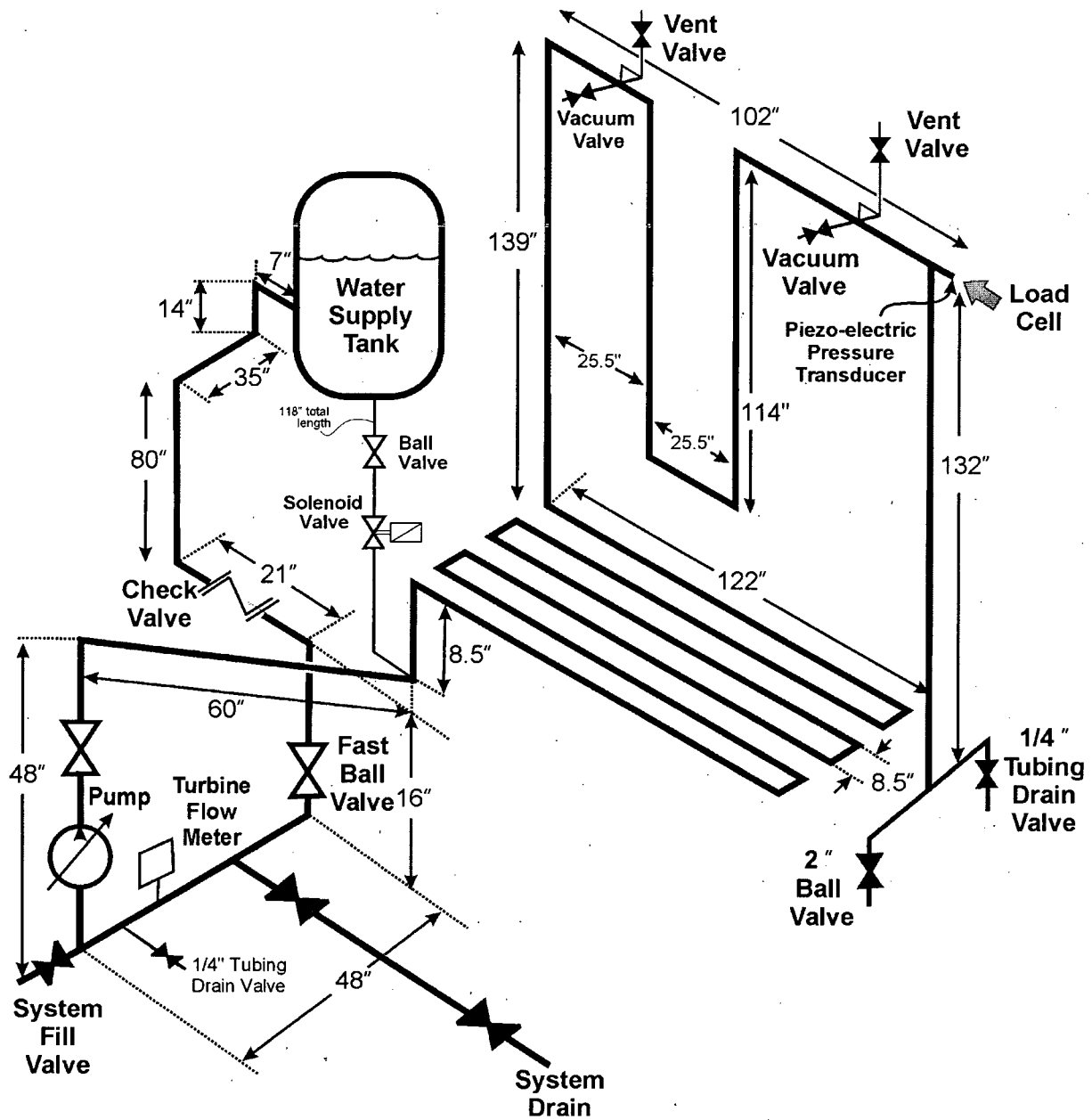
Figure 3-4: Schematic – experimental setup, including mini flow line.



NOT DRAWN TO SCALE

(modified "mini flow", JC 8/4/08) 20080512-1JC

Figure 3-5: Schematic of the test apparatus with two highpoint and two accumulated gas volumes.



NOT DRAWN TO SCALE

(modified "mini flow", JC 8/4/08) 20080512-1JC

4.0 EXPERIMENTAL CONDITIONS

4.1 Initial Conditions and Test Matrix

The test matrix is designed to investigate the forces induced by gas-water waterhammer events in various types of highpoint configurations. Table 4-1 presents the Test Matrix used to demonstrate the influence of the highpoint length on the magnitude of the force imbalance on the piping. As illustrated, the test matrix involves parametric variations for the following parameters:

- length of the highpoint,
- whether there is a check valve in the flow path,
- the initial gas volume,
- the initial gas pressure, and
- different high point configurations.

In addition to these parameters, the initial “water filled” condition was generated in two different manners: (a) by filling the system with tap water with the “water filled” condition determined using the highpoint vent and the low point drain, and (b) by flushing the system with a pumped flow rate that produces a Froude number well in excess of unity. Of these two techniques, the latter provides the condition that is closest to a true “water filled” system, but both of these conditions could be encountered in the plant systems.

Table 4-1
Test Matrix (Experimental Planning)

Test Number #	Length of High Point (inches)	Check Valve (Yes/No)	Initial Gas Volume (l)	Initial Gas Pressure Inches of Hg Vacuum	High Froude Number Flush (Yes/No)	File Number #	Water Volume Drained Depressurizing to 1 atm* (ml)	Mini Flow Line (Yes/No)
1A	102	Yes	0.5	-24	Yes	151	80	No
1A-R	102	Yes	0.5	-24	Yes	344	55	No
1B	102	Yes	0.5	-24	No	4	400	No
1G	102	Yes	0.5	-24	Yes	336	45	Yes
2A	102	Yes	1	-24	Yes	152	50	No
2A-R	102	Yes	1	-24	Yes	345	55	No
2B	102	Yes	1	-24	No	1	700	No
2G	102	Yes	1	-24	Yes	337	40	Yes
3A	102	Yes	1.5	-24	Yes	153	50	No
3A-R	102	Yes	1.5	-24	Yes	346	60	No
3B	102	Yes	1.5	-24	No	174	320	No
3G	102	Yes	1.5	-24	Yes	338	35	Yes
4A	102	Yes	2	-24	Yes	154	50	No
4A-R	102	Yes	2	-24	Yes	347	40	No
4B	102	Yes	2	-24	No	175	380	No
4G	102	Yes	2	-24	Yes	339	20	Yes
5A	102	Yes	0.5	-20	Yes	156	40	No
5B	102	Yes	0.5	-20	No	7	400	No
6A	102	Yes	1	-20	Yes	155	50	No
6B	102	Yes	1	-20	No	8	320	No
7A	102	Yes	1.5	-20	Yes	157	30	No
7B	102	Yes	1.5	-20	No	9	350	No
8A	102	Yes	2	-20	Yes	158	40	No
8B	102	Yes	2	-20	No	10	380	No
9A	102	Yes	0.5	-15	Yes	159	30	No
9A-R	102	Yes	0.5	-15	Yes	348	40	No
9B	102	Yes	0.5	-15	No	49	420	No
9G	102	Yes	0.5	-15	Yes	340	30	Yes
10A	102	Yes	1	-15	Yes	160	40	No
10A-R	102	Yes	1	-15	Yes	349	35	No

Test Number #	Length of High Point (inches)	Check Valve (Yes/No)	Initial Gas Volume (l)	Initial Gas Pressure Inches of Hg Vacuum	High Froude Number Flush (Yes/No)	File Number #	Water Volume Drained Depressurizing to 1 atm* (ml)	Mini Flow Line (Yes/No)
10B	102	Yes	1	-15	No	50	420	No
10G	102	Yes	1	-15	Yes	341	20	Yes
11A	102	Yes	1.5	-15	Yes	161	40	No
11A-R	102	Yes	1.5	-15	Yes	350	35	No
11B	102	Yes	1.5	-15	No	51	440	No
11G	102	Yes	1.5	-15	Yes	342	30	Yes
12A	102	Yes	2	-15	Yes	162	35	No
12A-R	102	Yes	2	-15	Yes	351	40	No
12B	102	Yes	2	-15	No	52	460	No
12G	102	Yes	2	-15	Yes	343	30	Yes
13A	102	Yes	0.5	-10	Yes	164	30	No
13B	102	Yes	0.5	-10	No	53	420	No
14A	102	Yes	1	-10	Yes	165	30	No
14B	102	Yes	1	-10	No	54	400	No
15A	102	Yes	1.5	-10	Yes	166	40	No
15B	102	Yes	1.5	-10	No	55	400	No
16A	102	Yes	2	-10	Yes	163	80	No
16B	102	Yes	2	-10	No	56	400	No
17A	102	Yes	0.5	-5	Yes	167	40	No
17B	102	Yes	0.5	-5	No	57	380	No
18A	102	Yes	1	-5	Yes	168	40	No
18B	102	Yes	1	-5	No	58	340	No
19A	102	Yes	1.5	-5	Yes	169	35	No
19B	102	Yes	1.5	-5	No	59	300	No
20A	102	Yes	2	-5	Yes	170	40	No
20B	102	Yes	2	-5	No	60	300	No
21A	102	No	0.5	-24	Yes	140	60	No
21B	102	No	0.5	-24	No	15	500	No
22A	102	No	1	-24	Yes	141	50	No
22B	102	No	1	-24	No	11	650	No
23A	102	No	1.5	-24	Yes	142	40	No
23B	102	No	1.5	-24	No	178	500	No
24A	102	No	2	-24	Yes	143	40	No

Test Number #	Length of High Point (inches)	Check Valve (Yes/No)	Initial Gas Volume (l)	Initial Gas Pressure Inches of Hg Vacuum	High Froude Number Flush (Yes/No)	File Number #	Water Volume Drained Depressurizing to 1 atm* (ml)	Mini Flow Line (Yes/No)
24B	102	No	2	-24	No	13	700	No
25A	102	No	0.5	-15	Yes	144	45	No
25B	102	No	0.5	-15	No	19	500	No
26A	102	No	1	-15	Yes	147	40	No
26B	102	No	1	-15	No	16	575	No
27A	102	No	1.5	-15	Yes	148	30	No
27B	102	No	1.5	-15	No	17	700	No
28A	102	No	2	-15	Yes	149	40	No
28B	102	No	2	-15	No	18	700	No
29A	51	Yes	0.5	-24	Yes	79	50	No
29C	51	Yes	0.5	-24	Yes	217	20	No
29D	51	Yes	0.5	-24	Yes	255	30	No
29E	51	Yes	0.5	-24	No	266	300	No
29G	51	Yes	0.5	-24	Yes	326	30	Yes
30A	51	Yes	1	-24	Yes	80	70	No
30B	51	Yes	1	-24	No	102	680	No
30C	51	Yes	1	-24	Yes	218	30	No
30D	51	Yes	1	-24	Yes	256	20	No
30E	51	Yes	1	-24	No	267	220	No
30F	51	Yes	1	-24	No	263	250	No
30G	51	Yes	1	-24	Yes	327	30	Yes
31A	51	Yes	1.5	-24	Yes	81	40	No
31C	51	Yes	1.5	-24	Yes	219	25	No
31D	51	Yes	1.5	-24	Yes	257	20	No
31E	51	Yes	1.5	-24	No	268	300	No
31G	51	Yes	1.5	-24	Yes	328	30	Yes
32A	51	Yes	2	-24	Yes	83	60	No
32B	51	Yes	2	-24	No	103	740	No
32C	51	Yes	2	-24	Yes	220	25	No
32D	51	Yes	2	-24	Yes	258	30	No
32E	51	Yes	2	-24	No	269	300	No
32F	51	Yes	2	-24	No	262	250	No
32G	51	Yes	2	-24	Yes	325	30	Yes

Test Number #	Length of High Point (inches)	Check Valve (Yes/No)	Initial Gas Volume (l)	Initial Gas Pressure Inches of Hg Vacuum	High Froude Number Flush (Yes/No)	File Number #	Water Volume Drained Depressurizing to 1 atm* (ml)	Mini Flow Line (Yes/No)
33A	51	Yes	0.5	-20	Yes	84	70	No
33C	51	Yes	0.5	-20	Yes	223	25	No
33E	51	Yes	0.5	-20	No	270	350	No
34A	51	Yes	1	-20	Yes	85	60	No
34C	51	Yes	1	-20	Yes	224	20	No
34E	51	Yes	1	-20	No	271	300	No
35A	51	Yes	1.5	-20	Yes	86	60	No
35C	51	Yes	1.5	-20	Yes	225	25	No
35E	51	Yes	1.5	-20	No	272	350	No
36A	51	Yes	2	-20	Yes	87	50	No
36C	51	Yes	2	-20	Yes	226	20	No
36E	51	Yes	2	-20	No	273	350	No
37A	51	Yes	0.5	-15	Yes	88	60	No
37C	51	Yes	0.5	-15	Yes	221	25	No
37D	51	Yes	0.5	-15	Yes	251	30	No
37E	51	Yes	0.5	-15	No	274	300	No
37G	51	Yes	0.5	-15	Yes	333	30	Yes
38A	51	Yes	1	-15	Yes	89	50	No
38C	51	Yes	1	-15	Yes	227	20	No
38D	51	Yes	1	-15	Yes	252	30	No
38E	51	Yes	1	-15	No	275	340	No
38F	51	Yes	1	-15	No	265	300	No
38G	51	Yes	1	-15	Yes	330	30	Yes
39A	51	Yes	1.5	-15	Yes	90	50	No
39C	51	Yes	1.5	-15	Yes	228	20	No
39D	51	Yes	1.5	-15	Yes	253	30	No
39E	51	Yes	1.5	-15	No	276	300	No
39G	51	Yes	1.5	-15	Yes	331	30	Yes
40A	51	Yes	2	-15	Yes	91	90	No
40C	51	Yes	2	-15	Yes	222	25	No
40D	51	Yes	2	-15	Yes	254	30	No
40E	51	Yes	2	-15	No	277	500	No
40F	51	Yes	2	-15	No	264	240	No

Test Number #	Length of High Point (inches)	Check Valve (Yes/No)	Initial Gas Volume (l)	Initial Gas Pressure Inches of Hg Vacuum	High Froude Number Flush (Yes/No)	File Number #	Water Volume Drained Depressurizing to 1 atm* (ml)	Mini Flow Line (Yes/No)
40G	51	Yes	2	-15	Yes	332	25	Yes
41A	51	Yes	0.5	-10	Yes	92	50	No
41C	51	Yes	0.5	-10	Yes	229	20	No
42A	51	Yes	1	-10	Yes	93	50	No
42C	51	Yes	1	-10	Yes	230	20	No
43A	51	Yes	1.5	-10	Yes	94	50	No
43C	51	Yes	1.5	-10	Yes	231	20	No
44A	51	Yes	2	-10	Yes	95	50	No
44C	51	Yes	2	-10	Yes	232	20	No
45A	51	Yes	0.5	-5	Yes	96	50	No
45C	51	Yes	0.5	-5	Yes	233	20	No
46A	51	Yes	1	-5	Yes	97	60	No
46C	51	Yes	1	-5	Yes	234	25	No
47A	51	Yes	1.5	-5	Yes	98	50	No
47C	51	Yes	1.5	-5	Yes	235	20	No
48A	51	Yes	2	-5	Yes	99	80	No
48C	51	Yes	2	-5	Yes	236	20	No
49A	51	No	0.5	-24	Yes	67	40	No
49C	51	No	0.5	-24	Yes	237	20	No
50A	51	No	1	-24	Yes	68	40	No
50B	51	No	1	-24	No	76	600	No
50C	51	No	1	-24	Yes	238	20	No
51A	51	No	1.5	-24	Yes	69	20	No
51C	51	No	1.5	-24	Yes	239	20	No
52A	51	No	2	-24	Yes	70	35	No
52B	51	No	2	-24	No	77	570	No
52C	51	No	2	-24	Yes	240	20	No
52D	51	No	2	-24	Yes	250	30	No
53A	51	No	0.5	-15	Yes	72	30	No
53C	51	No	0.5	-15	Yes	241	20	No
54A	51	No	1	-15	Yes	73	30	No
54C	51	No	1	-15	Yes	242	20	No
55A	51	No	1.5	-15	Yes	74	70	No

Test Number #	Length of High Point (inches)	Check Valve (Yes/No)	Initial Gas Volume (l)	Initial Gas Pressure Inches of Hg Vacuum	High Froude Number Flush (Yes/No)	File Number #	Water Volume Drained Depressurizing to 1 atm* (ml)	Mini Flow Line (Yes/No)
55C	51	No	1.5	-15	Yes	243	20	No
56A	51	No	2	-15	Yes	75	65	No
56C	51	No	2	-15	Yes	244	20	No
56D	51	No	2	-15	Yes	249	20	No
57A	25.5	Yes	0.5	-24	Yes	104	85	No
57C	25.5	Yes	0.5	-24	Yes	278	40	No
57G	25.5	Yes	0.5	-24	Yes	314	30	Yes
58A	25.5	Yes	1	-24	Yes	105	60	No
58B	25.5	Yes	1	-24	No	121	780	No
58C	25.5	Yes	1	-24	Yes	279	30	No
58E	25.5	Yes	1	-24	No	294	200	No
58G	25.5	Yes	1	-24	Yes	315	30	Yes
59A	25.5	Yes	1.5	-24	Yes	106	70	No
59C	25.5	Yes	1.5	-24	Yes	280	30	No
59G	25.5	Yes	1.5	-24	Yes	316	30	Yes
60A	25.5	Yes	2	-24	Yes	107	60	No
60C	25.5	Yes	2	-24	Yes	281	30	No
60E	25.5	Yes	2	-24	No	295	280	No
60G	25.5	Yes	2	-24	Yes	317	30	Yes
61A	25.5	Yes	0.5	-20	Yes	108	65	No
61B	25.5	Yes	0.5	-20	No	126	360	No
61C	25.5	Yes	0.5	-20	Yes	282	30	No
62A	25.5	Yes	1	-20	Yes	109	60	No
62B	25.5	Yes	1	-20	No	122	720	No
62C	25.5	Yes	1	-20	Yes	283	30	No
63A	25.5	Yes	1.5	-20	Yes	110	50	No
63C	25.5	Yes	1.5	-20	Yes	284	30	No
64A	25.5	Yes	2	-20	Yes	111	45	No
64C	25.5	Yes	2	-20	Yes	285	30	No
65A	25.5	Yes	0.5	-15	Yes	112	55	No
65B	25.5	Yes	0.5	-15	No	125	400	No
65C	25.5	Yes	0.5	-15	Yes	287	30	No
65G	25.5	Yes	0.5	-15	Yes	318	30	Yes

Test Number #	Length of High Point (inches)	Check Valve (Yes/No)	Initial Gas Volume (l)	Initial Gas Pressure Inches of Hg Vacuum	High Froude Number Flush (Yes/No)	File Number #	Water Volume Drained Depressurizing to 1 atm* (ml)	Mini Flow Line (Yes/No)
66A	25.5	Yes	1	-15	Yes	113	55	No
66B	25.5	Yes	1	-15	No	123	760	No
66C	25.5	Yes	1	-15	Yes	286	30	No
66E	25.5	Yes	1	-15	No	296	260	No
66G	25.5	Yes	1	-15	Yes	319	30	Yes
67A	25.5	Yes	1.5	-15	Yes	114	30	No
67C	25.5	Yes	1.5	-15	Yes	288	30	No
67G	25.5	Yes	1.5	-15	Yes	320	30	Yes
68A	25.5	Yes	2	-15	Yes	115	50	No
68C	25.5	Yes	2	-15	Yes	289	30	No
68E	25.5	Yes	2	-15	No	297	260	No
68G	25.5	Yes	2	-15	Yes	321	20	Yes
69A	25.5	Yes	0.5	-10	Yes	117	50	No
69C	25.5	Yes	0.5	-10	Yes	290	30	No
70A	25.5	Yes	1	-10	Yes	118	50	No
70C	25.5	Yes	1	-10	Yes	291	30	No
71A	25.5	Yes	1.5	-10	Yes	119	50	No
71C	25.5	Yes	1.5	-10	Yes	292	30	No
72A	25.5	Yes	2	-10	Yes	120	50	No
72C	25.5	Yes	2	-10	Yes	293	30	No
73A	25.5	No	0.5	-24	Yes	128	75	No
73C	25.5	No	0.5	-24	Yes	298	30	No
74A	25.5	No	1	-24	Yes	129	70	No
74B	25.5	No	1	-24	No	138	420	No
74C	25.5	No	1	-24	Yes	299	30	No
74E	25.5	No	1	-24	No	306	220	No
75A	25.5	No	1.5	-24	Yes	130	60	No
75C	25.5	No	1.5	-24	Yes	300	30	No
76A	25.5	No	2	-24	Yes	131	50	No
76C	25.5	No	2	-24	Yes	301	30	No
76E	25.5	No	2	-24	No	307	180	No
77A	25.5	No	0.5	-15	Yes	132	60	No
77B	25.5	No	0.5	-15	No	137	400	No

Test Number #	Length of High Point (inches)	Check Valve (Yes/No)	Initial Gas Volume (l)	Initial Gas Pressure Inches of Hg Vacuum	High Froude Number Flush (Yes/No)	File Number #	Water Volume Drained Depressurizing to 1 atm* (ml)	Mini Flow Line (Yes/No)
77C	25.5	No	0.5	-15	Yes	302	30	No
78A	25.5	No	1	-15	Yes	133	60	No
78B	25.5	No	1	-15	No	139	440	No
78C	25.5	No	1	-15	Yes	303	30	No
78E	25.5	No	1	-15	No	308	240	No
79A	25.5	No	1.5	-15	Yes	134	50	No
79C	25.5	No	1.5	-15	Yes	304	20	No
80A	25.5	No	2	-15	Yes	135	40	No
80C	25.5	No	2	-15	Yes	305	25	No
80E	25.5	No	2	-15	No	309	220	No
81A	102	Yes	2.5	-24	Yes	200	60	No
82A	102	Yes	3	-24	Yes	201	50	No
83A	102	Yes	4	-24	Yes	202	40	No
84A	102	Yes	5	-24	Yes	203	50	No
85A	102	Yes	2.5	-15	Yes	196	50	No
86A	102	Yes	3	-15	Yes	197	50	No
87A	102	Yes	4	-15	Yes	198	50	No
88A	102	Yes	5	-15	Yes	199	60	No
89A	102	No	2.5	-24	Yes	192	60	No
90A	102	No	3	-24	Yes	193	40	No
91A	102	No	4	-24	Yes	194	40	No
92A	102	No	5	-24	Yes	195	50	No
93A	102	No	2.5	-15	Yes	188	60	No
94A	102	No	3	-15	Yes	189	60	No
95A	102	No	4	-15	Yes	190	60	No
96A	102	No	5	-15	Yes	191	50	No
2V-1	51+25.5	Yes	1.5+0	-24	Yes	356	20+0	Yes
2V-2	51+25.5	Yes	1.4+.1	-24	Yes	370	15+10	Yes
2V-3	51+25.5	Yes	1.3+.2	-24	Yes	371	20+10	Yes
2V-4	51+25.5	Yes	1.2+.3	-24	Yes	368	20+10	Yes
2V-5	51+25.5	Yes	1.1+.4	-24	Yes	367	20+10	Yes
2V-6	51+25.5	Yes	1+.5	-24	Yes	354	70+20	Yes
2V-7	51+25.5	Yes	0+1.5	-24	Yes	372	0+15	Yes

Test Number #	Length of High Point (inches)	Check Valve (Yes/No)	Initial Gas Volume (l)	Initial Gas Pressure Inches of Hg Vacuum	High Froude Number Flush (Yes/No)	File Number #	Water Volume Drained Depressurizing to 1 atm* (ml)	Mini Flow Line (Yes/No)
2V-8	51+25.5	Yes	1+1	-24	Yes	366	20+10	Yes
2V-9	51+25.5	Yes	1.5+0	-15	Yes	373	15+0	Yes
2V-10	51+25.5	Yes	1+.5	-15	Yes	374	20+10	Yes
2V-11	51+25.5	Yes	0+1.5	-15	Yes	375	0+40	Yes
2V-12	51+25.5	Yes	.75+.75	-24	Yes	376	25+10	Yes
2V-13	51+25.5	Yes	.5+1	-24	Yes	377	20+10	Yes
2V-14	51+25.5	Yes	.25+1.25	-24	Yes	378	20+10	Yes
2V-15	51+25.5	Yes	.15+1.35	-24	Yes	379	20+10	Yes

A=Flushed

B=Unflushed

C=Tests performed with longer riser and flushed

D=Tests performed with support and flushed

E=Tests performed with longer riser and unflushed

F=Tests performed with support and unflushed

G=Tests performed with longer riser, flushed, and mini flow

R=Repeated tests used to compare the relative loads of a highpoint configuration

2V=Tests performed with two parallel high points (first number corresponds to primary high point located at the dead end, second number corresponds to the secondary highpoint)

*Value obtained during testing: for flushed system value was expected to be a few tens of mL and for the non-flushed system a few hundred mL.

4.2 Data Reduction and Interpretation

A large amount of data was collected during the air-water waterhammer experiments. The following section presents a sample of the data and what information was extracted for further analysis, comparison, and modeling. Plots are provided for pressure, force, and flow rate for conditions where the experimental setup was flushed (purged) with a flow rate at a high Froude number ($Fr > 0.54$) and for a system that was not flushed. Three sets of plots are provided (pressure – Figures 4-1, force (load) – Figures 4-2, and flow – Figures 4-3) with the following designations:

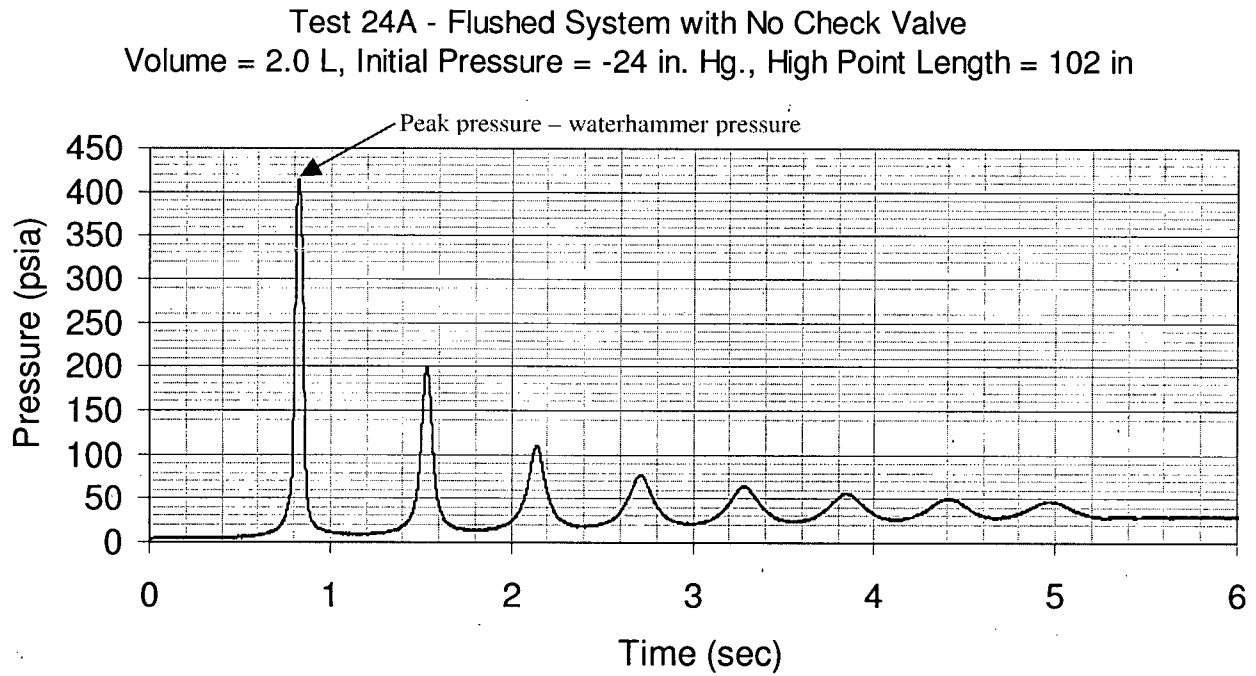
- a) flushed system with no check valve included,
- b) flushed system with check valve included,
- c) non-flushed system with no check valve included,
- d) case b, except that the initial pressure in the bubble for this case was -15 in Hg instead of -24 in Hg which was used for cases a, b, and c.

Case d plots are included since the force profile is significantly different from the other plots (cases a-c) in terms of the air-water waterhammer loads. The check valve slam loads still have the same signature, thus this additional force plot is only for the purpose of pointing out the difference in the air-water waterhammer loads.

4.2.1 Pressure Plots

Four pressure plots are included below as Figures 4-1a to 4-1d. Each plot points out the waterhammer pressure which was extracted from the data for further analysis, such as plots of peak pressure versus water volume drained for different initial pressure conditions. The flushed system pressure plots (cases a, b, and d) are very “clean”, where only one peak could be observed for the first oscillation (period). Thus, it is easy to determine the peak pressure for those tests. For the non-flushed system plots, there could be multiple peaks observed in each oscillation (period), such as in Figure 4-1c. Thus, each peak pressure value was collected and the highest peak pressure value was used for comparison between different tests.

Figure 4-1a: Sample pressure vs. time data plot with a flushed system and no check valve.



**Figure 4-1b: Sample pressure vs. time data plot
with a flushed system and check valve included.**

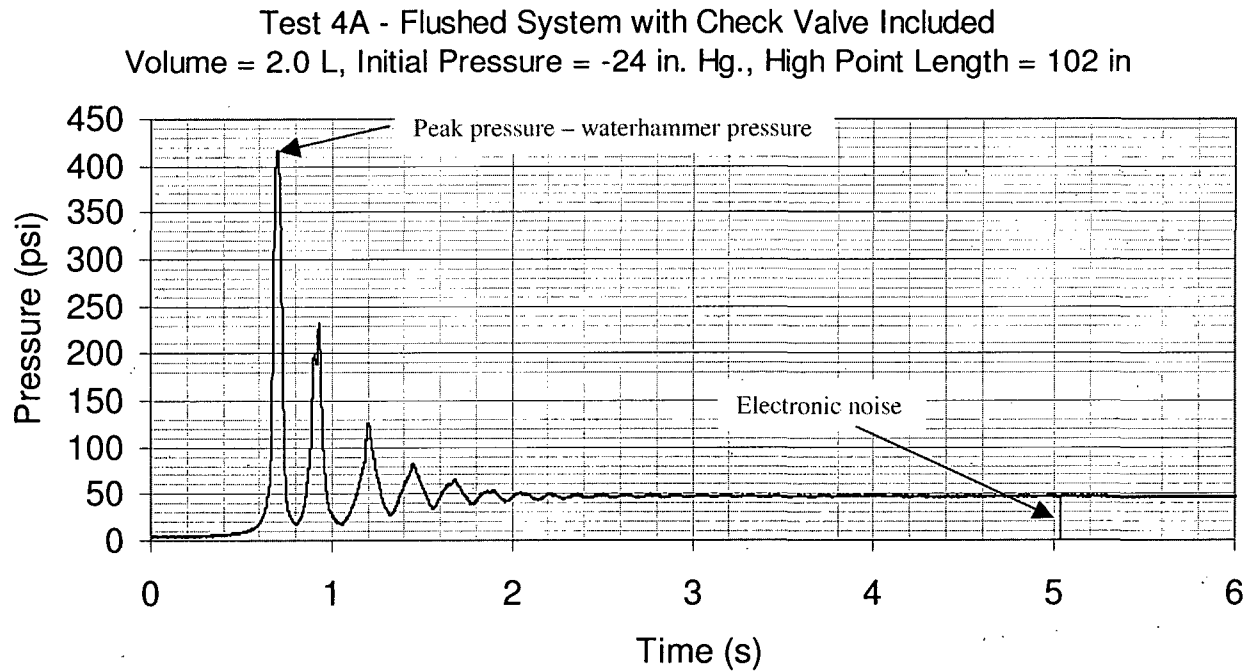


Figure 4-1c: Sample pressure vs. time data plot with a non-flushed system.

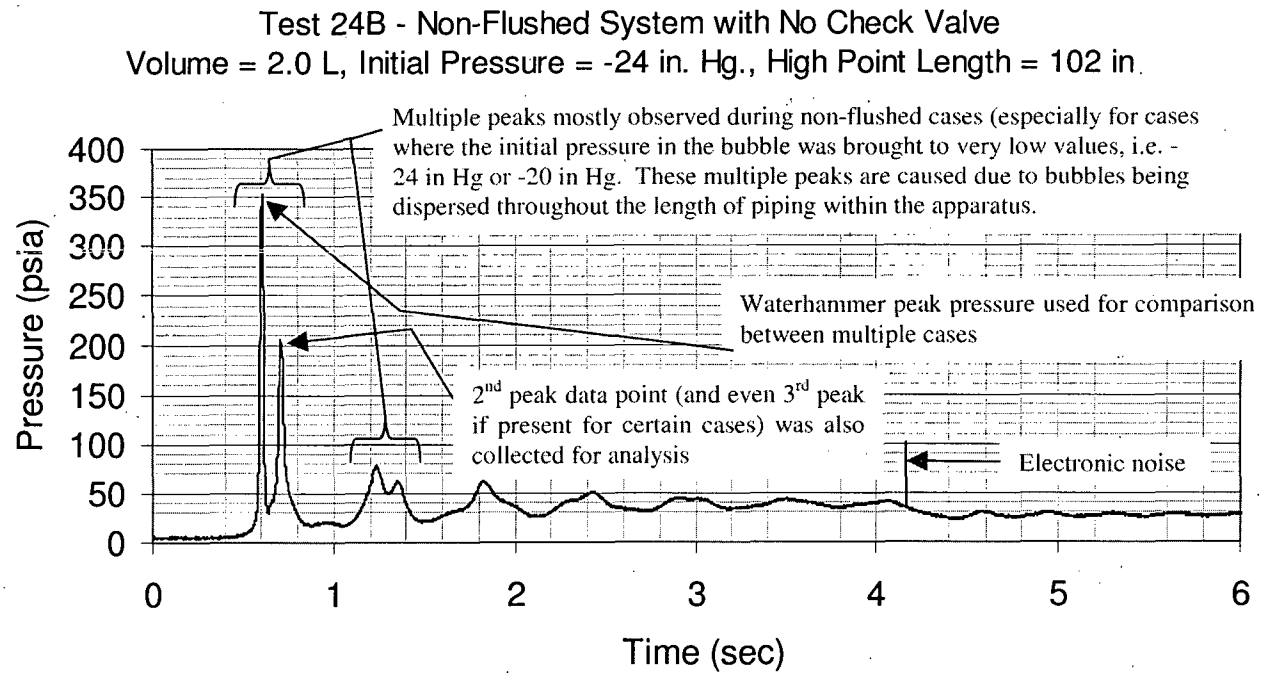
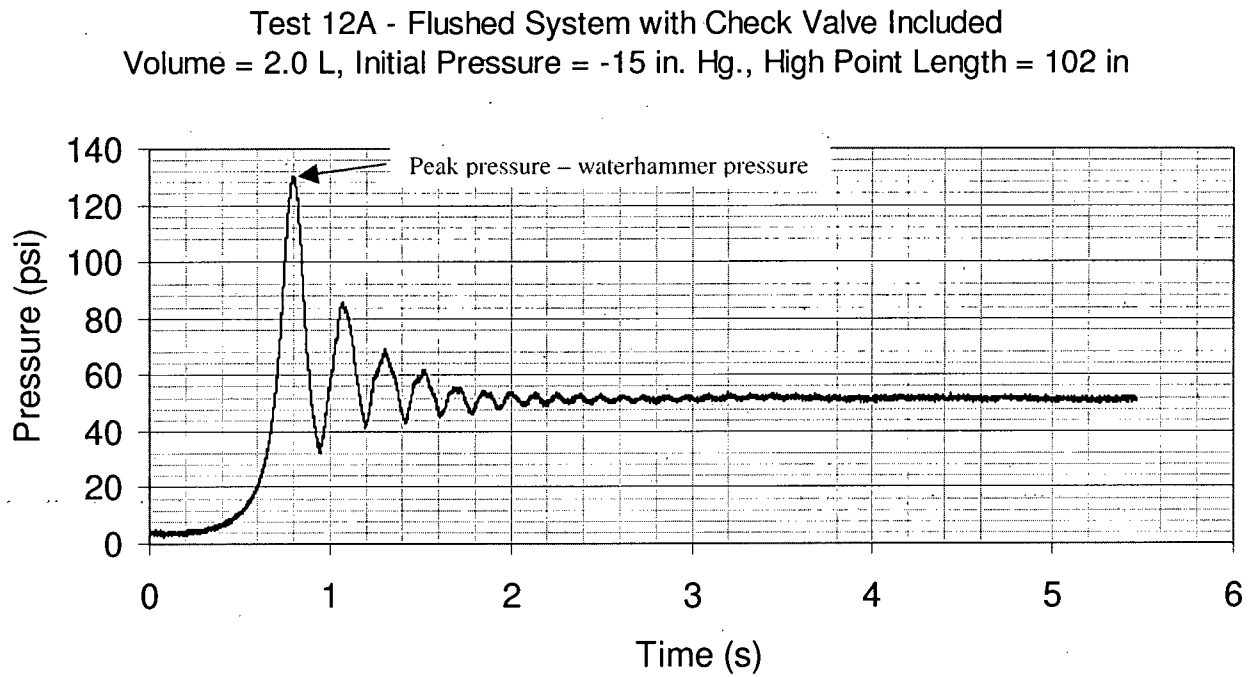


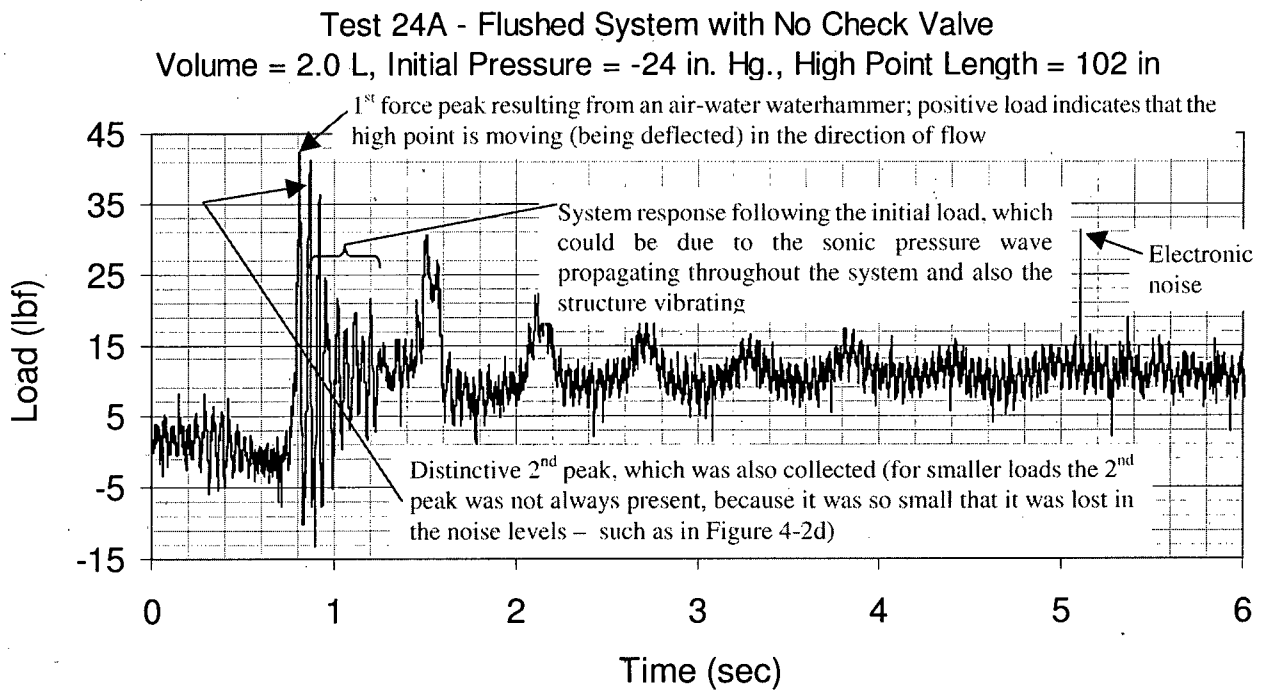
Figure 4-1d: Sample pressure vs. time data plot with a flushed system, check valve included, and the initial pressure in the bubble equal to -15 in. Hg.



4.2.2 Force Plots

Four force plots are included below as Figures 4-2a to 4-2d. These plots correspond to the pressure plots presented in Figures 4-1a to 4-1d. Each of the plots contains the initial force loads that are due to the air-water waterhammer and Figures 4-2b and 4-2d also contain additional loads that are due to a check valve slam (check valve was installed in the experimental apparatus for these cases). For tests with higher (higher refers to -24" Hg being higher then -15" Hg) air-water waterhammer pressures, multiple force peaks could be clearly identified during the transient, such as the ones noted in Figure 4-1b. For tests with lower (-15" Hg being lower then -24" Hg) pressures and thus loads, one distinctive peak (instead of multiple peaks) could be identified and data is only collected for that one peak. This is well illustrated in Figure 4-2d, which shows data for a test with an initial pressure of -15 in Hg instead of -24 in Hg. Note that the peaks being referred to here are for loads resulting from an air-water waterhammer and not from a check valve slam, which are discussed next. For cases with check valves, there is an additional set of data that is collected, which results from a check valve slam. A check valve slam occurs after the initial air-water waterhammer as a result of a rarefaction pressure wave propagating through the system and consequently imposing a significant load on the system. This load could be identified by first a significant negative force impulse (referred to as tensile load within this document) followed by a positive impulse (referred to as a compressive load). A negative load corresponds to the system high point moving in the opposite direction of flow and vice versa for the positive load. Refer to Figures 4-2a to 4-2d for more information on the different loads analyzed, since these plots contain extensive labels pointing out the different forces and how to identify them.

**Figure 4-2a: Sample load (force) vs. time data plot
with a flushed system and no check valve included.**



**Figure 4-2b: Sample load (force) vs. time data plot
with a flushed system and the check valve included.**

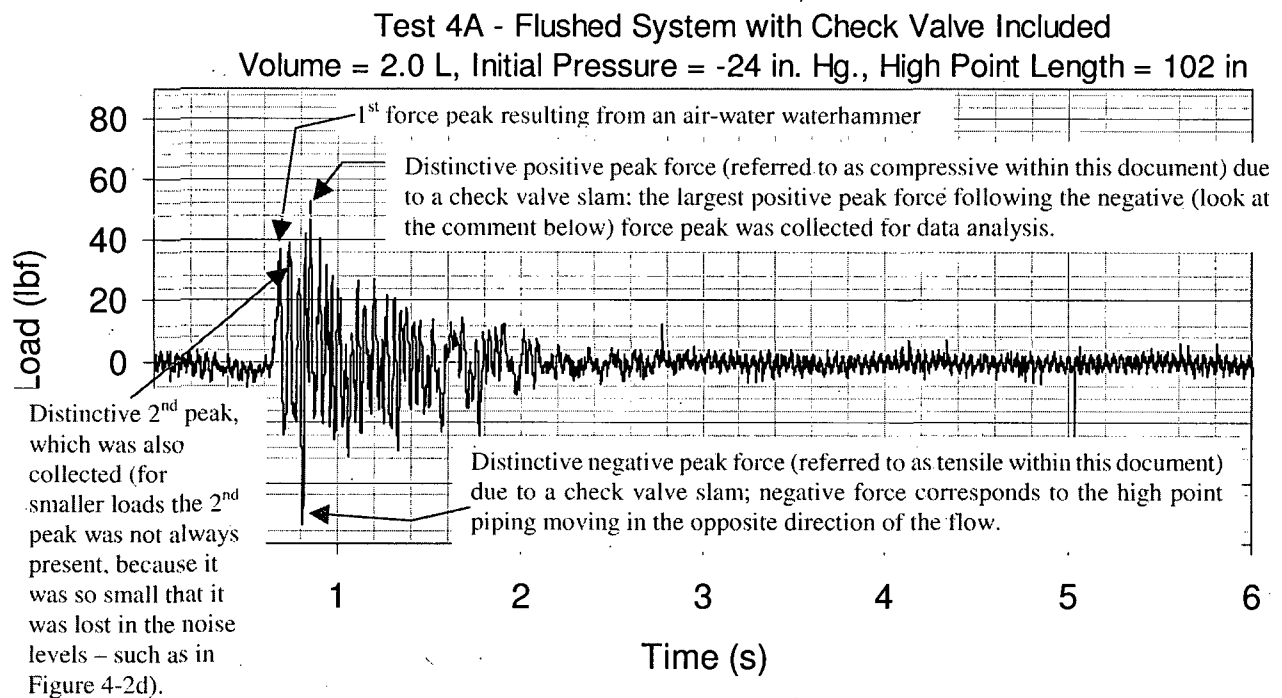


Figure 4-2c: Sample load (force) vs. time data plot with a non-flushed system.

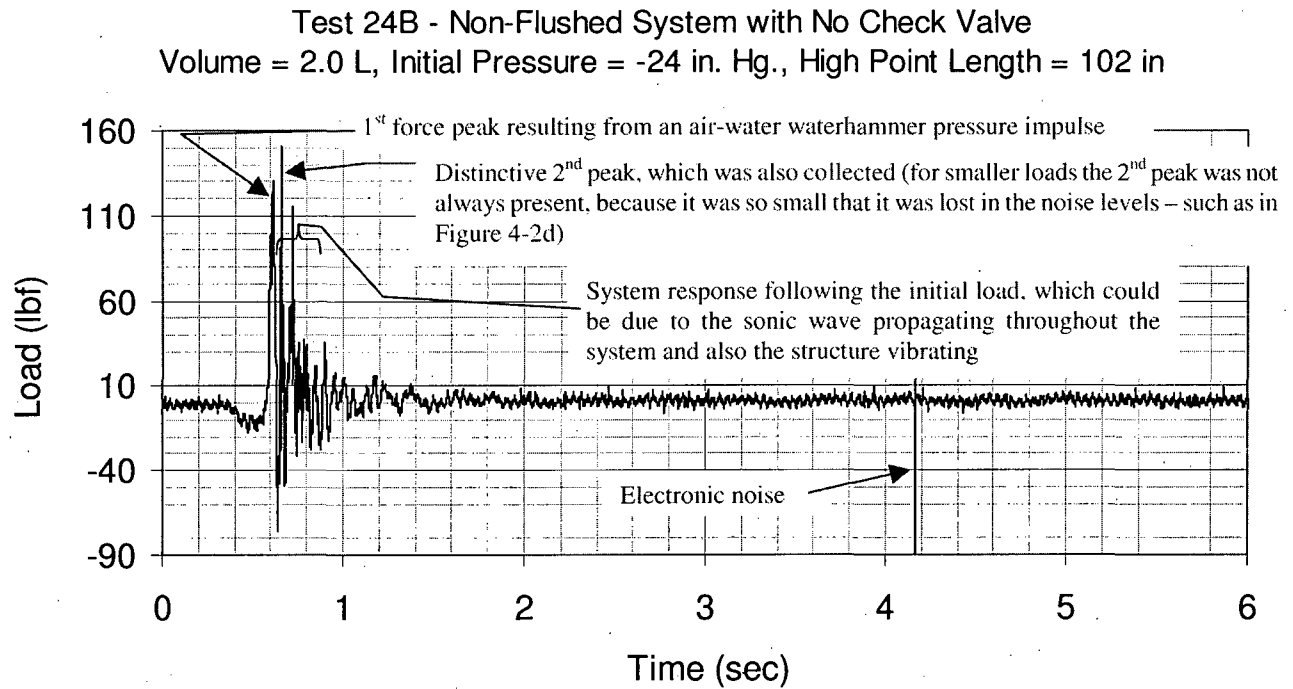
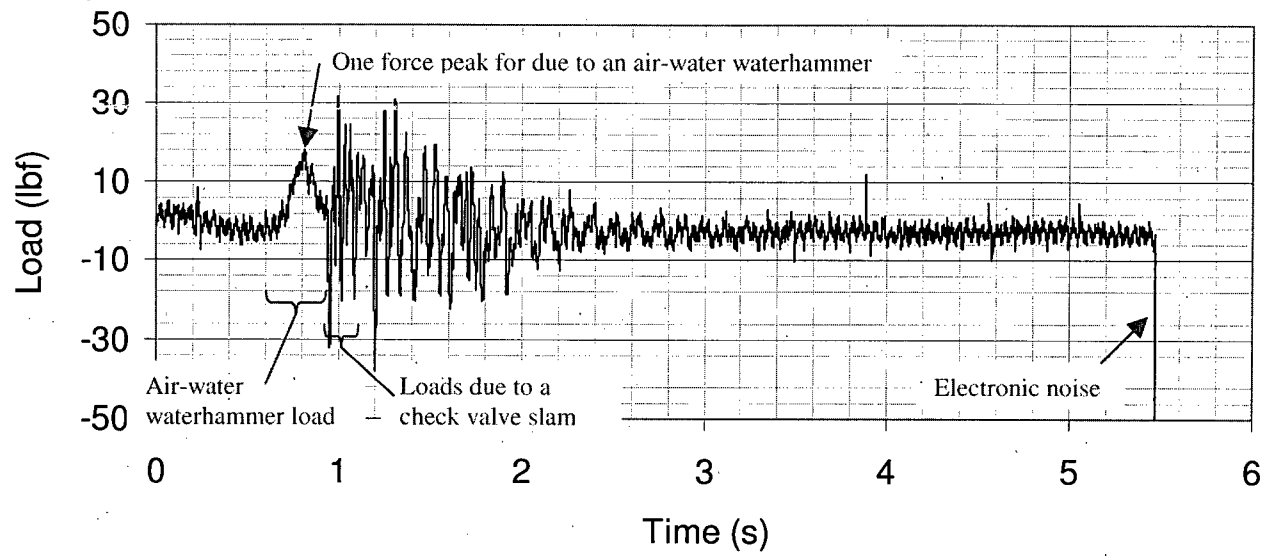


Figure 4-2d: Sample force vs. time data plot with a flushed system, check valve included, and the initial pressure in the bubble equal to -15 in Hg.

Test 12A - Flushed System with Check Valve Included
Volume = 2.0 L, Initial Pressure = -15 in. Hg., High Point Length = 102 in



4.2.3 Flow Rate Plots

The last set of four figures are flow rate plots which are included below as Figures 4-3a to 4-3d. These plots correspond to the pressure and force plots presented in Figures 4-1a to 4-1d and 4-2a to 4-2d, respectively. The flow rate plots are straight forward in terms of data collection when compared to the pressure and force plots. The flow rate data is only reliable up to the air-water waterhammer pressure peak, since following an air-water waterhammer event the flow within the system is constantly changing direction and the flow meter is not capable of measuring reverse flow.

Once the section of the plot that corresponds to the time prior to the air-water waterhammer pressure peak is identified, the peak flow rate from that section is collected for further data analysis. This procedure is performed for all four cases (a to d) and no special consideration is needed for cases where the check valve is included or where the system is not flushed. Refer to Figure 4-3a to 4-3d for a more information.

**Figure 4-3a: Sample flow rate vs. time data plot
with a flushed system and no check valve included.**

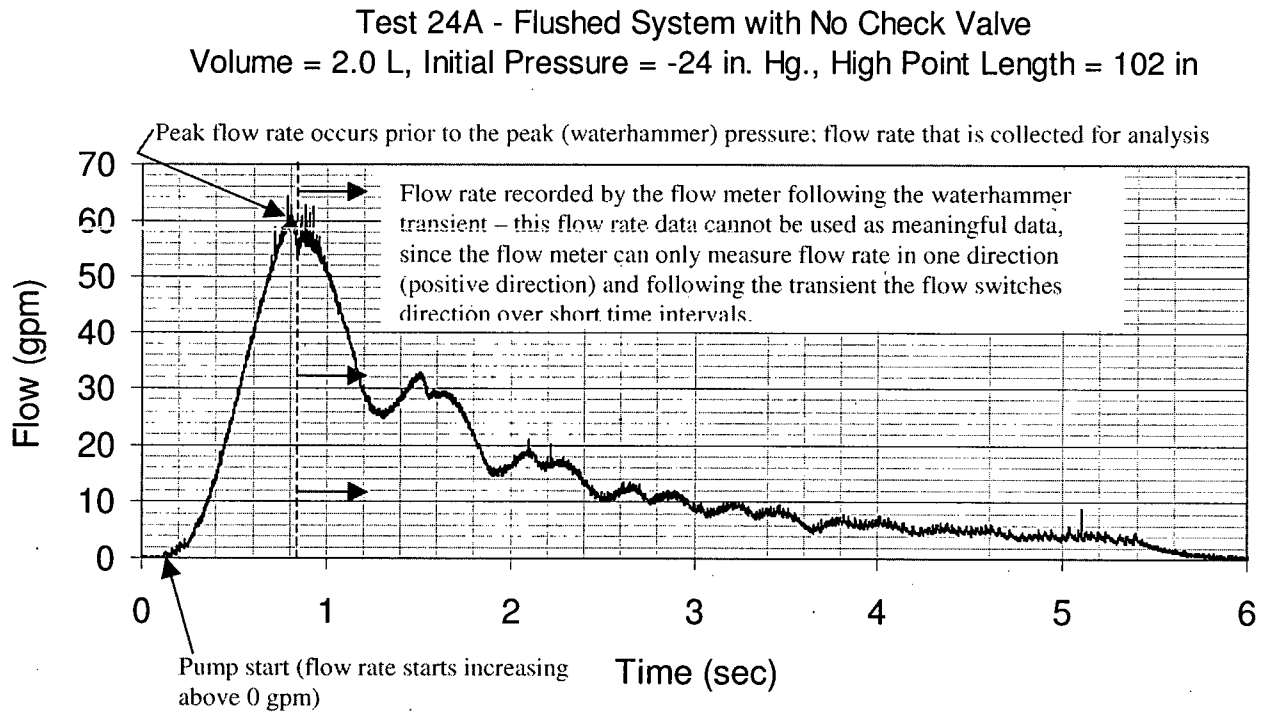
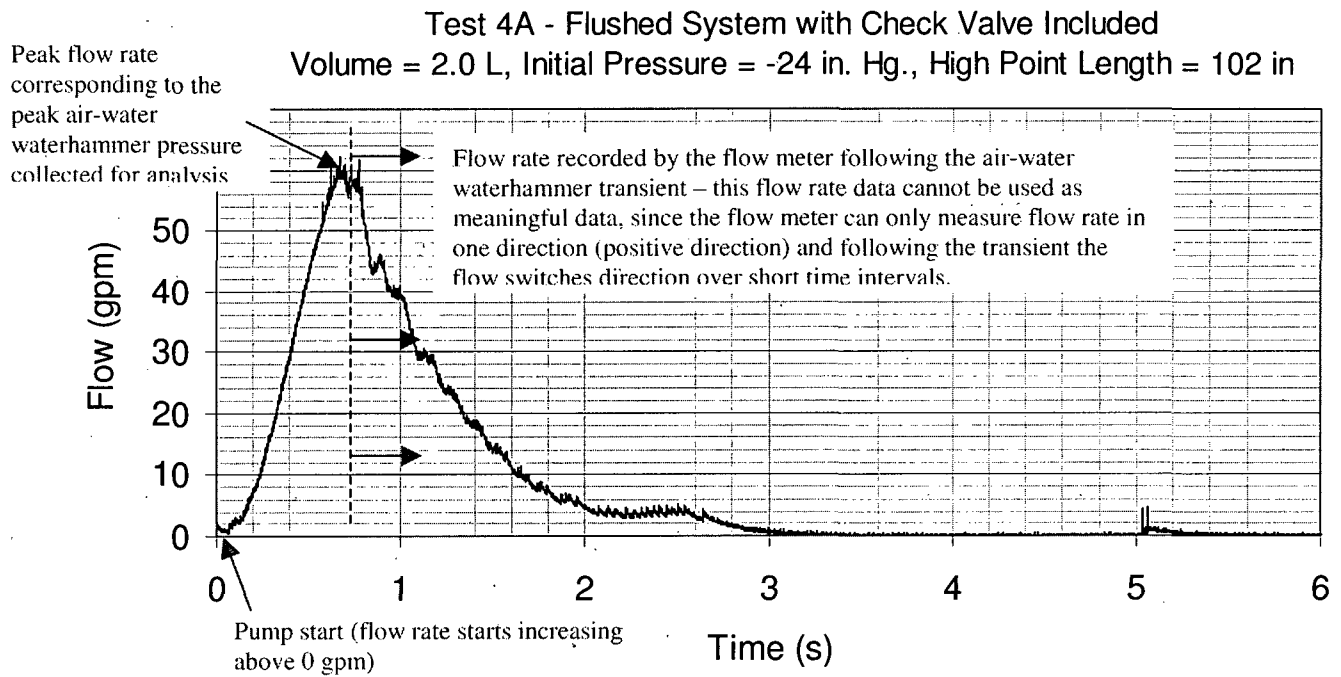


Figure 4-3b: Sample flow rate vs. time data plot with a non-flushed system and check valve not included.



**Figure 4-3c: Sample flow rate vs. time data plot with
a non-flushed system and check valve not included.**

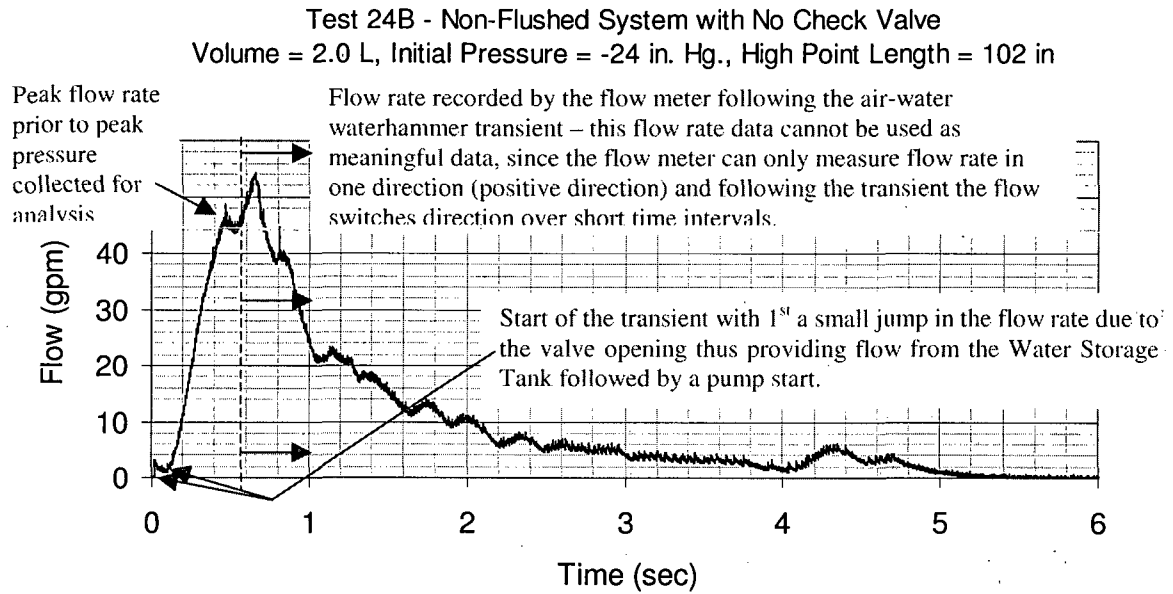
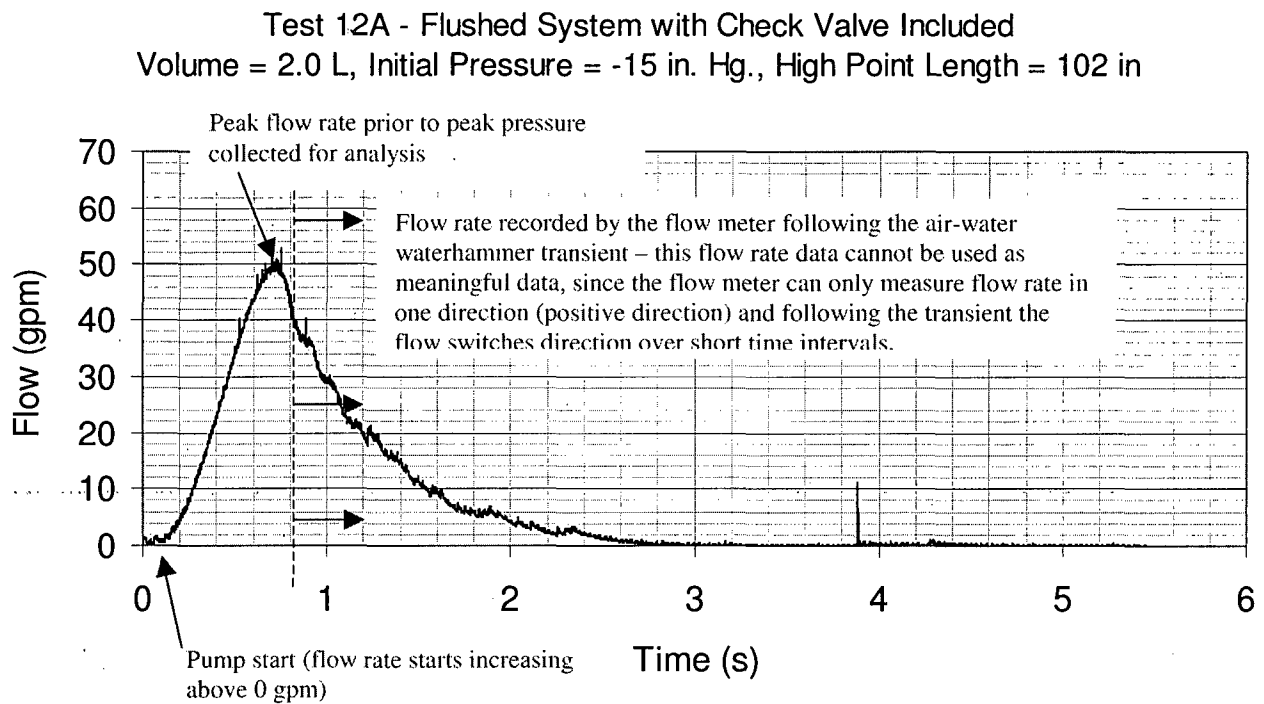


Figure 4-3d: Sample flow rate vs. time data plot with a flushed system, check valve included, and the initial pressure in the bubble equal to -15 in Hg.



5.0 TEST RESULTS

5.1 The Transparent Test Section

The transparent highpoint test section served two functions in this experimental program. Firstly, it confirmed the water velocity (Froude number) needed to “washout” an accumulated gas volume and secondly it illustrated the transient two-phase flow pattern as the gas volume was compressed in the stratified gas-water configuration. The results for both of these separate effect tests are discussed below.

5.1.1 “Washout” Water Velocity

These tests were performed by first forming a stratified gas volume in the piping highpoint under stagnant conditions and then sequentially increasing the water velocity through the test section and observing when the gas volume was swept out. This is important since this provides the user with a technical basis to determine whether a specific highpoint configuration has experienced system operational conditions sufficient to either prevent gas accumulation or purge existing accumulations, as well as to potentially provide a means to remove a gas volume that might accumulate. While not applicable to every system, there are systems where such considerations can be utilized such as those that have a “piggy-back” operational mode during a accident. For many of these systems, they have already exposed to a sufficient water flow rate to satisfy the Froude number criterion before the “piggy-back” operating mode begins. When this is the case, the “piggy-back” mode does not have to be evaluated.

Wallis et al (1977) performed tests on the liquid velocity that is sufficient to “washout” a gas bubble at the discharge of the pipe into a large reservoir. This resulted in a criterion of a Froude number equal to 0.54 as being sufficient to “washout” the gas volume where the Froude number is defined by:

$$N_{Fr} = U/[g D]^{0.5} \quad (5-1)$$

and the variables have the following definitions:

- D is the piping inner diameter,
- g is the acceleration of gravity and
- U is the water superficial velocity through the pipe (water volumetric flow rate divided by the total cross-sectional flow area of the pipe).

Our goal in these tests was to determine whether this same criterion could be used for piping highpoint configurations in terms of those conditions that are sufficient to sweep the gas volume into, and down through, the downcomer pipe. Obviously, the water velocity in the downcomer piping should be greater than the bubble rise velocity for the gas volume to be removed completely, but as we will see, this is generally satisfied.

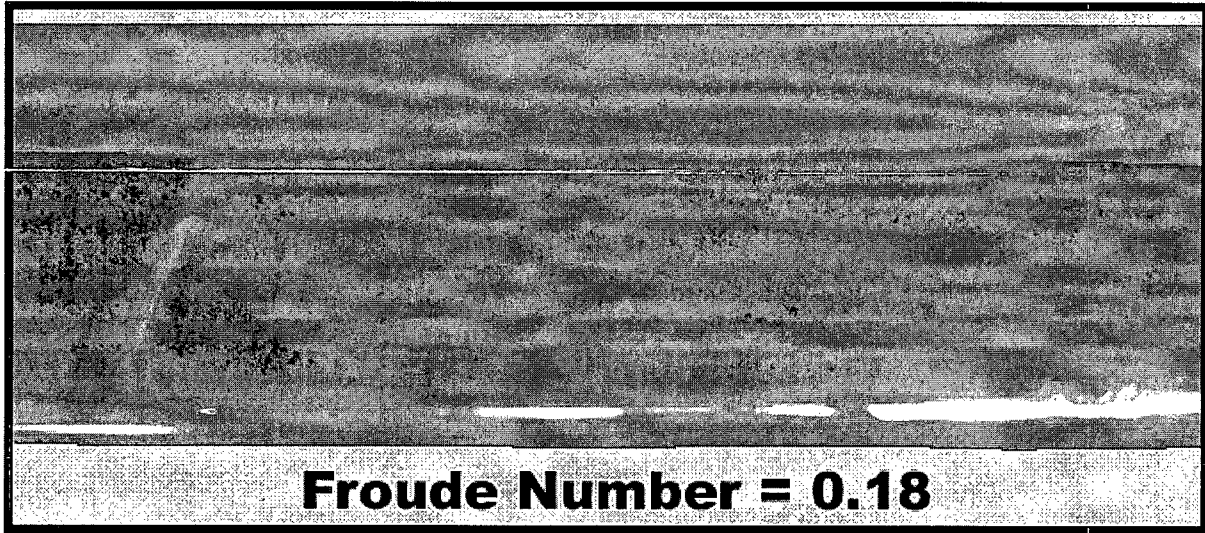
To examine the Froude number criterion, the transparent tests were performed with increasing velocities and Froude numbers as shown in Table 5-1 below.

Table 5-1

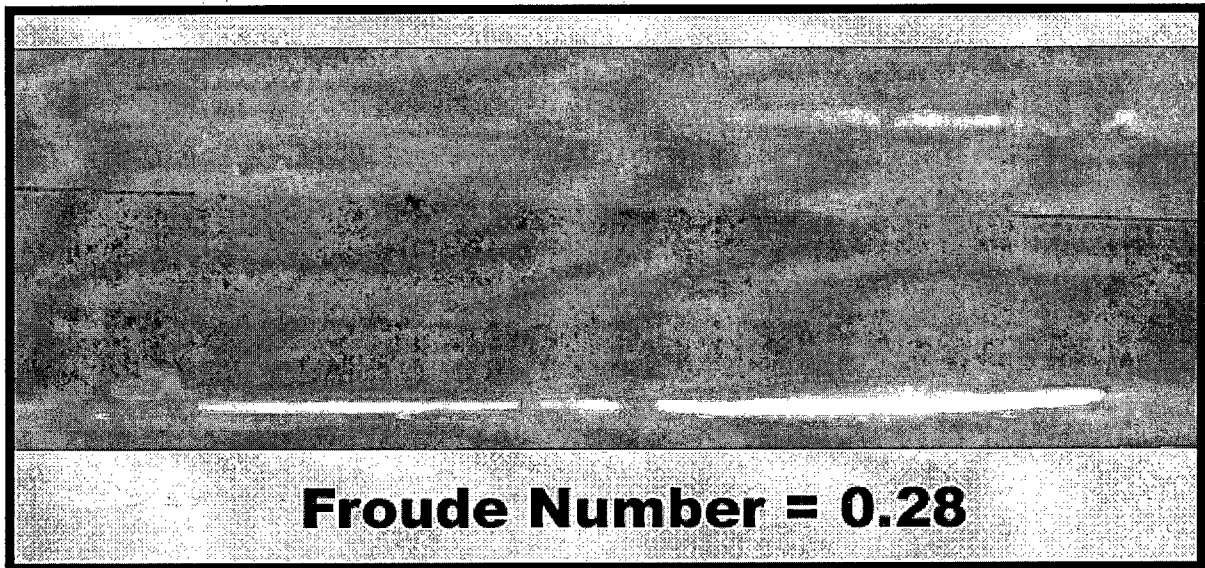
Measured Water Flow Rate (gpm)	Froude Number
4.5	0.18
7	0.28
10	0.41
11	0.45
13.5	0.55

The observed gas-water flow patterns are shown in Figures 5-1 through 5-4 with the water flowing from left to right. Consult Figure 3-3 for the locations of these views along the length of the transparent test section. As can be seen in the photographs, when the Froude number is 0.18 and 0.28, a stratified flow pattern is observed with the water flowing under the gas surface. Consistent with the driving potential for the water flow, the upstream side has a slightly greater depth than the downstream side and this differential increases with the Froude number. For a Froude number of

**Figure 5-1: Stratified air-water configuration
observed for a suction Froude number of 0.18.**



**Figure 5-2: Stratified air-water configuration
observed for a suction Froude number of 0.28.**



**Figure 5-3: Stratified air-water configuration
observed for a suction Froude number of 0.41.**

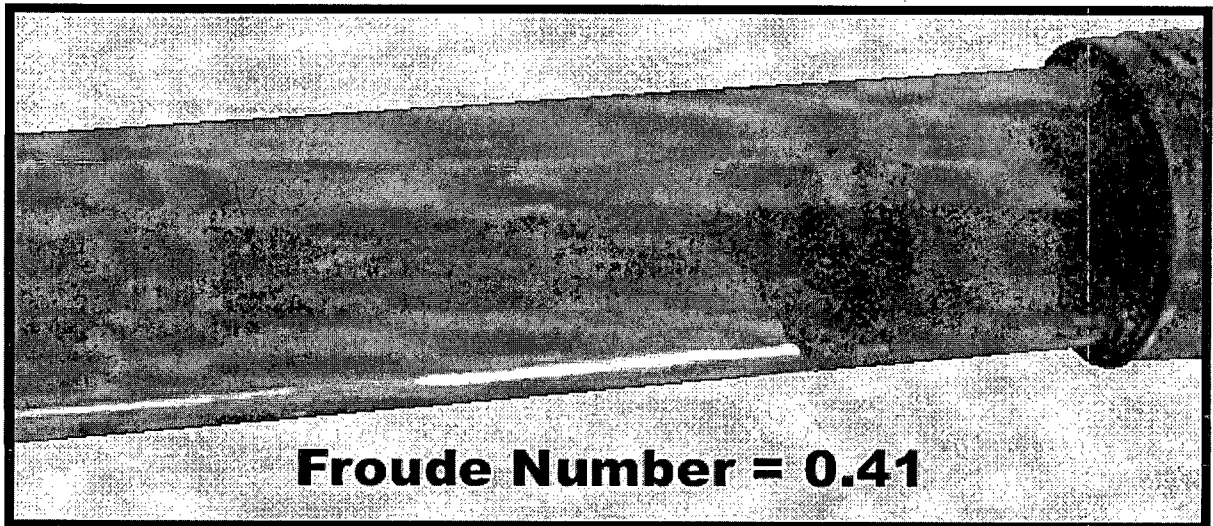
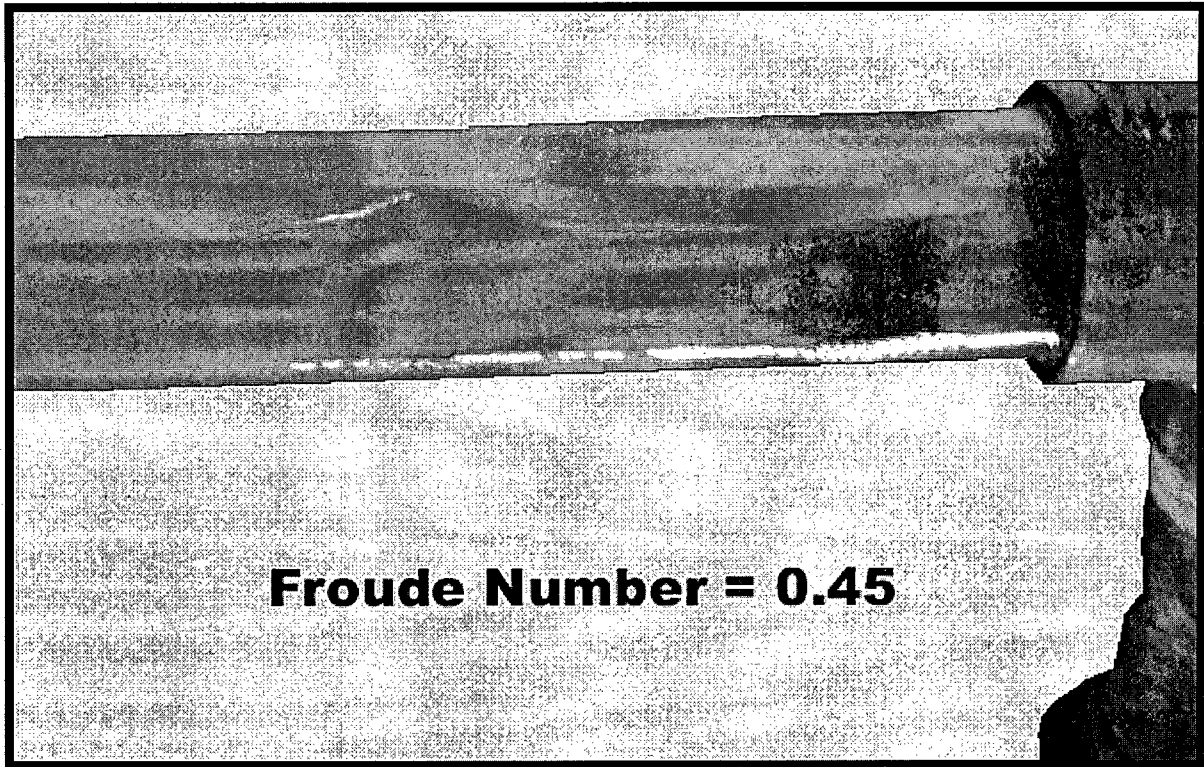


Figure 5-4: Air-water flow pattern observed for a suction Froude number of 0.45.



0.45, which approaches the 0.54 value, the gas volume is pushed to the downstream end of the pipe and some of the gas was pulled downward when the water velocity was greater than the bubble rise velocity. Figure 5-5 shows that the bubble rise velocity is approximately 1 ft/sec as demonstrated by the data of Haberman and Morton (1953) as given in Wallis (1969). For the reader's reference, the water velocity for a Froude of 0.54 exceeds 1 ft/sec for all pipes with an inner diameter greater than approximately 1-1/4 inches, i.e. for all practical cases of interest for gas intrusion. In these highpoint tests, when the water Froude number was increased to 0.55, there was no significant gas volume left in the highpoint volume between the riser and the downcomer.

From these data we conclude that the criterion developed by Wallis et al is directly applicable to the piping highpoint configuration. This can be used to determine if the recent hydraulic history shows that gas would have been removed due to the imposed water flow rate and it can also be used to evaluate whether an accumulated gas volume could be removed by the developed water volumetric flow rate as a plant strategy for controlling the extent of gas accumulations.

5.1.2 Gas-Water Flow Pattern for the Waterhammer Event

A stratified flow pattern can be produced in a piping highpoint with the accumulation of noncondensable gas in a stagnant system or one with a sufficient low water volumetric flow rate that the Froude number is much less than the 0.54 value discussed. With this flow pattern, the water flow rate induced by a pump start, or the opening of a control valve, will flow over the top of the water already resident in the highpoint as discussed in Section 2 (see Figure 2-3). Since the compression of the gas volume is a very dynamic event, it is helpful in understanding the nature and consequences of such events to determine if this stratified flow pattern is sustained during the rapid compression.

With the transparent test section in place, digital movies recorded the two-phase flow pattern as the gas volume became very small. Figures 5-6 (a), (b) and (c) show an example of the observed behavior as the final compression occurs for a test with the conditions of a drained volume of 1.5 liters and a pressure of -24 inches of Hg. It is clear from these pictures that the imposed water flow rate is moving over the stagnant water in such a manner that the local void fraction essentially

Figure 5-5: Terminal velocity of air bubbles in filtered or distilled water as function of bubble size (taken from Wallis, 1969).

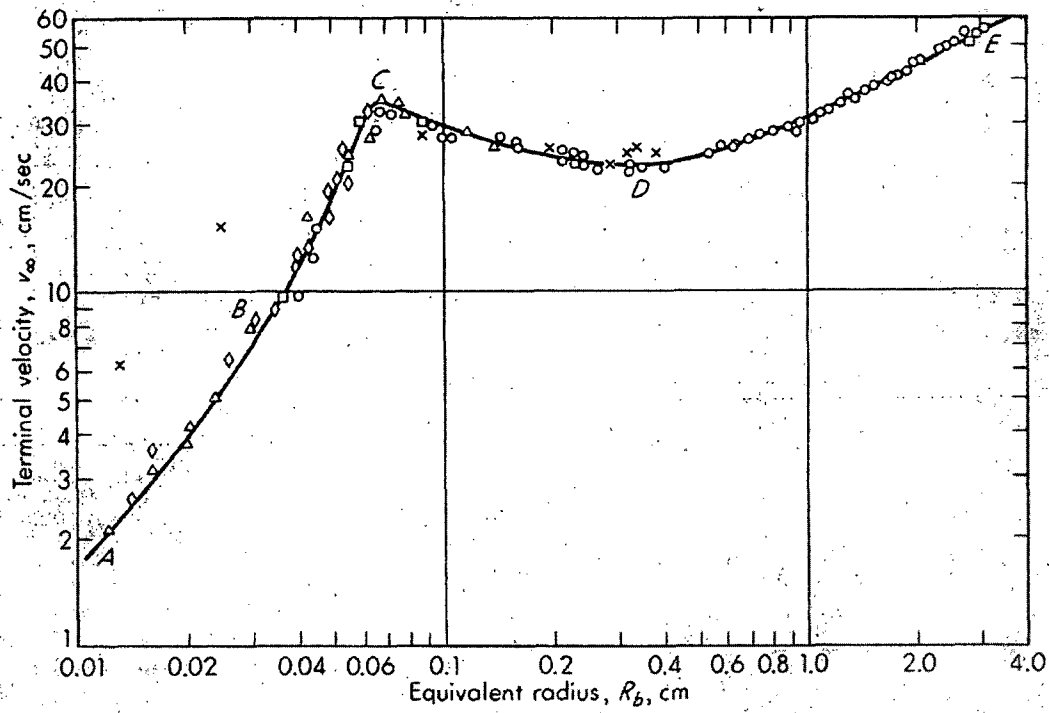
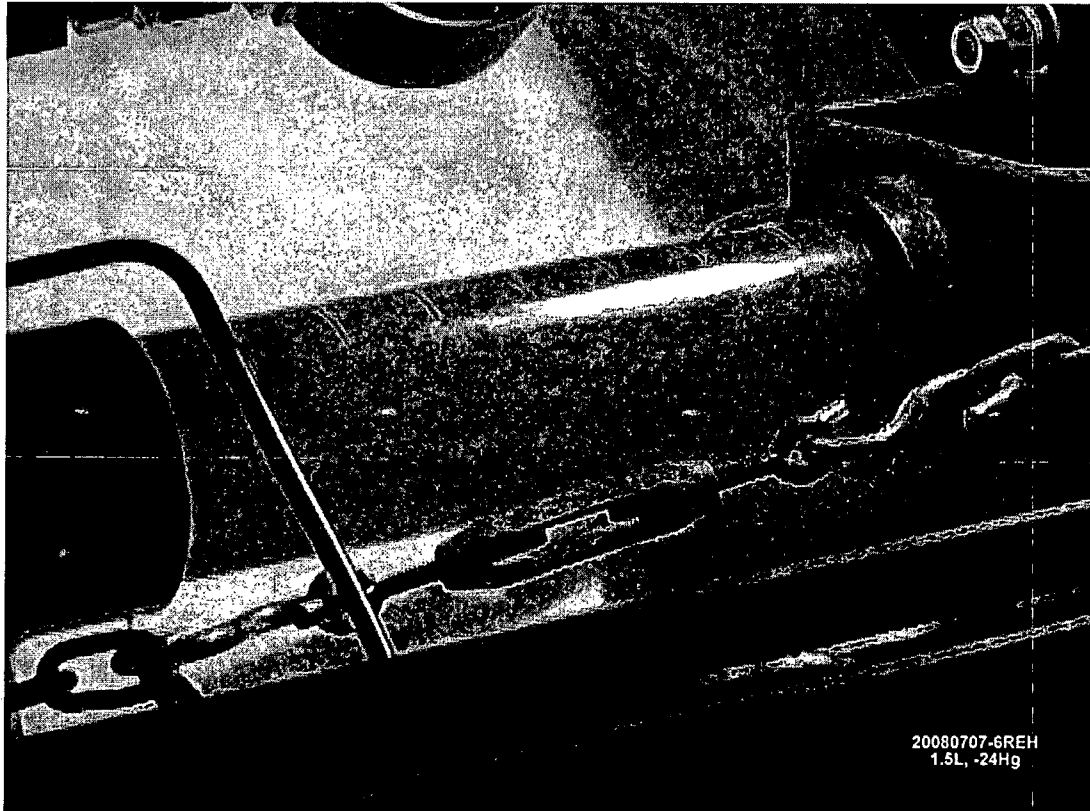


Figure 5-6a: Sequential pictures of the two-phase flow pattern for water compressing a gas volume with the initial conditions of -24 inches of Hg (2.5 psia) and 1.5 liters of water drained (initial void fraction = 0.25).



**Figure 5-6b: Sequential pictures of the two-phase flow pattern for water
compressing a gas volume with the initial conditions of -24 inches of Hg
(2.5 psia) and 1.5 liters of water drained (initial void fraction = 0.25).**

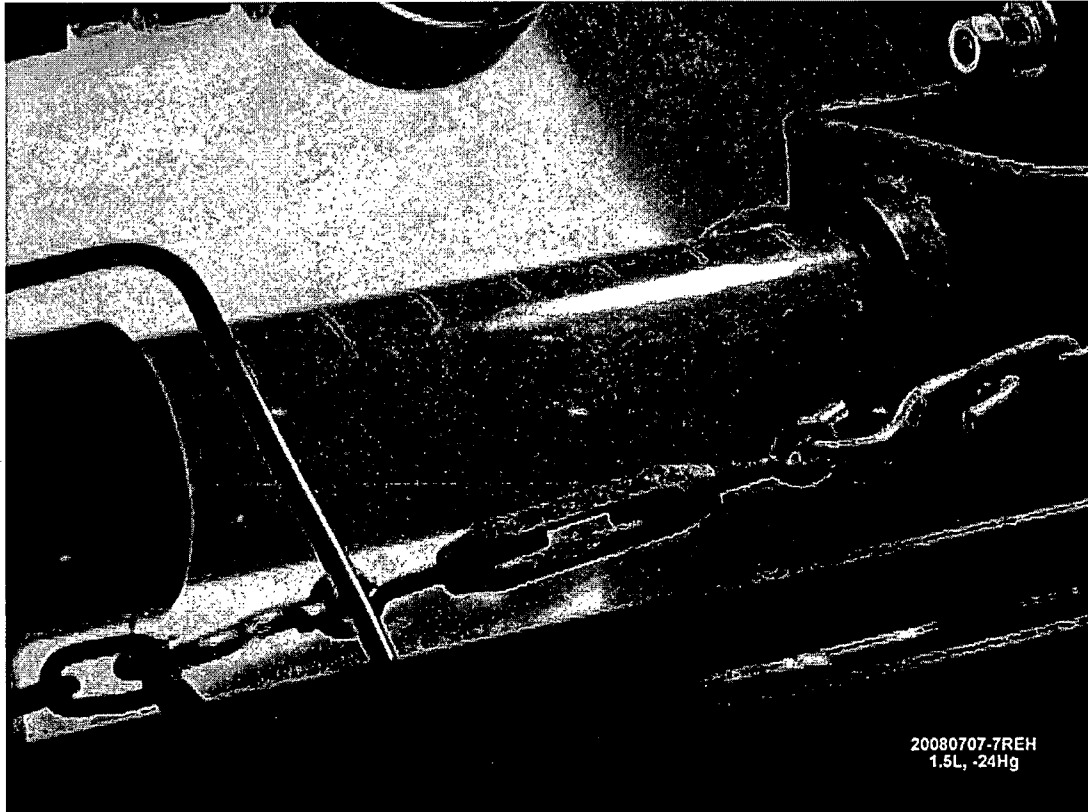
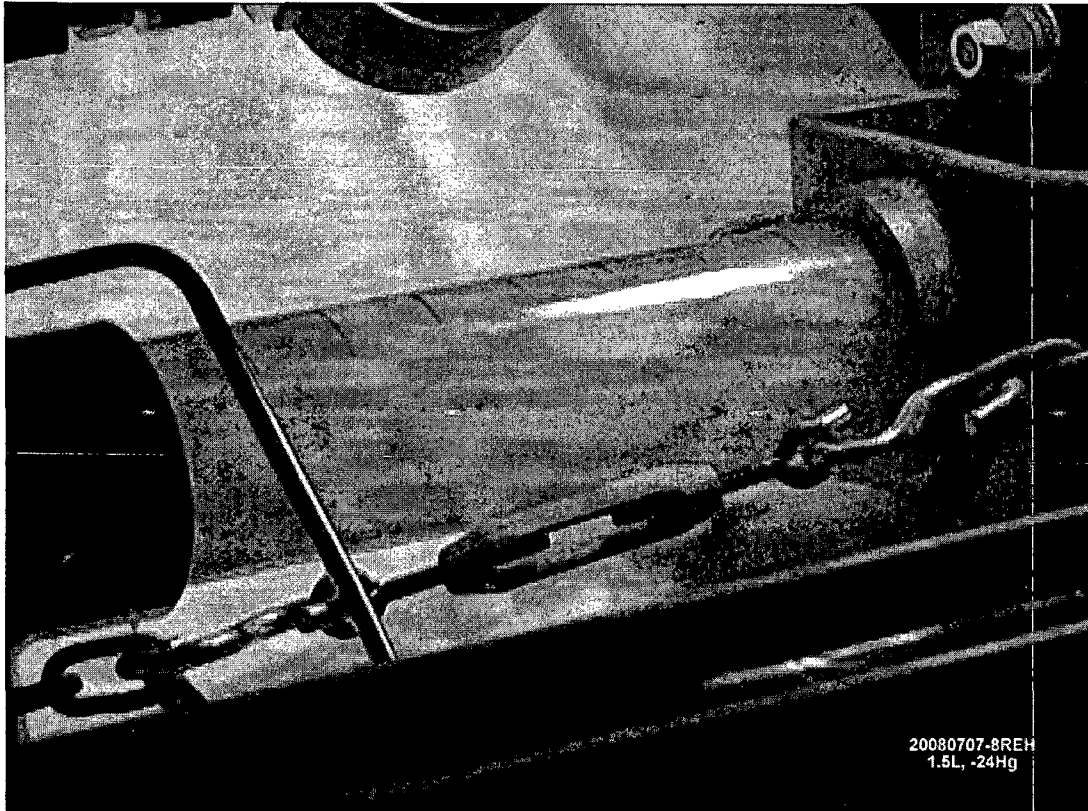


Figure 5-6c: Sequential pictures of the two-phase flow pattern for water copressing a gas volume with the initial conditions of -24 inches of Hg (2.5 psia) and 1.5 liters of water drained (initial void fraction = 0.25).



remains at the initial condition, where the gas region exists. Therefore, these experimental observations present a flow pattern like that depicted in Figure 2-3. This provides the basic knowledge of the stratified gas-water waterhammer events of interest for the plant conditions to be evaluated.

5.2 Measured Air-Water Waterhammer Pressures

As described above, air-water waterhammer data was taken for a spectrum of initial gas volumes, initial gas volume pressures as well as different highpoint lengths and configurations. In addition, the tests were performed with initial conditions in which the piping was “flushed” before developing the highpoint gas volume or not “flushed” before draining water to develop this gas volume. Lastly, the tests were performed with, and without, a swinging check valve in the system. To develop the insights gained from the data, we will start by examining how these various conditions influence the peak waterhammer pressures observed in the tests.

5.2.1 Influence of “Flushing” on the Peak Waterhammer Pressure

As discussed previously regarding the initial conditions, if the experimental piping was initially flushed with a high Froude number water flow rate, the air volume was only located in the instrumented horizontal highpoint section with a volume essentially equal to the volume of water drained. If it was not flushed in this manner, the largest air volume was in the instrumented horizontal highpoint with other smaller air volumes distributed to some extent throughout the two inch piping. This was illustrated by the extent of drainage obtained when the “water filled” test apparatus was depressurized from the pump shutoff head to atmospheric pressure. When the test apparatus had been flushed with a water flow rate having a Froude number substantially greater than the 0.54 criterion discussed above, the water volume drained was a few tens of milliliters. For those tests where this flushing technique was not performed, the water volume drained varied from a few hundred to several hundred milliliters, i.e. thereby illustrating that air volume(s), albeit small, were captured in other segments of the piping. As the apparatus was constructed, care was taken to ensure that the “horizontal” parts of the piping, including the alternate switchback segments, were installed

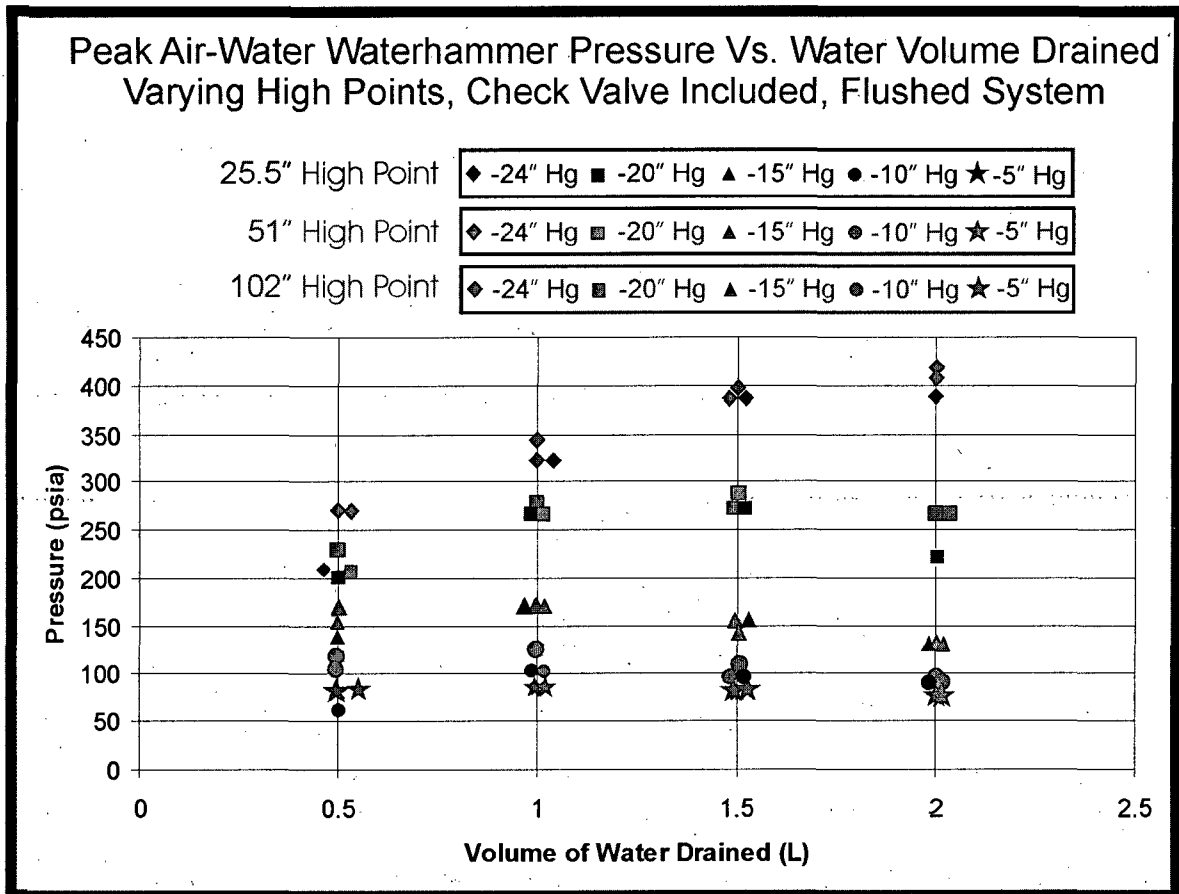
to be sloped slightly upward in the direction of the highpoint. Hence, the capture of air was either in the pump, the pipe fittings (unions) used to connect the straight piping lengths in the switchback arrangement, or as distributed air bubbles captured along the top surface of the piping. Whatever the actual gas volume configuration, the water volume drained was included in the total volume drained from the test apparatus used to define the test initial condition.

As a result of this difference in the location of the air in the test piping configuration, the tests performed using flushing to produce the initial condition provide the most controlled set of initial conditions to investigate the influences of the initial gas volume, the initial gas pressure, etc. Those tests performed without using flushing to establish the initial condition are also useful in that they illustrate the influence of having a given gas volume distributed throughout the piping. Depending on the source of the accumulated gas, either of these could be experienced in the field. Therefore, these experiments examined the gas-water waterhammer response of both sets of conditions.

Figure 5-7 shows the peak waterhammer pressures measured for those tests performed with a swing check valve installed and using a dynamic flush to produce a controlled set of experimental conditions. As is discussed later, the presence of a swing check valve in the flow path does not influence the peak waterhammer pressure. This figure shows the influence of the water volume drained, the initial gas pressure and the length of the piping highpoint. (From a practical perspective, the volume drained is the initial gas volume plus the small volume associated with the water compressible. We show this as the water volume drained in liters since this is the parameter measured. For a drained volume of 0.5 liters, the contribution to this volume due to the water compressible is approximately 2% and would be 1% for a drained volume of 1 liter.) Please note that for those data points that experienced the same waterhammer pressure, the data are displaced slightly to the left or right to illustrate all of the test observations.

Several key results are immediately apparent from Figure 5-7. Firstly, when compared on the basis of the peak pressure as a function of the accumulated gas volume, there is no influence of the length of the piping highpoint. This agreement between test sections with highpoints of different

Figure 5-7: Comparison of the measured peak gas-water waterhammer event pressures for the three highpoint lengths tested with controlled initial conditions.



lengths is true for the three highpoint lengths tested and is observed for all of the initial gas pressures and volumes. Fundamentally, the total gas volume available controls the extent of the pump run-up condition at the instant that the waterhammer occurs, and therefore, the peak gas-water waterhammer pressure. Basic knowledge of this nature is important in the assessment of whether a specific gas volume could result in a waterhammer pressure sufficient to lift a relief valve should such an event occur.

Secondly, examining the results for peak waterhammer pressure as a function of the initial gas volume (volume of water drained) shows that for initial pressures of -20, -15, -10 and -5 inches Hg the data exhibit a maximum in the waterhammer pressure observed as the initial gas volume is increased. Moreover, the data also shows that the greater the initial gas volume pressure, the lower the maximum waterhammer pressure. Since there are several different manners in which gas could be accumulated (outage manipulations, back leakage of nitrogen saturated water from accumulators and safety injection tanks, radiolytic gas accumulation, keep-full systems, etc.), there are a variety of initial gas volume pressures that could be experienced in the field.

Thirdly, these experimental results show that substantial noncondensable gas-water waterhammer pressures (in excess of 400 psia) can be developed with a pump that has a run-up time of about 1 sec. and an effective shutoff head at the highpoint elevation of approximately 18 psig. Considering the pump run-up times, shutoff heads and design flow rates available for the plant systems it is apparent that events sufficient to cause relief valves to lift could result from such noncondensable gas-water events depending on the initial conditions in the piping and the characteristics of the initiating event (pump start, opening of a valve, etc.).

Given the evidence that there is a maximum in the peak gas-water waterhammer pressure as a function of the water volume drained, additional experiments were performed in the full length highpoint (102 inches) for the lowest initial gas pressure tested. These results are given in Figure 5-8 and show that such a maximum peak waterhammer pressure was also observed for an initial gas pressure of -24 inches of Hg.

Figure 5-8: The measured peak waterhammer pressures for the full length highpoint with (a) larger volumes of water drained, (b) initial gas volume pressures of -24 and -15 inches Hg and (c) the test section flushed to establish the initial condition.

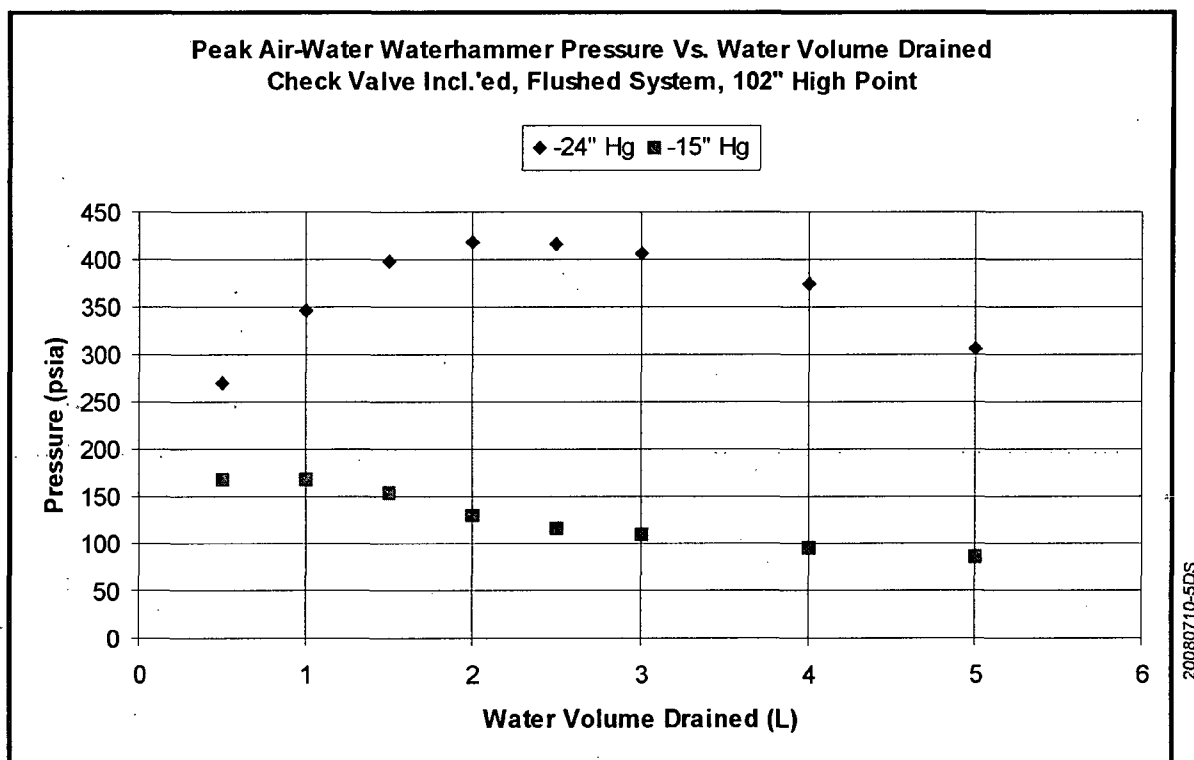


Figure 5-9 compares the results for tests taken with, and without, the pre-test, high Froude number flushing process for the 102 inch highpoint length, and shows the influence of a distributed gas void fraction on the resulting waterhammer peak pressure. In general, the peak pressures for the non-flushed tests are consistent with, but somewhat less than those obtained with a single gas volume (flushed tests) of the same size. Therefore, the occurrence of a distributed gas volume can be considered as having a peak pressure that is bounded by that measured using the same parameters but with the initial condition developed from a flushed state.

5.2.2 Influence of the Check Valve on the Peak Waterhammer Pressure

As a result of the subsequent frictional and expansion losses in the piping network, the peak waterhammer pressures typically occur during the first compression event, even though there may be several follow-on events due to the oscillatory nature of the response. Figures 5-10, 5-11 and 5-12 illustrate the manner in which a swing check valve would respond to a downstream gas-water waterhammer event. Note that in the hydraulic response to the pump start, the check valve opens to provide the flow required by the pump and remains open during the compression of the noncondensable gas that generates the noncondensable gas-water waterhammer event. Once the compression waves propagate back to the large diameter, atmospheric conditions, storage tank and are reflected as rarefaction waves that eventually reverse the water flow rate, the swing check valve in the example would eventually respond by closing the flapper with the closure rate being equal to the water velocity induced by the rarefaction waves. Since the role of the check valve on the hydraulic response in the piping system occurs only after the compression waves are reflected from the large volume and low pressure in the water storage tank, it is expected that the check valve should have no influence on the peak pressure developed by the noncondensable gas-water waterhammer events, regardless of the highpoint configuration.

This is clearly illustrated by the comparison of tests with and without a check valve shown in Figures 5-13 and 5-14 that show the measured water flow rates and waterhammer pressures for these two tests respectively. The initial conditions for these tests were (1) the full length high point, (2) a two liter water volume drained to establish the initial gas volume and (3) and an initial gas pressure

Figure 5-9: Comparison of peak gas-water waterhammer pressures for flushed and non-flushed systems.

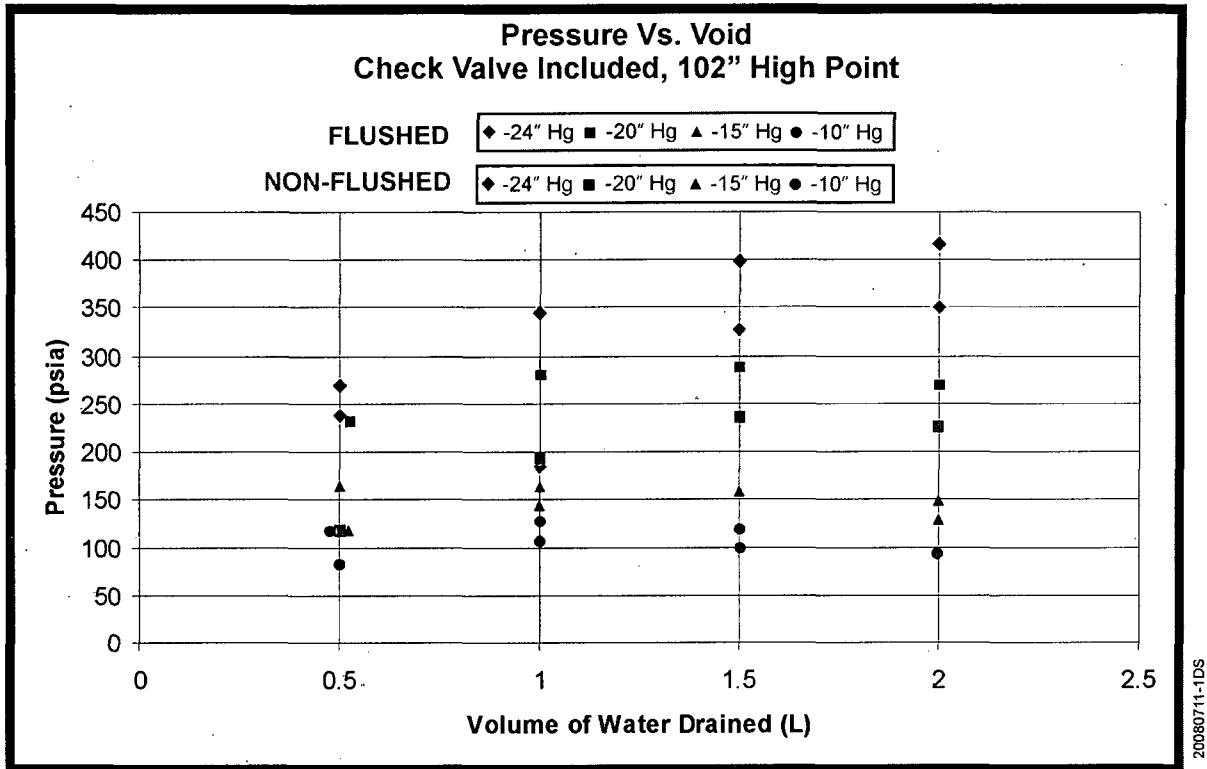


Figure 5-10: Response of a check valve to a downstream gas-water waterhammer event.

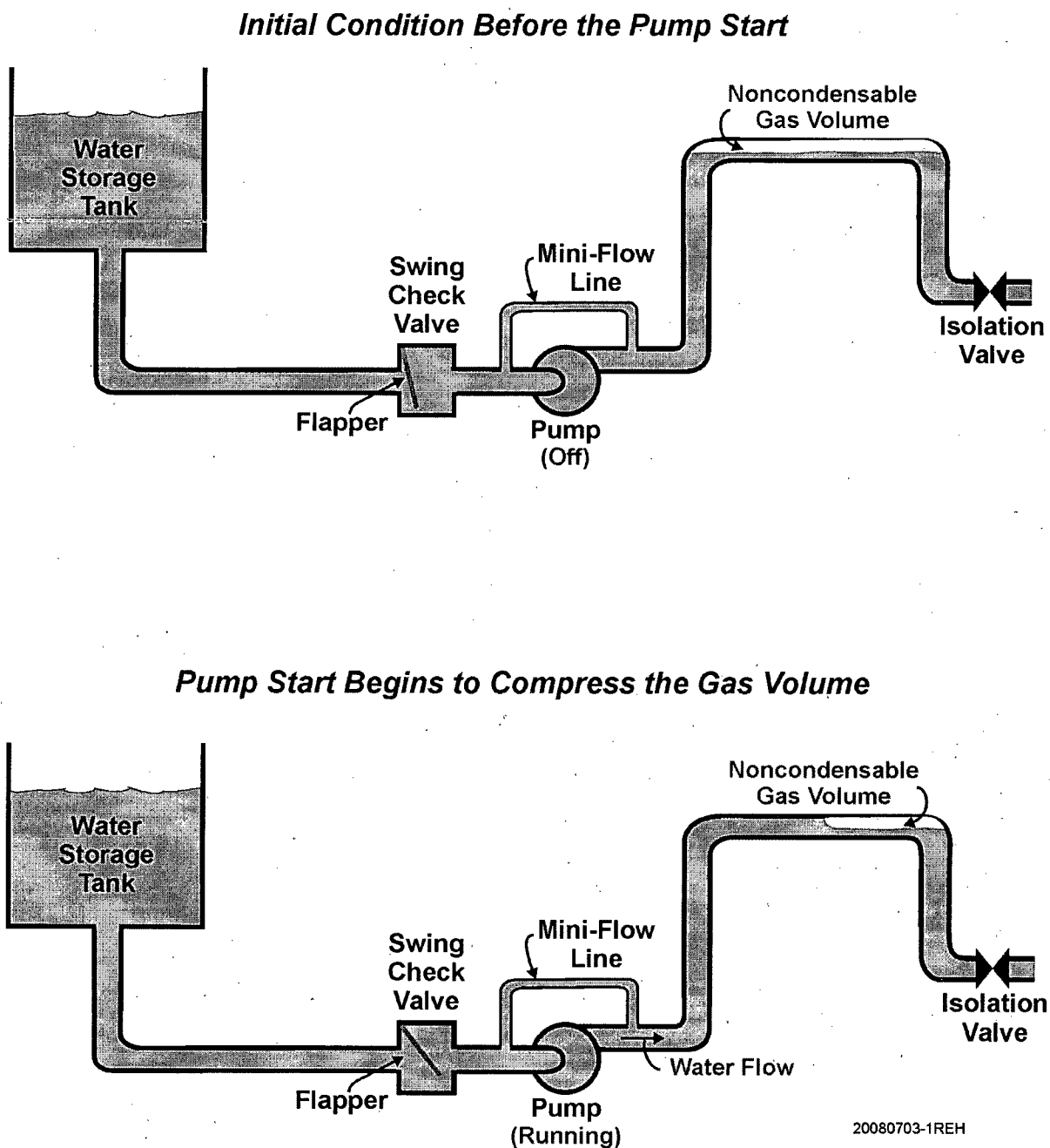
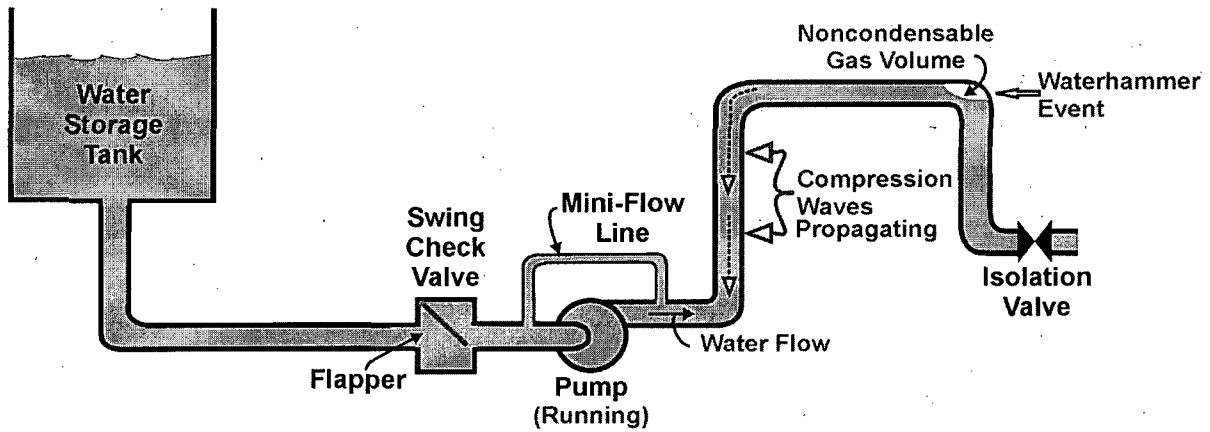
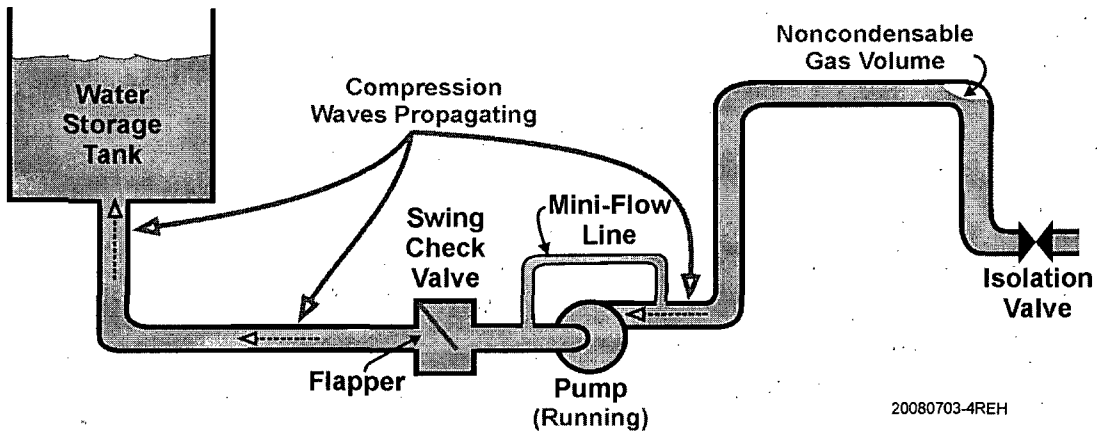


Figure 5-11: Response of a check valve to a downstream gas-water waterhammer event.

Gas-Water Waterhammer Event Occurs With a Rise Time of the Order of 100 Milliseconds



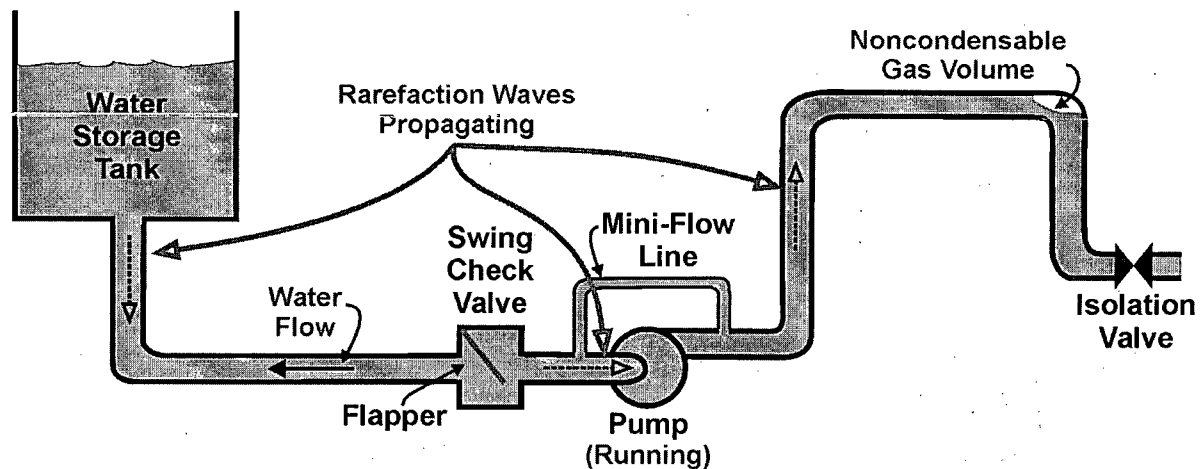
Compression Waves Stagnate the Flow and Propagate to the Free Surface in the Water Storage Tank



20080703-4REH

Figure 5-12: Response of a check valve to a downstream gas-water waterhammer event.

Rarefaction Waves are Reflected from the Water Storage Tank and the Water Flow is Reversed



With the Flow Reversed for a Few Hundred Milliseconds, Check Valve Slam Will Occur and Cause a Waterhammer With a Rise Time of the Order of 10 Milliseconds

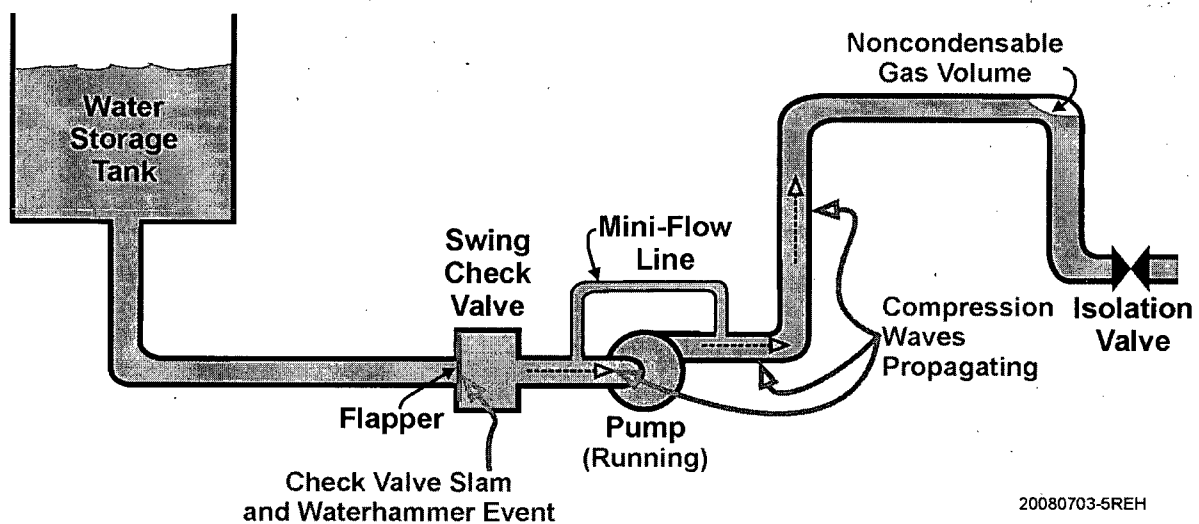


Figure 5-13: Comparisons of the measured water flow rates for the tests in the full length highpoint with (blue), and without (red), a swing check valve installed.

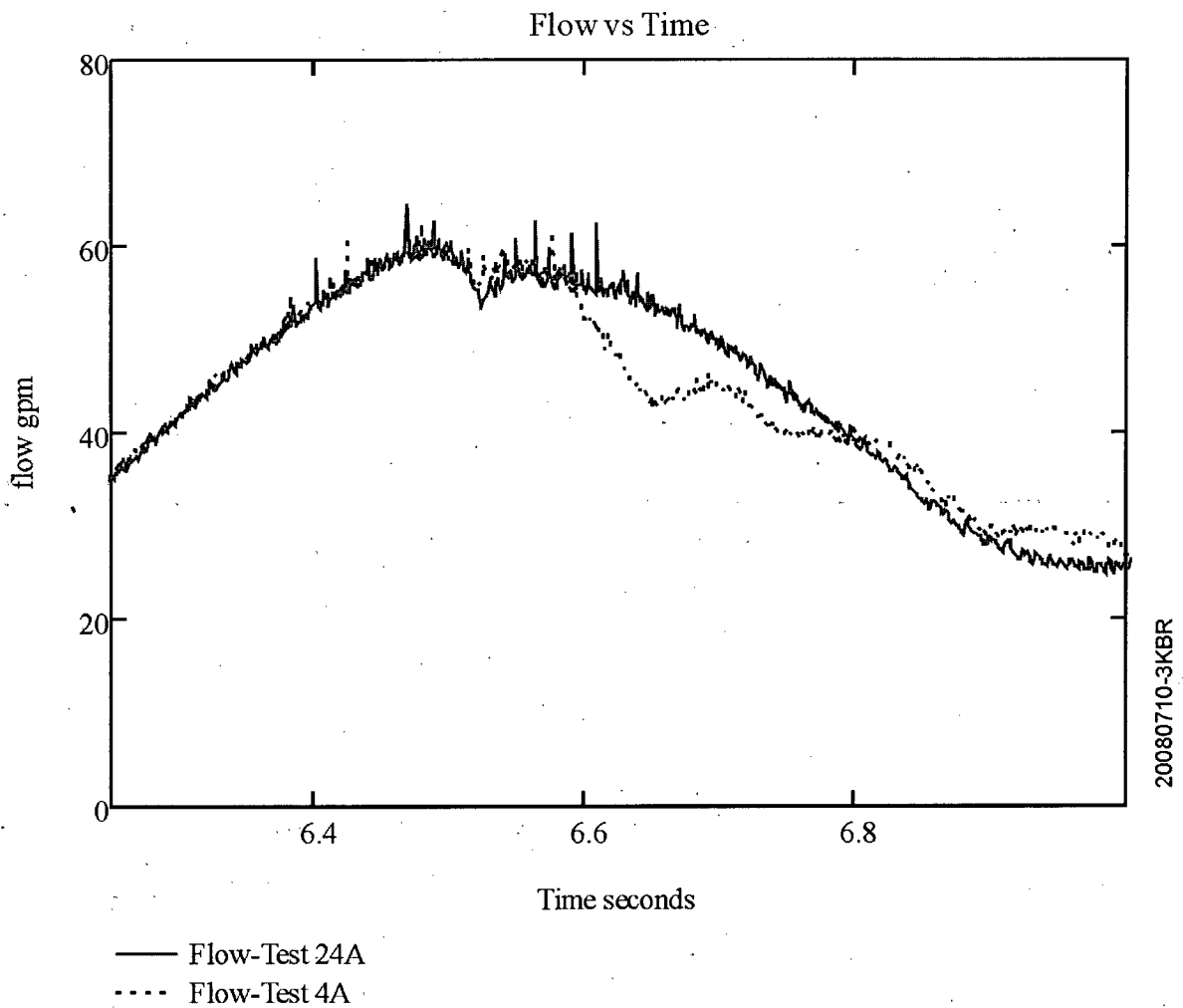
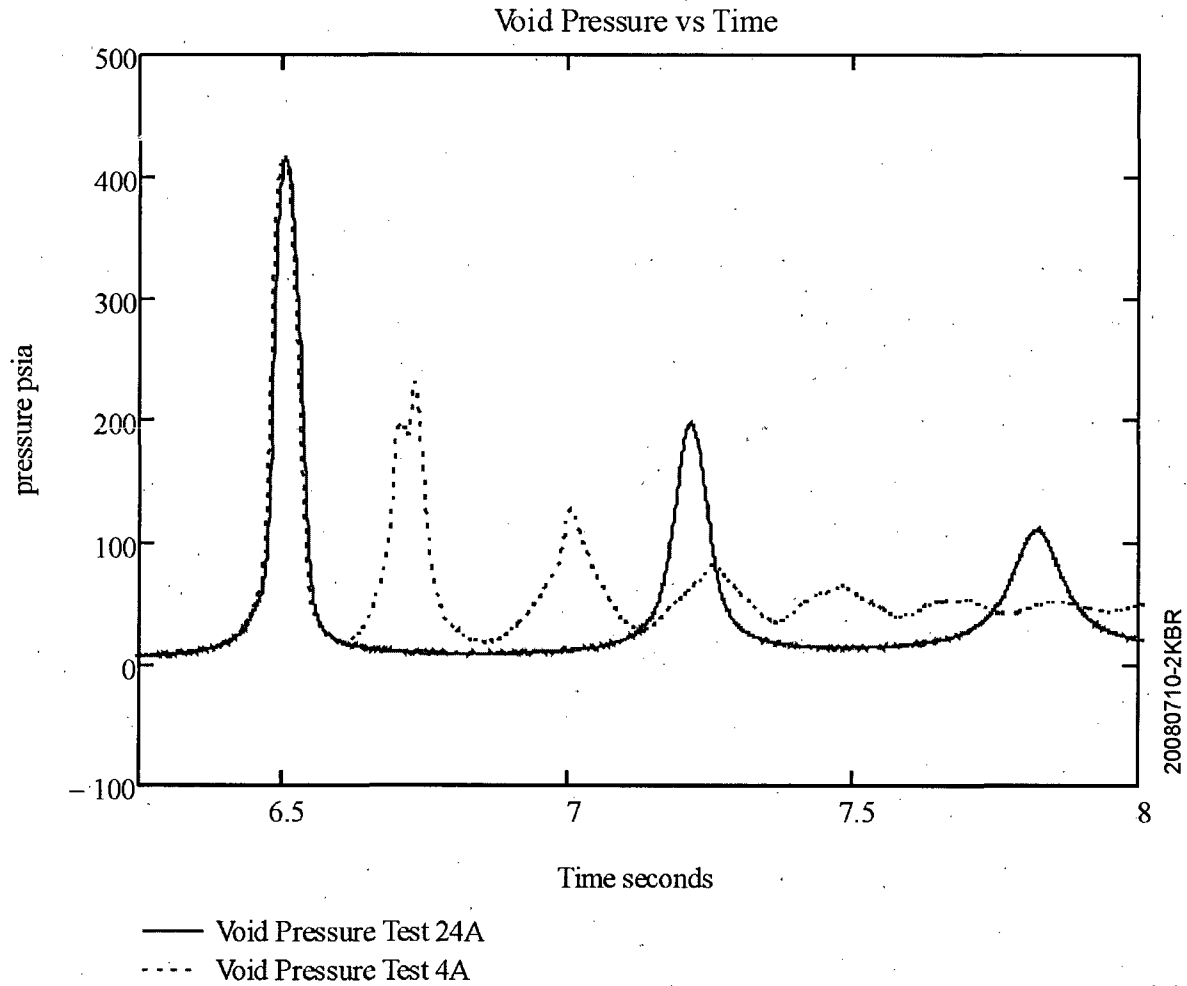


Figure 5-14: Comparisons of the measured air-water pressure histories for the tests in the full length highpoint with (blue), and without (red), a swing check valve installed.

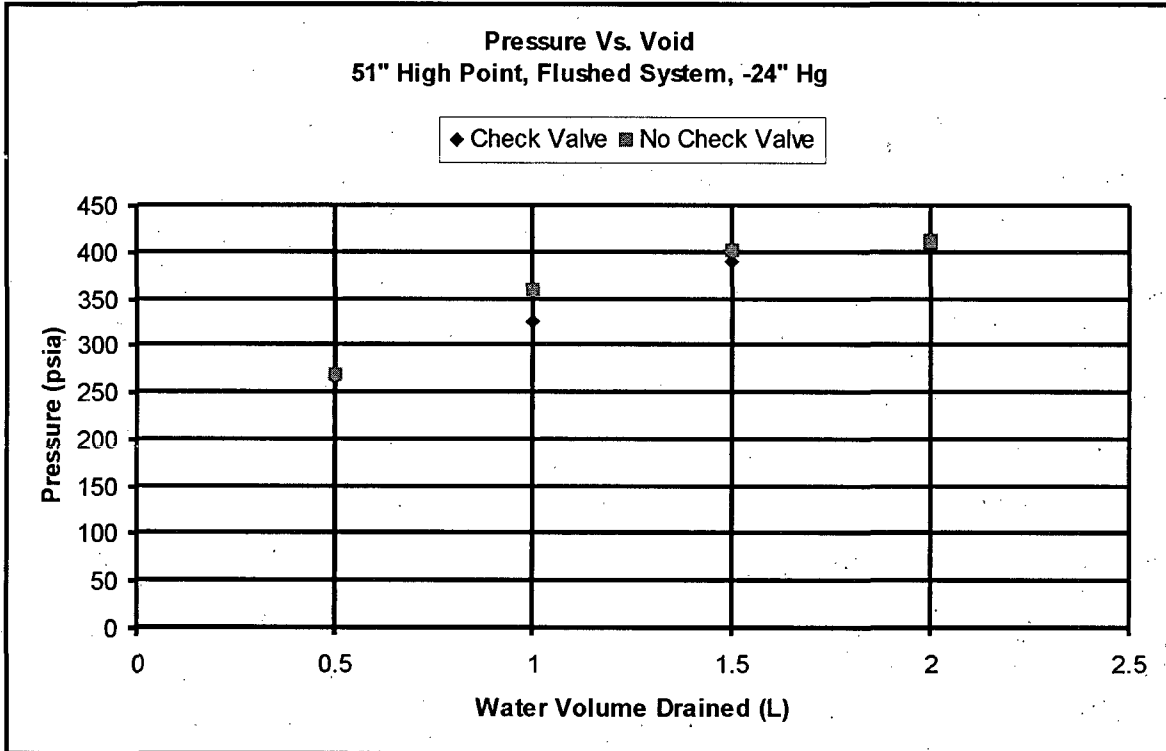


of -24 inches of Hg, i.e. an absolute pressure of about 2.5 psia (17,241 Pa). As shown by these two figures, the pressures overlay perfectly during the gas-water waterhammer event (the first pressurization), which also produces the peak pressure during the transient. As would be expected with this good agreement, the measured water flow rates are also in excellent agreement until the waterhammer event occurs at about 6.5 seconds following the start of the data acquisition. (As discussed in Section 3, the output of the turbine is only reliable up to the time of the waterhammer event and it is not used thereafter.) Figure 5-14 also shows that the transient pressure histories differ substantially after the first pressurization event which is due to the check valve preventing reverse flow towards the water storage tank. How the presence of the check valve influences the measured axial force imbalance on the highpoint piping will be discussed later.

With this background, Figures 5-15 compares the measured peak waterhammer pressures for tests performed with, and without, a swing check valve in the system for the 51 inch long highpoint and an initial pressure of -24 inches of Hg. These tests were all conducted using the high Froude number flushing process to establish a well controlled initial condition with void volumes ranging from 0.5 to 2.0 liters, i.e. initial void fractions from 0.2 to 0.8. As illustrated, there is no significant influence of the check valve on the measured peak pressure in the noncondensable gas-water waterhammer event.

Similar tests were performed with the same initial gas volumes and pressures but with the system not exposed to the flushing condition. As previously noted, this resulted in the initial gas volume being somewhat distributed within the piping system. Nonetheless, except for the smallest water drained, this is a small part of the gas volume. Consequently, this is not a major influence on the peak pressure as illustrated for all of the highpoints in Figure 5-9. These show that the peak pressures are bounded by those observed when the flushing is used as the initial condition. This was also observed for all of the initial conditions and highpoint configurations investigated.

Figure 5-15: Comparisons of the measured peak waterhammer pressure for the 51" long highpoint as a function of whether the test apparatus includes a swing check valve.

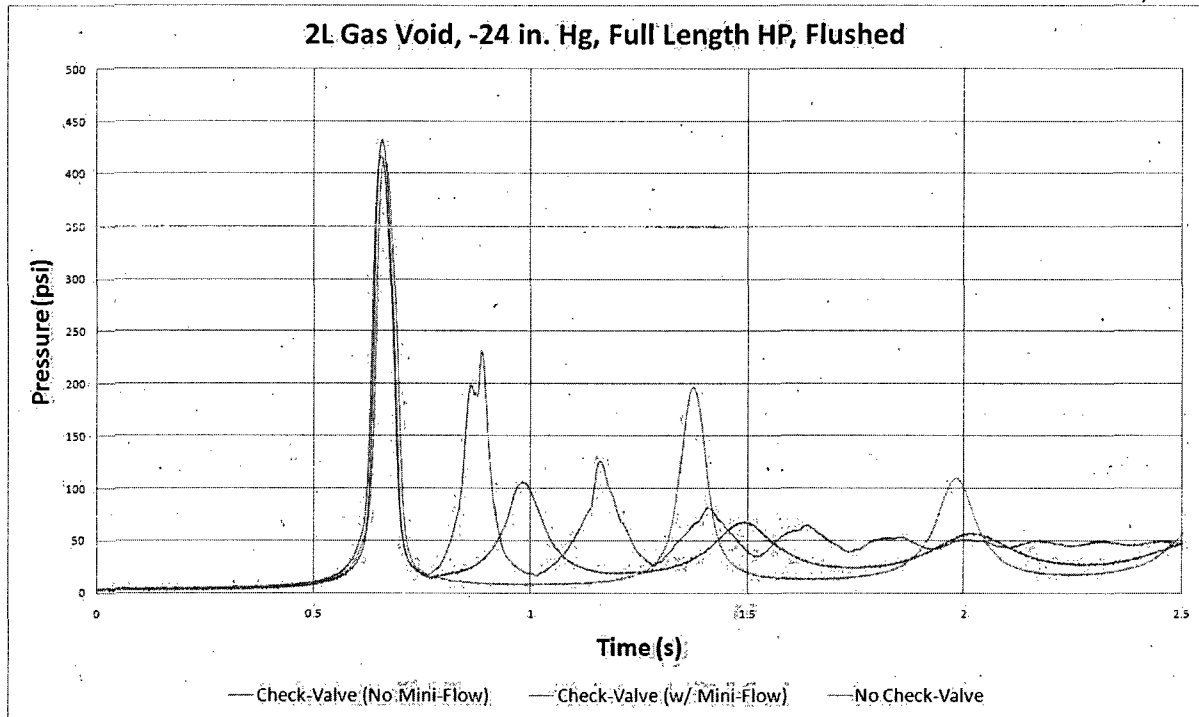


5.2.3 Influence of the Mini Flow Line on the Peak Waterhammer Pressure

All tests including the mini flow line were conducted using the high Froude number flushing process to establish a well controlled initial condition with void volumes ranging from 0.5 to 2.0 liters. The mini flow line was initially isolated by a solenoid valve. During the individual tests, the isolation valve was opened on the same signal as the fast ball valve, i.e. at the pump start. The mini flow line then returned a volumetric flow rate to the water supply tank according to the development of the flow in this line as the pump run-up progressed with the maximum flow rate being approximately 5gpm at the full pump flow rate. Therefore, the transient flow rate at the piping highpoint may be slightly reduced. The flow meter is located upstream of the pump and was observed to record a slightly higher flow rate because the flow resistance is somewhat lower i.e. the pipeline is not "dead ended" downstream of the pump compared to the setup without a mini flow line. The length of the mini flow line is 118" resulting in a total system length (from the bottom of the water supply tank, via the mini flow line, to the end of the highpoint) of 1142". Therefore, the mini flow line provides a smaller, but shorter acoustic pathway in the piping system. As a result, the frequency of the subsequent pressurization events may be higher, but because the mini-flow line is well removed from the location of the gas-water waterhammer, no significant change in the pressure increase is for the initial waterhammer event.

Figure 5-16 shows the pressure history for three tests with equal initial conditions. One can see that the frequencies of the pressure peaks for the tests with a check valve or a mini flow line are higher which is expected since the system is, in the overall sense, shorter. As expected, the magnitude of the first pressure peak is essentially the same for all tests. It is notable is that the subsequent pressure peaks decay faster for tests performed with a check valve or a check valve plus mini flow line.

Figure 5-16: Pressure versus time - comparison for mini flow line tests.

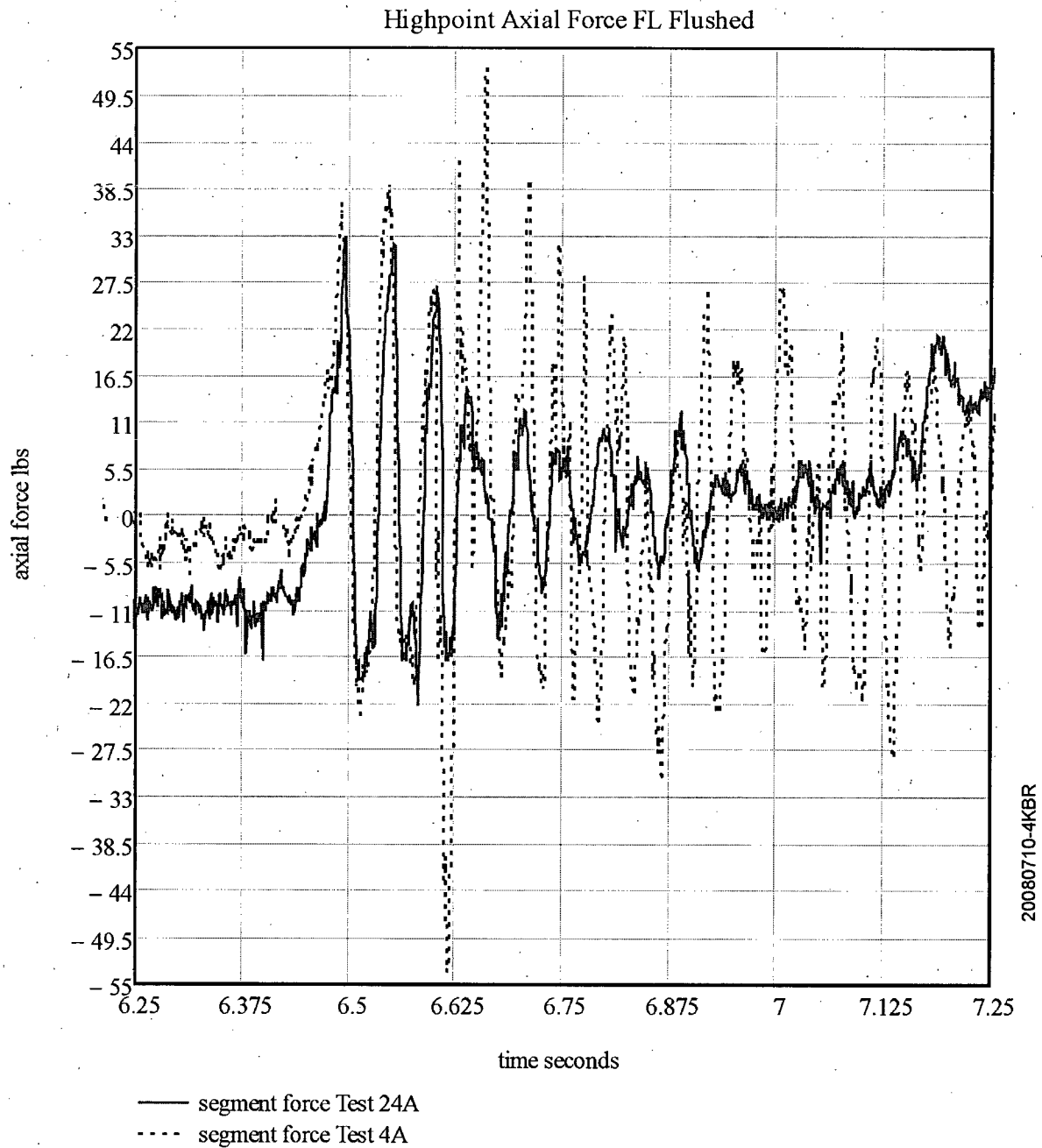


5.3 Axial Forces Generated on the Piping by the Waterhammer Event

While the internal pressures produced by a gas-water waterhammer event are, in general, not sufficient to challenge the piping integrity, the axial forces generated by the pressure differences caused by the event, as well as the subsequent hydraulic response can be sufficient to shake the piping and potentially cause damage to the piping restraints and supports. As noted in Section 1, steam-water waterhammer piping loads have been evaluated (Van Duyne and Merilo, 1996) using the product of the waterhammer pressure increase (Joukowsky/waterhammer equation) and the pipe cross-sectional area. As we will see through some examples below, this is a very conservative approach to evaluating the axial forces produced by noncondensable gas-water events, in fact, in general it is too conservative to be of practical use for noncondensable gas-water waterhammer events. Nonetheless, it is a conservative representation of the force developed and if the piping restraints and supports are sufficient to cope with this calculated force, no further evaluation would be needed.

In contrast to the assumed instantaneous loading represented by the use of the waterhammer equation (Joukowsky-Frizell equation) in this manner, the rise times of noncondensable gas-water waterhammer events are typically an order of magnitude longer than those of steam-water waterhammer events. Hence, the response of the piping is more related to the integral response of the entire system. This is effectively illustrated by revisiting the comparison of tests with, and without, a check valve installed for a full length highpoint test that was discussed previously in this section with respect to the measured flow rate and pressurization histories. In a similar manner Figure 5-17 compares the measured axial force histories for the highpoint with, and without, the check valve installed. For the initial conditions of -24 inches Hg (2.5 psia) gas pressure and 2 liters drained to produce the gas volume, the measured waterhammer pressure was about 400 psia. With a cross-sectional flow area of $3.355 \text{ in}^2 / 0.02330 \text{ ft}^2$ (2 inch Schedule 40 pipe (Crane, 1976)), the product of the waterhammer pressure and the flow area yields a force of 1342 lbf, which two orders of magnitude greater than the measured value for the waterhammer event of about 38.5 lbf. As discussed in Appendix A, the force measurement is influenced by the response of the supporting structures for the test facility. Therefore, while the measured response may differ somewhat from the

Figure 5-17: Comparison of the measured axial forces histories for the 102" length highpoint with, and without a swing check valve installed.



hydraulic forces imposed on the pipe and only provide a general representation of these forces, the measured values are generally within a factor of two of the imposed hydraulic forces and are certainly of the same order of magnitude. Moreover, the measured peak force for a given test can be used to estimate the effective pressure differential that would produce this value. Dividing the maximum measured force by the flow area, results in a pressure difference across the full length highpoint pipe of approximately 12 psi, i.e. an order of magnitude less than the maximum waterhammer pressure of 400 psia. This simple calculation illustrates the extent of the conservatism introduced when using the product of the waterhammer equation and the pipe flow area. As noted previously, this large conservatism is due to the long rise time for noncondensable gas-water events compared to the interval for the pressurization event to be propagated along the length of the highpoint pipe. In other words, the only time that the total pressure increase calculated by the waterhammer should be used is when the rise time is so fast that the entire pressurization occurs before the wave can propagate to the other end of the highpoint piping.

To assess the maximum hydraulic forces imposed on the pipe by the waterhammer event, we must formulate an approximate means of evaluating the pressurization rate that was generated for the individual experiments. As illustrated by the pressure histories shown above for tests 4A and 24A, the initial part of the pressurization is comparatively slow and, as expected, the most rapid rate of pressurization occurs when the gas volume is compressed the most. To approximate this rapid rate of rise, reference pressure was selected that is greater than the pump shutoff head but considerably less than the waterhammer pressure. This is only a reference value used to (a) assess the hydraulic forces developed in these tests and (b) compare the calculated forces with the recorded values from the load cell. For this interpretation a reference pressure of 100 psi was used and the corresponding rate of pressure increase is then given by:

$$(dP/dt)_R = [P_{\max} - 100]/[t_{\max} - t_{100}] \quad (5-2)$$

where:

- P_{\max} is the maximum pressure (psia) during the noncondensable gas-water waterhammer,
- t_{\max} is the time that this maximum pressure occurs and

- t_{100} is the time that the increasing pressure passed through 100 psia.

Using this definition, we analyzed the measured results for the various highpoint configurations and initial conditions in the test matrix. Figures 5-18, 5-19 and 5-20 illustrate the calculated reference pressurization rates for the full length and half length test configurations for initial gas volume pressures of -15, -20 and -24 inches of Hg respectively. These figures show the very close agreement of the calculated reference pressurization rates when the values for the two highpoint lengths are compared as a function of the initial gas volume (water volume drained). Two other important facets of these comparisons are: (1) the decreasing values of the pressurization rates as the initial gas volume increases and (2) the observation of a maximum value of the rate as a function of initial gas volume. This latter point is clearly seen in Figure 5-19 for the initial pressure of -20 inches Hg with the maximum value in Figure 5-18 being at an initial volume less than 0.5 liters and for an initial volume greater than 2 liters for an initial gas pressure of -24 inches Hg.

With this reference pressurization rate, we can estimate the maximum axial force acting on the highpoint piping segment from the expression:

$$F = A_p (dP/dt)_R t_c \quad (5-3)$$

where:

$$t_c = L_{HP}/C_w \quad (5-4)$$

In this expression, A_p is the cross-sectional flow area, which for a 2 inch Schedule 40 pipe is 3.355 in². For the peak pressures accompanying the measured forces shown in Figure 5-17, tests were conducted with initial gas pressures and volumes of -24 inches Hg and 2 liters respectively. From Figure 5-20 we see that the reference pressurization is 9800 psi/sec. Using this rate along with the test length of 102" (8.5 ft) and a water sonic velocity of 4500 ft/sec a force of 62.1 lbf is calculated as compared to the measured value of 38.5 lbf. While the calculated value somewhat overstates the measured maximum force, the measured force is mitigated by the response of the supporting

Figure 5-18: Comparison of the calculated reference pressurization rates for the full and half length highpoint segments with an initial gas pressure of -15 inches Hg.

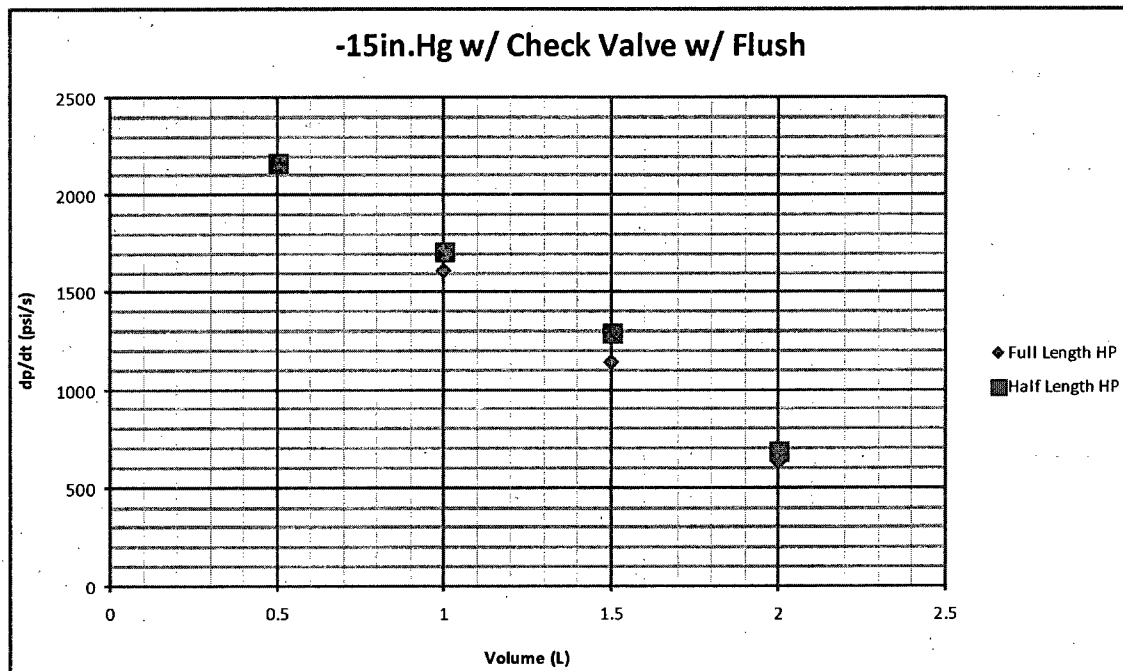


Figure 5-19: Comparison of the calculated reference pressurization rates for the full and half length highpoint segments with an initial gas pressure of -20 inches Hg.

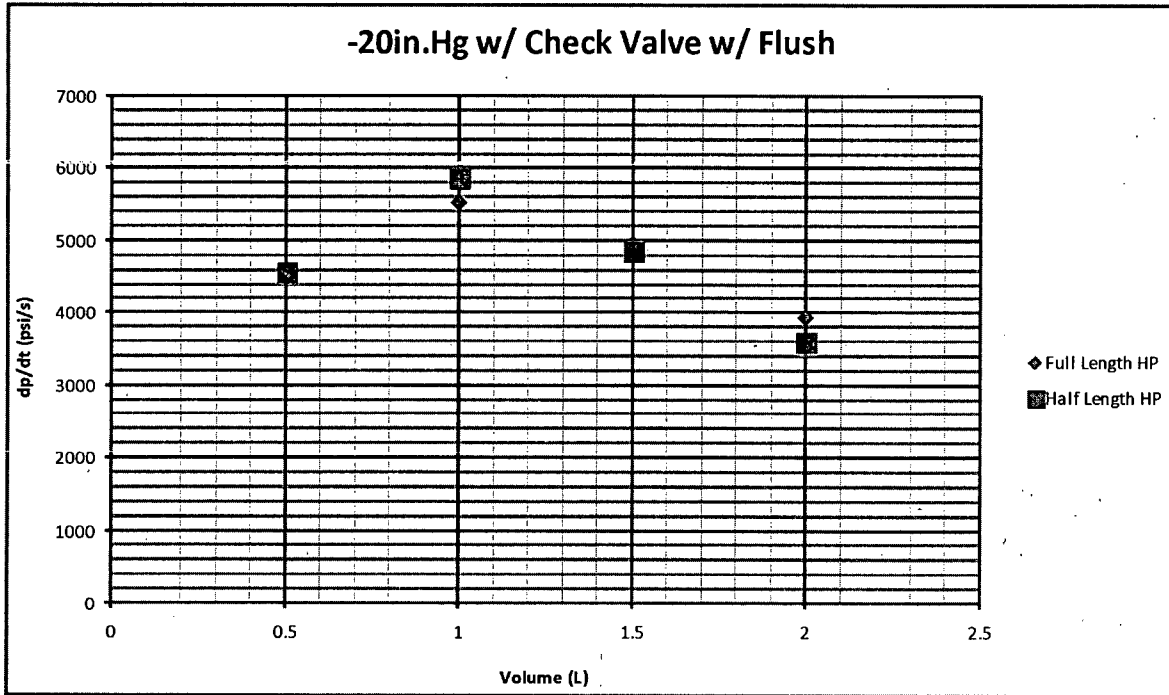
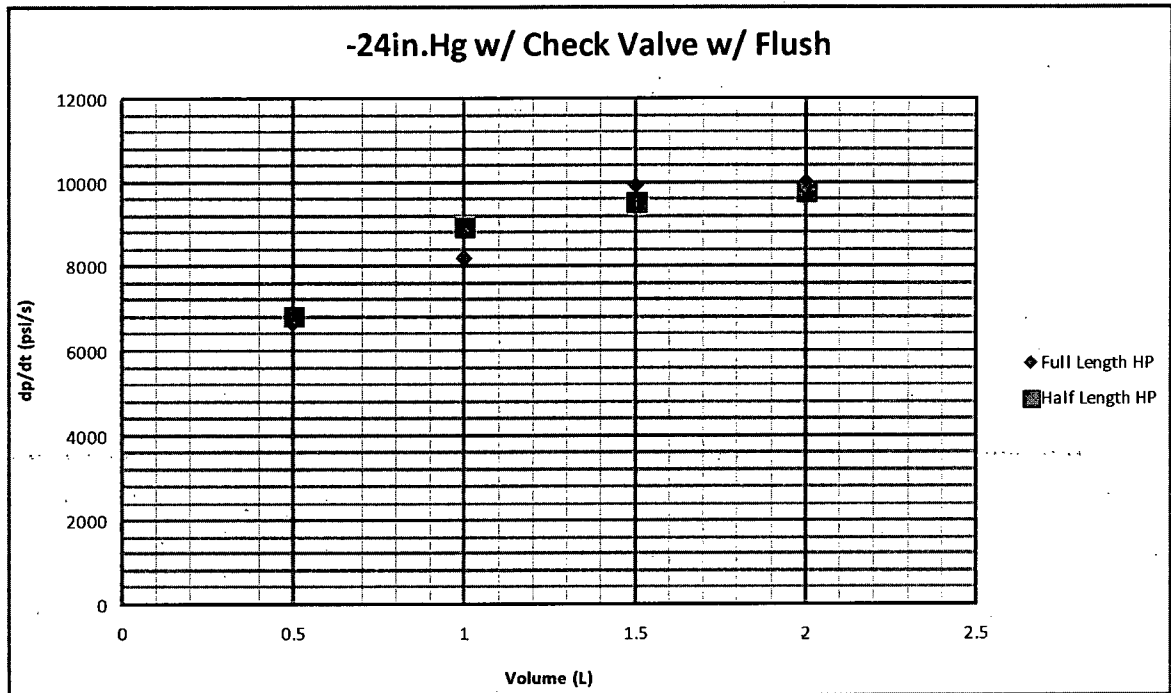


Figure 5-20 Comparison of the calculated reference pressurization rates for the full and half length highpoint segments with an initial gas pressure of -24 inches Hg.



structure as discussed in Appendix A. Of particular importance, the force calculated using the reference pressurization rate provides a conservative representation of the measured value and it is representative of the hydraulic pressure force imposed on the piping.

Considering the agreement of the calculated reference pressurization rates for the two different length highpoint configurations and the conservative representation of the measured force on the piping system, the reference pressurization rate is a technique that can be used to estimate the forces that could be imposed on the piping for a given plant set of conditions. This is discussed further in the Section 6.

5.4 Axial Forces Generated on the Piping by the Check Valve Slam

Returning to Figure 5-17 we observe the expected behavior that the measured force histories are virtually identical for the first 100 msec, which is the response due to the gas-water waterhammer event, the water mass has been brought to rest. However, after this point in the hydraulic response the compressed water and gas begin to experience a reverse flow due to the rarefaction waves propagating from the water storage tank. Because one has a check valve, there is a significant departure in the two force histories that persists for the remainder of the flow transient. Specifically, a negative force, comparable in magnitude to the initial waterhammer force, is observed for the test with the swing check valve installed. This negative force occurs because the upstream end of the highpoint pipe has a higher pressure than the downstream end, which results from a compression wave, generated by the check valve slam, propagating from the check valve to the highpoint piping segment. As noted above, this check valve slam results from the rarefaction (depressurization) waves reflected from the water storage tank eventually reversing the water flow and causing the flapper in the swing check valve to close rapidly ("slam"). Such a rapid closure stagnates the water immediately downstream (toward the highpoint) of the valve flapper and the corresponding waterhammer pressure increase needed to bring the water velocity to zero (stagnating the flow) propagates toward the highpoint. (This pressure increase is described by the waterhammer equation with the water velocity being the reversed flow velocity to which the flow was accelerated by the rarefaction waves at the time that the check valve closes.) Note that because this reversed flow

velocity is only that which can be developed as the check valve flapper is moving toward closure, it is related to the integral of the velocity in the reversed direction. Therefore, it is smaller in magnitude than the water velocity that caused the gas-water waterhammer, which is related to the integral of the volume of water pumped during the pump run-up interval. Hence, as noted previously when comparing the test results with, and without a check valve in the flow path (Figure 5-14), the measured peak pressure following the check valve slam is considerably less than the maximum pressure generated by the noncondensable gas-water waterhammer. We can reach a similar conclusion by considering that the nature of the reverse flow is to reduce the pressure in the compressed gas bubble (volume) and as a result, the combination of the gas depressurization and the smaller water velocity that generates a waterhammer when the check valve closes causes the pressure increase to be less than that experienced by the gas-water waterhammer. Lastly, it is noted that this considerably smaller pressure increase for the check valve closure was observed in every experiment performed with the check valve in the flow path.

However, as discussed above, the force imbalance imposed on the piping segments is a function of the rate of the pressure increase and not of the magnitude of the system pressure. Therefore, if the final closure of the check valve generates a rate of pressure increase that is greater than that produced by the relatively slow gas-water waterhammer event, the piping loads resulting from the check valve slam can be greater than those produced by the gas-water waterhammer. Consulting the check valve data in the literature, we find that the swing check valves have been observed to generate pressurization events with rise times of the order of 10 msec (Thorley, 1983), which is an order of magnitude faster than those observed in the data taken in this study. This more rapid closure interval causes the measured force associated with this 2nd event (check valve slam) to be higher than that generated by the original waterhammer event.

While the force is somewhat larger, it is the impulse that represents the energy delivered to the piping segment. Therefore, integral of the force versus time needs to be compared.

5.5 Influence of Mini Flow Line on Axial Forces

Previous tests, without the simulation of a mini-flow line, have shown that the check valve slam is capable of generating force imbalances on the instrumented highpoint that exceeds those produced by the initial waterhammer event and tend to move the highpoint in opposite direction compared to the gas-water waterhammer. Simulation of the mini-flow line creates a second path to partially relieve the compression wave caused by stopping the water column as the check valve closes. This second path acts to mitigate the consequences of the valve slam. This is best illustrated by the comparisons given in Figure 5-21 and 5-22. Note that the force imbalances that arise from the gas-water waterhammer (those that occur between 0.6 and 0.7 seconds) are essentially unaffected by the presence of the mini-flow line. At about 0.7 seconds check valve slam occurs and the propagation to the highpoint causes a force in the reverse direction (herein referred to as a tensile force since it tends to unload the load cell). These two figures show that the presence of the mini-flow line reduces the magnitude of the force imbalance to a value that is approximately equal to the maximum generated by the gas-water waterhammer. Perhaps equally important is the observation that it acts to quickly dampen the subsequent oscillations.

Figures 5-23 and 5-24 compare the measured force imbalance for tests with a check valve with tests with a check valve plus a mini flow line at equivalent initial conditions. Figure 5-23 shows the forces that are induced by the gas-water waterhammer event and it is seen that: (a) the values are very close and (b) those tests taken with the mini-flow line open have slightly lower peak forces. An explanation for this might be a slightly lower flow toward the gas bubble and therefore less momentum to be stagnated at the highpoint. Figure 5-24 compares the tensile force imbalances (those force direction that is opposite to that generated by the initial waterhammer) that are produced by the check-valve slam. We observe that the forces generated by the check valve slam are substantially mitigated by the presence of the open mini-flow line. For the test with void volumes of 1 liter or greater the forces were reduced to one-half of those observed with the mini-flow line closed. This resulted in the maximum check valve forces being about the same as those generated by the gas-water waterhammer but in the opposite direction. In addition, during the course of the tests the test personnel reported a less powerful audible response from the check valve and piping.

Figure 5-21: Comparison of the highpoint force imbalance measured for a 2 Liter-gas volume with and without a mini-flow line.

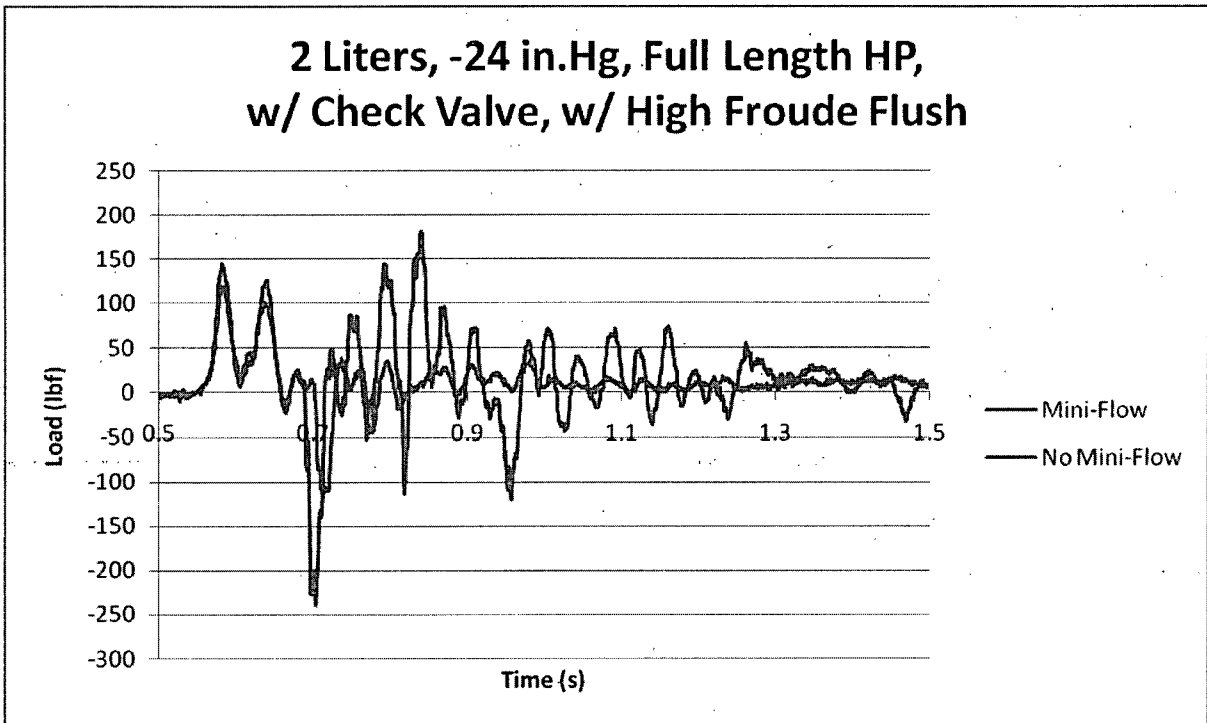


Figure 5-22: Comparison of the highpoint force imbalance measured for a 1 Liter gas volume with and without a mini-flow line.

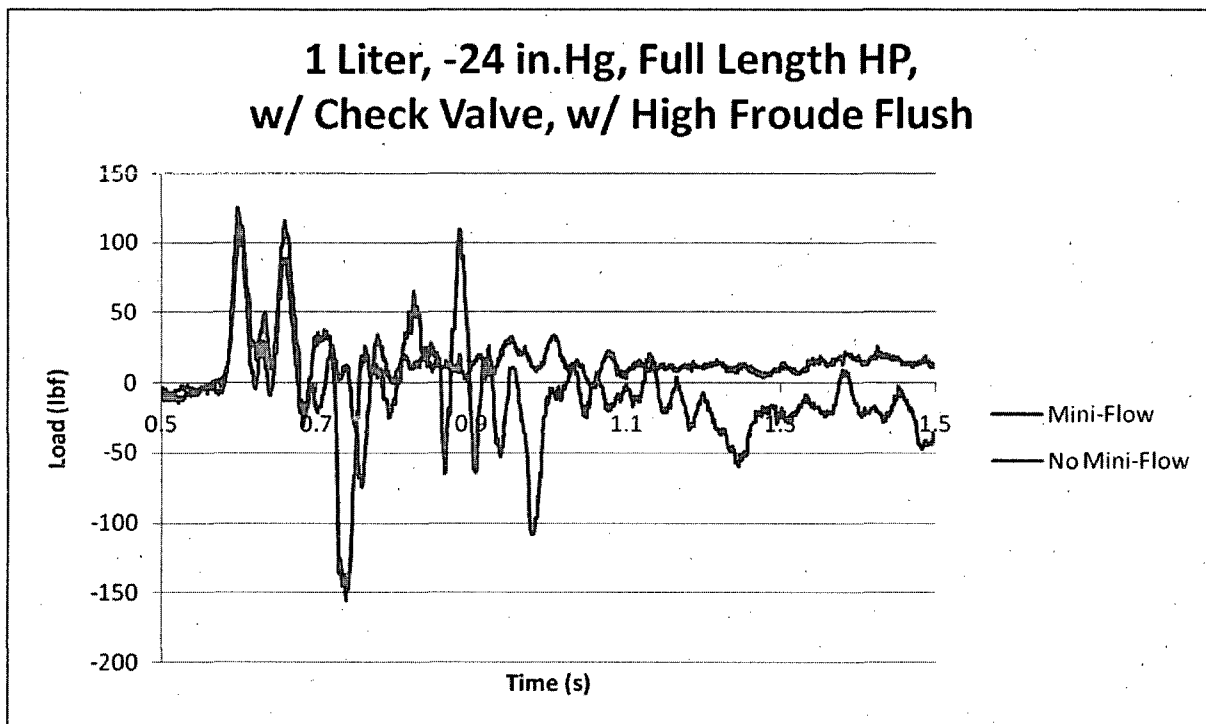


Figure 5-23: Force comparison for mini flow line tests.

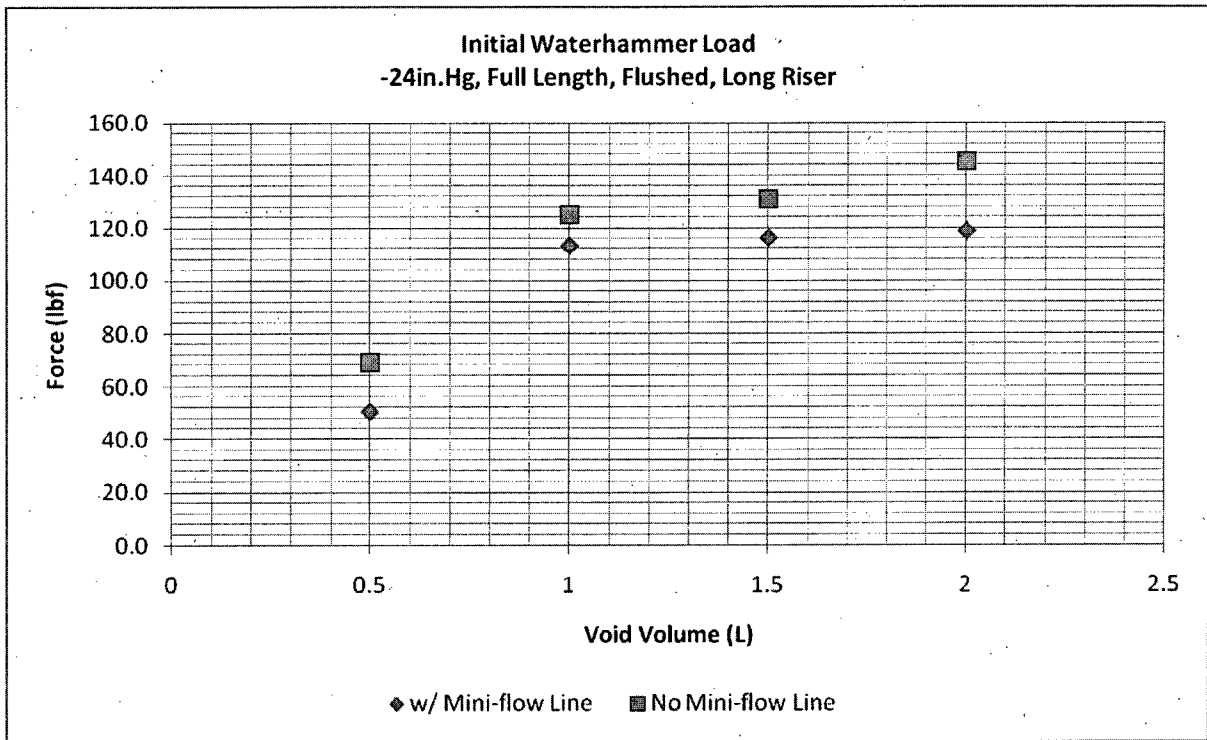
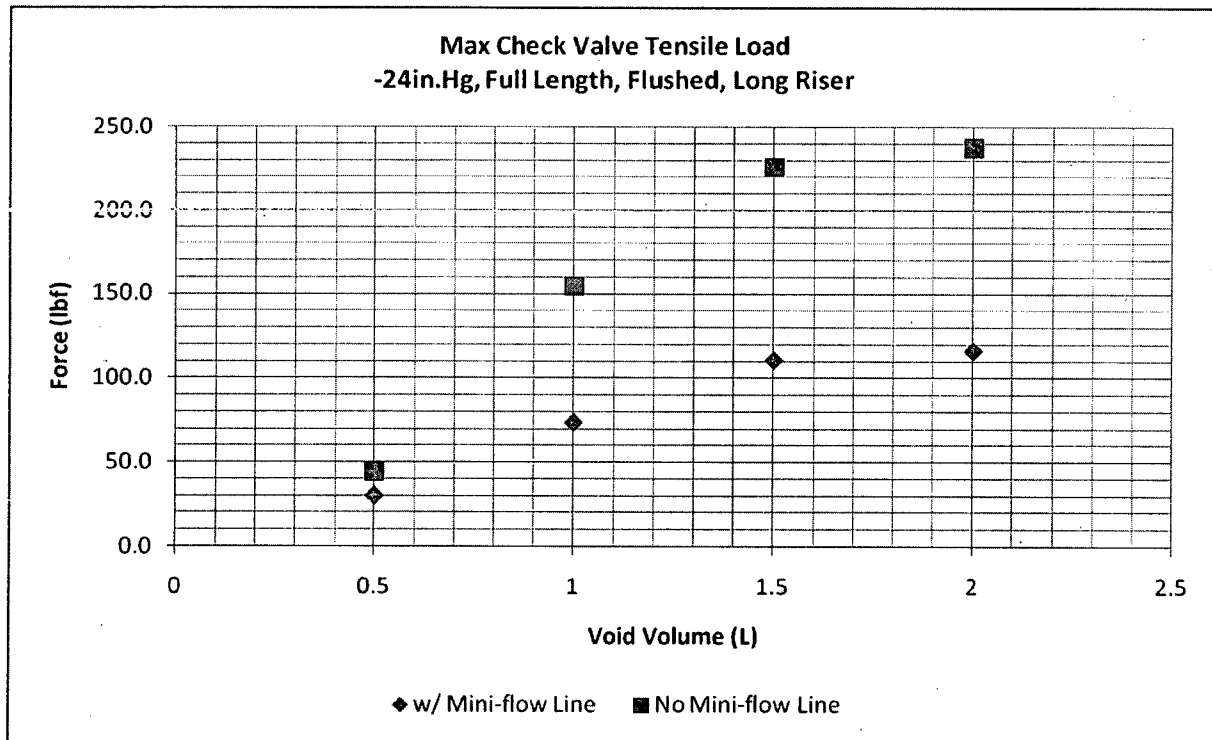


Figure 5-24: Force comparison for mini flow line tests.



5.6 Multiple Bubble Tests

A number of tests were performed in the test apparatus shown in Figure 3-5 to examine the influence of distributed gas volumes. These test conditions are listed in Table 4-1 and varied the gas volumes in the different highpoints between 0 and 1.5 liters for an initial gas pressure of -24 inches of Hg. The data for these tests are shown in Figure 5-25 and 5-26 for the influences on the maximum gas-water waterhammer pressure and the force imbalance on the half length highpoint respectively. With respect to the maximum pressure, the data show that the pressure is essentially the same when the data is evaluated on the basis of the total gas volume. This is particularly helpful to plant analyses where one of the important features to assess is the possibility that relief valves could be lifted by a gas-water waterhammer event. Specifically, this means that the simplified methodology can be used to conservatively estimate the peak pressure that could be developed.

Conversely, the measurements of the force imbalances generated in the multiple gas bubble tests (Figure C-3) show that the maximum force can be increased as compared to the force generated when a single bubble with the same total volume exists in the downstream highpoint. From this observation we conclude that if a multi-bubble configuration is known to exist, the evaluation of the force imbalance on the piping segments for that system should be assessed using a multiple bubble model.

Figure 5-26 clearly shows that the forces at the highpoint stay in the same range if only one bubble is present in the multiple highpoint configuration. However, for multiple bubble tests substantial forces were recorded. For example, for a total void volume of 1.5 L, where 0.5 L were drained from the quarter length high point, the resulting waterhammer force increased by a factor of seven compared to single high point tests. The reason for such a force increase could be that the two bubbles are oscillating out of phase which results in a greater force imbalance. We find a similar behavior for the tensile forces (reverse flow direction). As a result, we can say that if a piping system were to have multiple void volumes, the resulting forces can only be modeled with a single bubble model as long as there is one large void volume followed by very small other voids.

Figure 5-25: Comparison of the single and multiple highpoint measurements of the peak gas-water waterhammer pressure as a function of the gas volume distribution. (Variable Vg2 is the volume of water drained from the quarter length highpoint, i.e. 25.5 inches.)

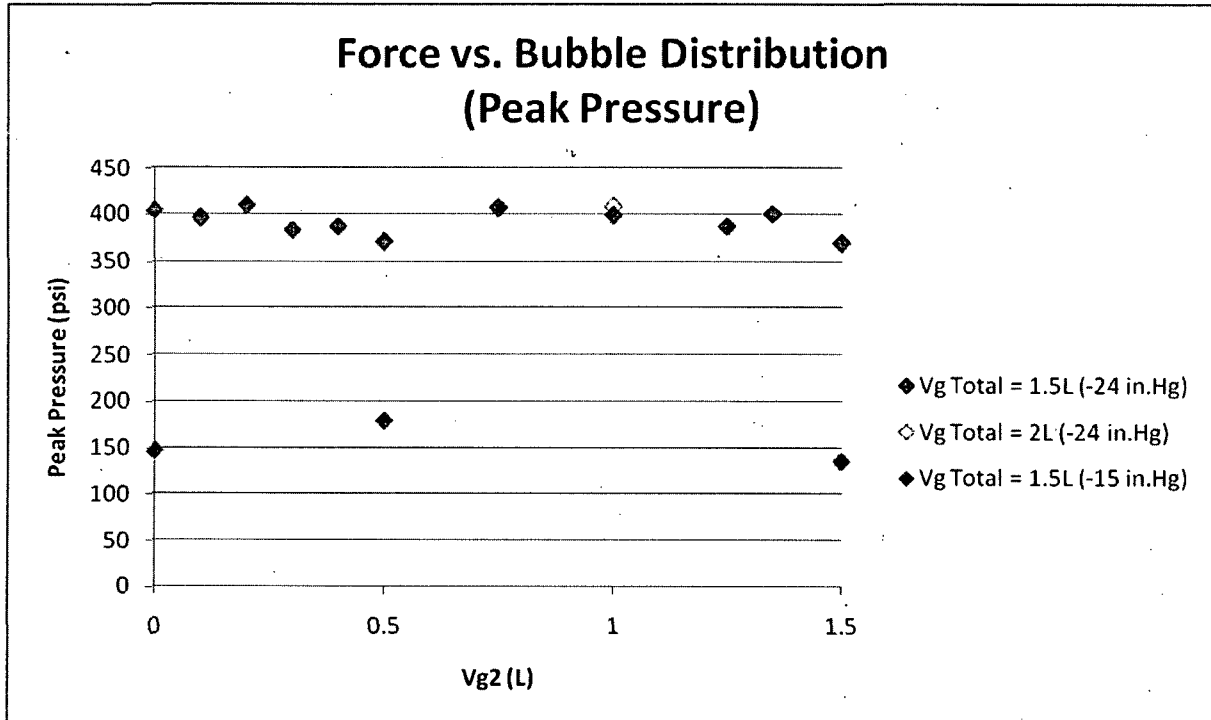
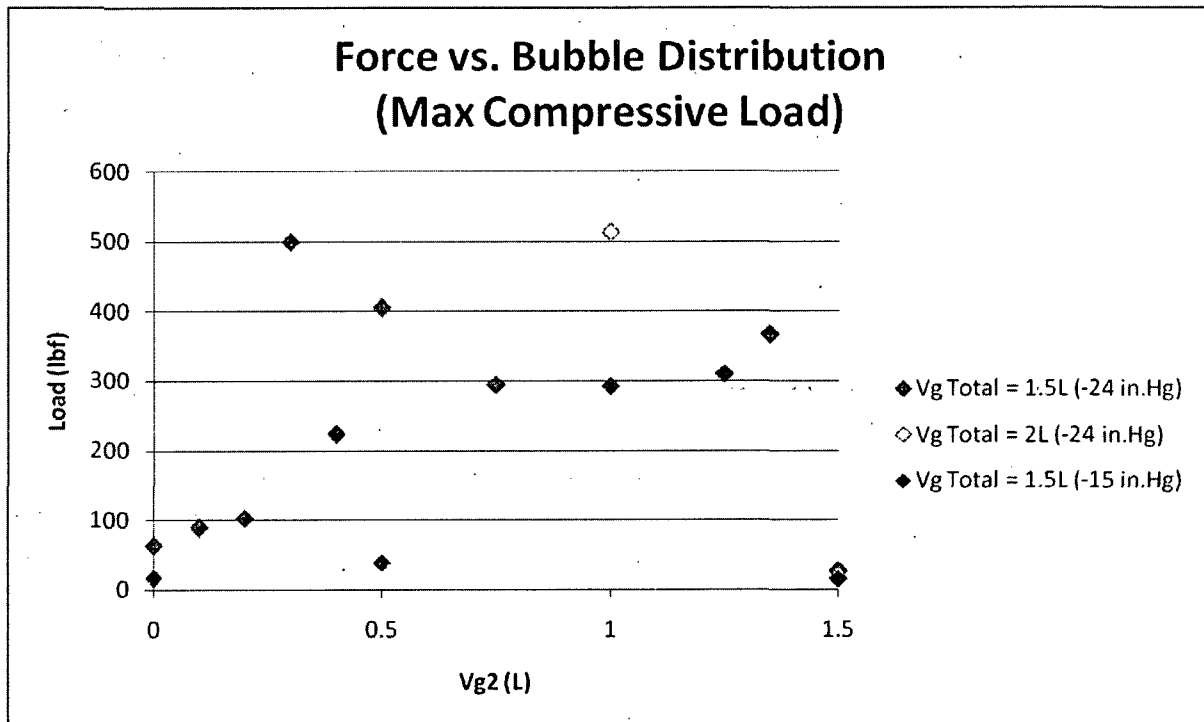


Figure 5-26: Comparison of the single and multiple highpoint measurements of the maximum compressive force as a function of the gas volume distribution.
(Variable Vg2 is the volume of water drained from the quarter length highpoint.)



6.0 APPLICATIONS TO PLANT EVALUATIONS

6.1 Cautions and Limitations in Plant Applications

Fundamentally, these experiments illustrate the relative importance of various aspects of system conditions and configurations that need to be assessed during plant specific evaluations. Specifically, these are: the volume of the gas bubble, the initial gas volume pressure, the flow run-up behavior, the length of the highpoint, the response of a check valve, the role of the min-flow line and the behavior of multiple highpoints. As part of this, simplified calculational tools have been developed to conservatively estimate the consequences of an accumulated gas volume in the piping given a flow transient. While the experimental data and the calculational tools all provide substantial insights, there are equally important cautions and limitations to be considered in the application of these insights. These are listed below.

1. One of the evaluations to be performed is the peak pressure developed by a gas-water waterhammer event since this pressure could be imposed on the system relief valve(s) and such an event could potentially result in causing a valve to lift and stick open. The peak pressure resulting from a gas-water waterhammer event is a function of the total gas volume available, the initial gas pressure and the flow run-up transient. The transients to be considered include the pump run-up as part of a pump surveillance test, the starting of an ECCS pump under LOCA conditions and the opening of a valve in the transition to RHR cooling. In addition, the considerations of a pump run-up transient need to include how the flow could be modified (limited) by flow balancing orifices if the accumulated gas volume is downstream of the balancing orifice(s). Each plant evaluation needs to carefully consider these sequences at a minimum and represent the flow run-up transient for each.
2. The test data clearly shows that the presence of a check valve does not influence the peak pressure and the force imbalances generated by the gas-water waterhammer event itself. However, the subsequent rapid closure of the check valve does introduce a second waterhammer transient that has a lower peak pressure but a faster rate of rise. With this faster

pressurization rate, the magnitude of the force imbalances can be increased. The test data also demonstrate that the presence of an open mini-flow line substantially mitigate the increased force imbalances by bleeding off some of the imposed water flow rate and slowing the rate of the pressure rise. It is conservative to not represent the influence of the mini-flow line but this may also overstate the peak force imbalances developed by a factor of three to five.

3. Perhaps the most interesting data reported is that taken with two highpoints and gas volumes in each. These data show that the peak gas-water waterhammer pressure is determined by the total gas volume given the same initial gas pressure and flow run-up transient. Therefore, when assessing the potential for lifting the system relief valve(s), the total gas volume needs to be considered. However, the data also demonstrate that the force imbalances on a specific highpoint can be increased due to the out-of-phase oscillations of the two gas volumes. Therefore, if the force imbalances are to be evaluated for a condition of multiple gas volumes accumulated, then the simplified methodology should not be used and the calculation should be performed using a multiple bubble model.
4. This simplified is intended to provide a means to conservatively estimate the loads on the piping due these relatively slow waterhammer events. If the calculated values are sufficient to possibly challenge the success criteria for the piping supports, then a more detailed piping system calculation should be performed. Also, these conservatively estimated forces should only be used to develop criteria for determining the size of accumulated gas volumes that would not challenge the functionality of the pumping system. They should not be used to develop design basis force-time histories for these piping systems.
5. The simplified methodology to estimate the maximum force imbalances acting on piping segments will conservatively estimate these force imbalances but should not be used to develop force-time histories as inputs to a detailed model of the piping system and the supports/restraints.

6.2 Evaluation of Sufficient Conditions to "Washout" a Gas Volume

For some systems the operating conditions can lead to water velocities that are sufficient to remove (washout) an accumulated gas volume in the piping highpoint. To determine if this applies for a specific system, evaluate the Froude number for the piping highpoint at the operating conditions using the following equation:

$$N_{Fr} = U/[g D]^{0.5} \quad (6-1)$$

where the variables are defined as:

- D is the highpoint inner diameter in ft or m,
- g is the acceleration of gravity in ft/sec² or m/sec² and
- U is the one-dimensional water velocity in ft/sec or m/sec.

Of course this needs to be evaluated in consistent system of units and if the resulting Froude number is larger than the "bubble washout" criterion developed by Wallis et al (1977), the highpoint experimental results included in this report show that the gas volume would be removed.

6.3 Gas-Water Waterhammer Pressures

The pressures developed by noncondensable gas-water waterhammer events (as opposed to steam-water waterhammer events) are a function of; (1) the flow run-up interval, (2) the pump shutoff head pressure or the stagnation pressure of the flow behind an opening valve, (2) the initial volume of the accumulated gas and (3) the initial pressure of the gas volume. This waterhammer pressure is the maximum value exhibited in the hydraulic transient which includes the subsequent gas volume oscillations for those systems without a check valve as well as the subsequent events caused by the induced check valve closure and rebound when one or more check valve(s) is (are) installed in this system. This peak pressure is of particular interest in terms of evaluating whether the gas-water waterhammer would be sufficient to lift a relief valve in the piping network of interest.

The results of these experiments show that the peak waterhammer pressure can be evaluated from the superficial water velocity corresponding to the maximum water flow rate and this flow rate can be evaluated from the pump run-up or the valve opening characteristic and the available gas volume to be compressed as the water is accelerated into the voided region. During the water acceleration phase of the event, the pressure increases from the gas volume initial pressure to the pump shutoff head pressure, or the static pressure upstream of the opening valve, and can be assumed to follow an isentropic thermodynamic path ($PV^n = \text{Constant}$; $n = 1.4$). Hence, this results in:

$$P_1 V_1^n = P_2 V_2^n$$

where:

- P_1 is the initial gas volume pressure,
- P_2 is the pump shutoff pressure or the static pressure upstream of the opening valve,
- V_1 is the initial gas volume and
- V_2 is the gas volume at the pump shutoff pressure (pump surveillance or LOCA transients) or the system pressure (transfer to RHR cooling).

Solving for the gas volume change during the acceleration phase we find:

$$V_g = V_1 - V_2 = V_1 [1 - (P_1/P_2)^{1/n}] \quad (6-2)$$

As discussed in Section 2, the pump discharge flow rate during the run-up interval can be approximated as a linear increase with time (Shulman, 1977): As noted above in Section 6.1, there are several flow transients that need to be addressed. One is the pump surveillance transient and this approximation is appropriate for this run-up behavior. It is also appropriate to use in evaluating the gas volume response for LOCA transients in which the pump is started but the injection can not be initiated due to either a closed injection valve or check valve. The linear run-up approximation is given by:

$$Q_{\text{pump}}(t) = Q (t / t_{\text{run-up}}) \quad (6-3)$$

With this we can conservatively assess the time required for the pump to fill the available volume (V_g) as:

$$t = [2 V_g t_{\text{run-up}} / Q]^{0.5} \quad (6-4)$$

The time calculated from this expression can not be longer than the run-up interval and therefore the calculated flow rate can not be larger than Q .

When the flow run-up transient is caused by a valve being opened, such as is the case when transfer to RHR cooling, the flow transient can be approximated in terms of the gas pressure increasing with the square of the time. This is consistent with a pump run-up being linear in time, but the run-up interval related to the compression/pressurization of the noncondensable gas volume should be a small fraction of the valve opening interval (t_o). As a general representation of the valve opening characteristics, it is recommended to consider that the gas volume pressurization occurs within 10% of the minimum measured opening interval. For this sequence, the change in the volume due to the compression is given by the initial and RCS pressures as described above. Consistent with an assumed linear increase for the flow compressing the gas volume, the peak flow rate at the time that the gas volume reaches the system pressure is given by:

$$Q_f = 2 V_g / (K t_o) \quad (6-5)$$

where K is the fraction of the opening interval that results in essentially full flow to compress the gas volume and is recommended to have a value of 0.1.

Using the appropriate flow transient interval, the maximum volumetric flow rate can be calculated, which enables the practitioner to estimate the waterhammer pressure increase, i.e.

$$\Delta P_{\text{WH}} = \rho C_w Q / A_{\text{pipe}} \quad (6-6)$$

In this equation, Q_1 is either Q_{pump} or Q_f depending on the sequence that is being evaluated. It is important to note that this calculation must be done in consistent units, but the resulting gas-water waterhammer pressure increase should be added to the pump shutoff head, or the pressure of the upstream flow for the opening of a valve, to determine if the waterhammer event could potentially exceed the opening pressure of a relief valve in the piping. Appendix C of this report includes sample problems for each of the flow transients discussed above.

6.4 Force Imbalances Developed by the Gas-Water Waterhammer Event

As discussed in this report, the force imbalance on an axial piping segment is determined by the rate of rise of the pressurization, or depressurization event. Rapid compression of the accumulated gas volume is the mechanism that produces the noncondensable gas-water waterhammer which occurs when the latter phase of this compression takes place during an interval that is short compared to the acoustic relief time constant of the piping in question. When assessing the piping force imbalances generated by noncondensable gas-water waterhammer events, it is especially important to note that the maximum rate of pressurization is the controlling parameter; not the maximum waterhammer pressure.

The experimental studies presented in this report show that the peak axial force imbalance for the waterhammer event is determined by the system configuration, the initial pressure and volume of the accumulated gas, the pump shutoff head and, to a minor extent, the initial condition of whether the gas volume is distributed or in a single location. As determined from the analysis of the data, the hydraulic force imbalance imposed on a piping segment can be estimated by the equation (Eq. 2-12, but slightly in a different form):

$$F = A_{\text{pipe}} (dP/dt)_R (L_{\text{HP}} / C_w) \quad (6-7)$$

As was discussed in Section 5, the reference pressurization rate needs to be defined in terms of a pressure that is greater than the pump shutoff head and less than the maximum pressure caused by

the event. To provide a consistent basis for plant evaluations as well as to approximate that segment of the transient that has the most rapid rate of increase, this pressurization should be taken as the difference of one half of the calculated waterhammer pressure increase over the interval that is defined in the following paragraph.

Once the waterhammer pressure increase is calculated, evaluate the extent of gas compression (the resulting volume) from the initial pressure and volume state (P_1, V_1) to a higher pressure (P_2) equal to the pump shutoff pressure plus one half of the waterhammer increase using an isentropic thermodynamic path ($n = 1.4$). Therefore, volume V_2 at the specified pressure is again calculated by:

$$V_2 = V_1 (P_1 / P_2)^{(1/n)} \quad (6-8)$$

Consistent with the Joukowsky (1898) –Frizell (1898) water hammer equation, when the pressure has increased to this level, the water velocity would have been decreased by a factor of 2. We can also use the above equation to calculate the gas volume (V_3) at the peak pressure (P_3). By taking the difference between V_2 and V_3 and dividing by the pipe cross-sectional flow area, we calculate the effective length of travel ($L_{sg} = (V_2 - V_3) / A_{pipe}$) needed for the last half of the waterhammer pressure increase.. The time required for this pressurization is taken to be the time needed for the water to travel the effective length of travel given a water velocity consistent with the pressure (P_2), which as discussed above is ($U_{sw} = Q_{pump} / (2 A_{pipe})$). Thus, the reference pressurization derivative is calculated as:

$$dP/dt)_R = (P_3 - P_2) / (L_{sg} / U_{sw}) \quad (6-9)$$

With this specified, all of the parameters are known to calculate a conservative estimate of the hydraulic force imbalances acting on the highpoint piping segment as a result of the gas-water waterhammer event. This calculation is performed using the above equation for the force imbalance. A set of sample calculations for evaluating the force imbalance are given in Appendix C.

While the above estimates the maximum force imbalance acting on the highpoint where the gas-water waterhammer occurs, the force imbalances on other piping segments in the system can be estimated in a similar manner. Since the same pressurization rate will propagate through the system piping configuration, the maximum force imbalance acting on other straight segments of the piping will be linearly related to the calculated force imbalance for the highpoint. In particular, if the segment is half the length of the highpoint, the maximum force imbalance on this other segment would be half of that on the highpoint; if the segment was twice as long, the maximum force imbalance would be twice as large.

This simplified is intended to provide a means to estimate the loads on the piping due these relatively slow waterhammer events. If the calculated values are sufficient to possibly challenge the success criteria for the piping supports, then a more detailed piping system calculation should be performed.

6.4.1 Force Imbalances Developed by a Check Valve Closure Induced by a Gas-Water Waterhammer Event

A check valve can become an important consideration because the gas-water waterhammer induces compression waves to propagate backward through the system piping and the pump. This propagation continues through the suction piping until it reaches a very large increase in the cross-sectional flow area (such as a large tank) or a free surface such as that in the RWT, the RWST or the BWST. If such a large increase in the flow area and/or a free surface is encountered, these compression waves will be reflected as rarefaction waves that travel forward through the piping toward the location of the waterhammer. The rarefaction waves induce decreases in the water velocity and also enable the compressed gas volume to expand. Eventually, the rarefaction waves, combined with the expanding gas volume, cause the water velocity to be reversed such that it flows toward the large diameter change and/or the free surface. It is this reverse water velocity that causes the check valve to close. However, the aspect that is most influential is the closure rate of the check valve (particular a swing check valve). As discussed in the report, a swing check would tend to close with the induced water velocity such that the developing reverse velocity would continue

unmitigated until the valve experiences the final closure. This effective rapid closure has been demonstrated by these experiments to produce potentially larger force imbalances even though the pressures generated are considerably smaller than the peak pressure generated by the noncondensable gas-water waterhammer event. However, the experiments also show that the presence of the mini-flow line, if it is located downstream of the check valve, acts to strongly mitigate the rate of pressurization cause by the check valve slam and, therefore mitigates the force imbalances developed. These experiments show that the resulting force imbalances with the mini-flow line open limit the highpoint net forces to values typical of the gas-water waterhammer event. Hence, for those systems that have an open mini-flow line downstream of the check valve that experiences this rapid closure, this simplified methodology can be used. If the check valve is located downstream of the mini-flow line, or if the mini-flow line is closed, a detailed piping calculation should be performed.

7.0 CONCLUSIONS

Numerous conclusions can be derived from the experimental results presented in this report. These are related to the conditions that would remove an accumulated gas volume, the dynamic two-phase flow regime that accompanies a noncondensable gas-water waterhammer event and those system specific conditions that influence the net force imbalance on the piping components of a given system. These insights and conclusions are listed below.

1. If the operating history, or the maintenance strategy, involve a sufficient flow rate through the piping highpoint to produce a Froude number greater than 0.54 the accumulated gas volume will be "washed-out" of the highpoint.
2. With the stratified two-phase flow pattern that would be produced with gas accumulated in a piping highpoint, the initial void fraction for the gas would be essentially preserved in the vicinity of the dynamic waterhammer event. In essence, the induced water flow rate moves over the top of the water inventory initially in the highpoint.
3. The peak waterhammer pressure is determined by the initial gas pressure and volume, the pump shutoff head and whether the system is flushed before the test conditions are established. This pressure is greater than the subsequent oscillations of the gas volume for those systems without a check valve and also greater than the pressures resulting from the induced check valve closure and rebound when one or more check valve(s) is (are) installed.
4. The peak force imbalance generated by the gas-water waterhammer event is determined by the peak pressure and the rate of rise of the waterhammer pressurization.
5. If the system piping includes a swinging check valve, the closure induced by the waterhammer event can cause subsequent force imbalances, in both axial directions (upstream and downstream), that are larger than the waterhammer induced force imbalance.
6. The peak force imbalances are a function of both the piping configuration (pipe highpoints, check valves, etc.), the pump parameters as well as the initial gas volume and pressure.

7. Data taken with a check valve with, and without, an open mini-flow line show that the acoustic relief path through the mini-flow line substantially reduces the force imbalance on the remainder of the piping as a result of the check valve slam. For the test configuration, this reduced the force imbalance due to the check valve slam to values comparable to those generated by the gas-water waterhammer.
8. With respect to the maximum transient pressure generated for a multi-bubble configuration, the test data show that these gas-water waterhammer pressures are essentially the same as those recorded for a single gas bubble with the same total gas volume. Therefore, the simplified methodology can be used to conservatively estimate the peak pressure that could be developed for a multiple gas bubble situation.
9. Conversely, the measurements of the force imbalances generated in the multiple gas bubble tests show that the maximum force can be increased compared to the force generated when a single bubble, with the same total volume, exists in the downstream highpoint. This increase is due to an increase in the rate of pressurization to the maximum pressure cause by the interaction between the bubbles and the water inertial mass between the gas volumes. From this observation we conclude that if a multi-bubble configuration is known to exist, the evaluation of the force imbalances on the piping segments for that system should be assessed using a multiple bubble model.

8.0 REFERENCES

- Crane Co., 1976, "Flow of Fluids Through Valves, Fittings, and Pipe" Crane Co. Technical Paper No.410.
- Epstein, M., 2008, "A Simple Approach to the Prediction of Waterhammer Transients in a Pipe Line with Entrapped Air", Nuclear Engineering and Design, 238, pp 2182-2188.
- Frizell, J.P., 1898, "Pressures resulting from changes of velocity of water in pipes," Transactions of the ASCE 39, Paper 819 (presented 6 October 1897).
- Haberman, W.L. and R.K. Morton, David W. Taylor Model Basin Report 802.
- Henry, R.E., et al, 1971, "Pressure-Pulse Propagation in Two-Phase One- and Two-Component Mixtures", Argonne National Laboratory report ANL-7792.
- Joukowsky, N., 1898, "Über den hydraulischen Stoss in Wasserleitungsrohren" ("On the hydraulic hammer in water supply pipes") Memoires de l'Academie Imperiale des Sciences de St.-Petersbourg (1900), Series 8, 9(5), 1-71 (in German).
- Shulman T.M., et al, 1977, "Motor Starting Protection by Impedance Sensing," presented at the IEEE Power Engineering Society meeting, Mexico City, July.
- Thorley, A.R.D., 1983, "Dynamic Response of Check Valves", 4th International Conference on Pressure Surges, University of Bath, England, September 21-23, Paper F1,
- Van Duyne, D.A. and Merilo, M., 1996, "Water Hammer Handbook for Nuclear Plant Engineers and Operators", EPRI Final Report TR-106438, Project No. 2856-03.
- Wallis, G.B., 1969, One-dimensional Two-phase Flow, McGraw-Hill Book Company, New York, N.Y.
- Wallis, G.B., 1977, "Conditions for a Pipe to Run Full When Discharging Liquid Into a Space Filled With Gas," Journal of Fluids Engineering, June, pp 405 - 413.

APPENDIX A

Sensitivity of Force Measurements to System Structural Characteristics

Introduction

The measurement of force at the highpoint is accomplished through the use of a load cell situated at one end of the highpoint. The force measurement is affected by the waterhammer load as well as the system structural response to that load. A series of tests with the mid-length highpoint were performed to highlight the differences that accrue from changes in structural configuration.

Configurations Tested

Three mid-length highpoint configurations were compared :

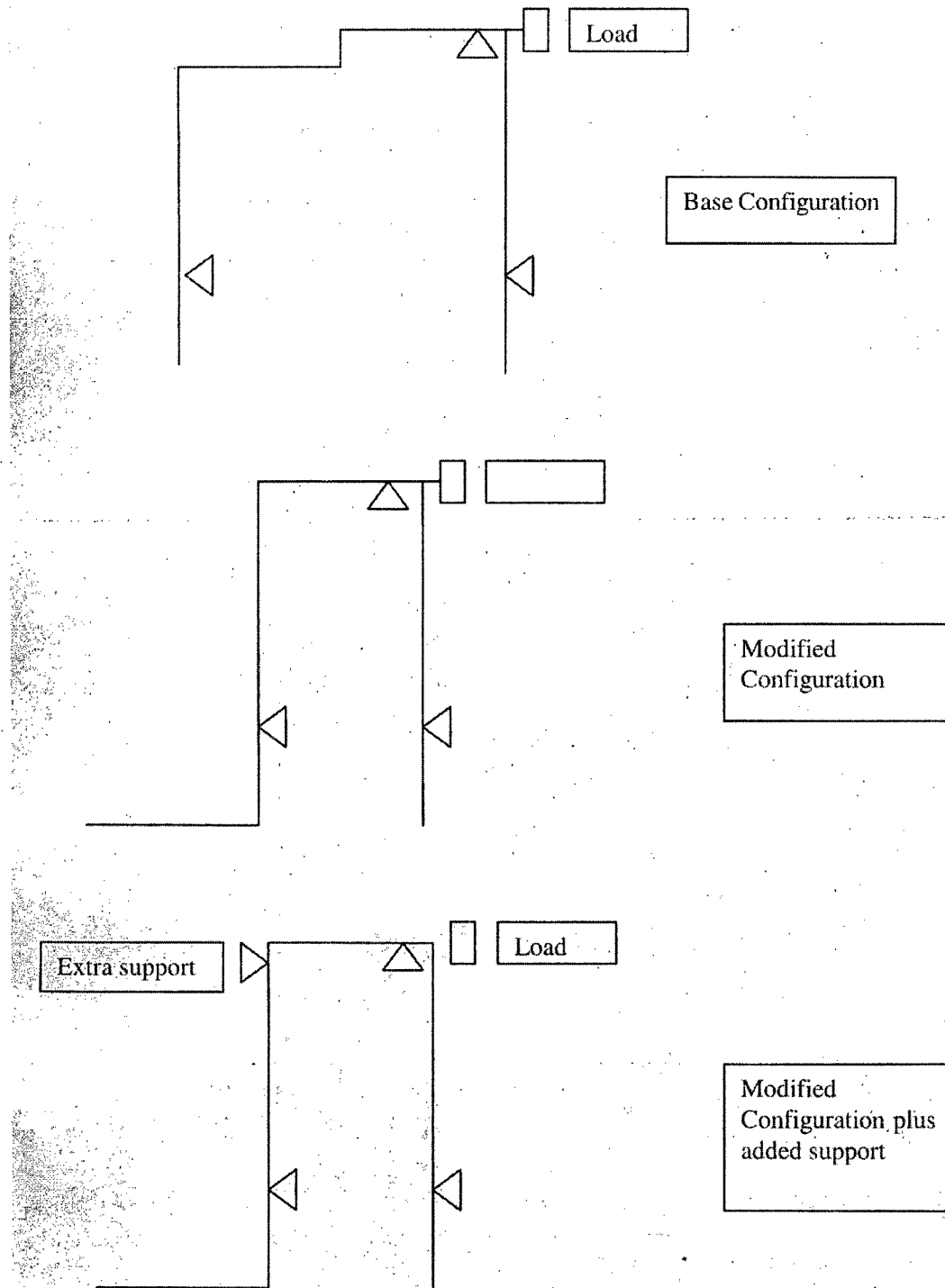
- 1) Original mid-length setup, with short riser (about 9 inches) at the upstream elbow (Test Numbers 32A and 52A).
- 2) Modified mid-length setup, with long riser (about 11 feet) at the upstream elbow (Test Numbers 32C and 52C).
- 3) Modified mid-length setup, with long riser (about 11 feet) at the upstream elbow plus and additional support located on the riser directly below the upstream elbow (Test Numbers 32D and 52D)

Diagrams of the three configurations are shown in Figure A-1. The original configuration was fairly stiff, with limited lateral flexibility. The modified mid-length setup proved to be fairly flexible, particularly at the riser pipe. The additional support provided in the third configuration limited the lateral flexibility as well as providing a stiffer structure in the highpoint axial direction.

Initial Conditions

The same initial conditions were selected for this comparison. A 2 liter void with -24 in Hg pressure was applied for each case. Comparisons with check valve installed and without check valve installed were also performed. The 32 series tests included installed check valve, where the 52 series tests had no check valve installed.

Figure A-1 Diagram of Different Midpoint Configurations



Results

Flow Comparison

Figures A-2 through A-4 show the measured flow response for the non-check valve installed cases. Figures A-5 through A-7 provide the same information for the check valve installed cases. Inspection of these figures shows that the initial flow increase and peak value is virtually identical for all six tests, which confirms the results presented in Section 5. The non check valve cases show a somewhat different behavior after the peak, which can be attributed to the system pressure oscillation including the suction piping beyond the check valve. Figure A-32 provides an overlay of the three check valve cases that demonstrates the similarity. The principal observation is that the six cases are being driven comparably.

Pressure Comparison

Figures A-8 through A-10 provide the void pressure response for the non-check valve installed cases. Figures A-11 through A-13 provide the same information for the check valve installed cases. The peak pressures are very close for all six cases. The post –peak pressure response is different for the check valve cases. The pressure oscillation frequency is higher for the check valve cases, which is consistent with the expectation that the check valve closure will “shorten” the system, driving the oscillation frequency up (this was also shown in Figure 5-14). Figure A-33 provides an overlay of the three check valve cases that demonstrates the similarity between the cases. The most significant aspect of the pressure behavior is the slope of the curve , particularly during the approach to the first pressure peak, since this value, combined with the acoustic transport speed of the fluid in the highpoint, determines the unsteady pressures and forces seen by the highpoint.

Statistical Comparison of Flow and Pressure

The mean maximum flow for the six cases is 63.74 gpm. The sample standard deviation for the flow is 2.16 gpm or 3.4% of the mean maximum flow. The mean maximum pressure for the six cases is 413.5 psia. The sample standard deviation for the pressure is 9.72 psi, or approximately 2.4% of the mean maximum pressure. These results support a conclusion that the transient response is very consistent between cases and the forces would be expected to be comparable.

Force Measurement Comparison

Figures A-14 through A-16 show the measured force vs time for the overall transient for the non-check valve cases. Figures A-17 through A-19 expand the time scale to show details of the first second of the transient. The first peak represents the key point of interest, as it is the direct response to the initial flow transient. The subsequent behavior includes aspects of the structural response to the event. Physically, one way to characterize the structural response is that the initial compression transient tends to impart strain energy to the structure which is then released over time, essentially as ringout. For these cases, the initial transient is the dominant feature and structural response decays fairly rapidly. It is readily apparent that the initial peak forces and subsequent response are different for the three cases.

Figures A-20 through A-22 show the measured force vs time for the check valve cases, and Figures A-23 through A-25 provide the expanded time scale views. The presence of the check valve introduces additional forces in the interval subsequent to the initial peak. These forces are due to pressure pulses with very short rise time (roughly 10 milliseconds) created when the check valve slams shut. The check valve slam forces are comparable to and in fact tend to exceed the bubble compression forces seen at the beginning of the transient. One effect seen in the force behavior that results from the check valve response is that the forces continue for an extended time relative to the non-check valve cases. Essentially, the structural response is sustained by the additional energy provided by the check valve pulses.

The mean first peak force measured for all six cases is 57.8 lbs. The sample standard deviation is 25 lbs, or approximately 43% of the mean. This shows that the structure clearly affects the initial peak force measurement. The plots also show that the structure effects the ringout behavior as well. Figure A-34 provides an overlay of the measured forces for the three check valve cases.

Force Measurement Frequency Domain Comparison

The power spectral densities (PSDs) of the measured forces were computed to allow the comparison of the different configuration frequency responses. Figures A-26 through A-31 provide the plots for

the six cases. Frequency content up to 100 Hz was examined, but the dominant responses were found to be below 40 Hz.

Figure A-26 shows the measured force PSD for the original (short riser) mid-length highpoint. It clearly shows the dominant response at the bubble oscillation frequency. There is some higher frequency content near 22 and 24 Hz that represent structural response.

Figure A-27 shows the measured force PSD for the modified (short riser) mid-length highpoint. It also displays the dominant response at the bubble oscillation frequency. A frequency peak at 14 Hz is evident, as well as some additional content in the 18-22 Hz range. In comparison to the original configuration, it is clear that there are more frequency components evident.

Figure A-28 shows the measured force PSD for the modified mid-length highpoint with the added support present. Comparing this plot to A-27 demonstrates the impact of the support, namely to virtually eliminate response in the 10-22 Hz range. There is one peak at about 25 Hz which is consistent with stiffening the structure and raising its natural frequency.

Figure A-29 shows the measured force PSD for the original mid-length highpoint configuration, with check valve installed. A key feature evident is the shift in bubble oscillation frequency that characterized the check valve cases. (Compare with Figure A-26) This case demonstrates considerably more harmonic response at higher frequencies than the non-check valve case. Responses are observed at 12, 18, 20, 25, and 27 Hz. These are most likely due to the check valve behavior.

Figure A-30 shows the measured force PSD for the modified mid-length highpoint configuration with check valve installed. It displays the same bubble frequency shift noted in A-29. The 14 Hz peak noted in the non-check valve case (Figure A-27) is also present. A number of additional frequency responses appear due to the presence of the check valve. These are seen at 8, 12, 17, 25, 29, 31 and 34 Hz.

Figure A-31 shows the measured force PSD for the modified mid-length highpoint configuration with the check valve installed and the additional support present. Comparing to Figure A-30, the support effectively eliminates the 14 Hz peak as well as most of the response up to 24 Hz. The 25 Hz peak observed in Figure A-28 remains present and appears to be somewhat broadened.

Conclusions/Recommendations

A sensitivity study considering the effects of the structure on the measured highpoint forces has been performed. The following observations are salient:

- 1) The hydraulic transient is highly reproducible, with little variance in flow or pressure. The force applied would necessarily be highly comparable.
- 2) The measured forces show large variance, and differ significantly between structural configurations.
- 3) Frequency domain evaluations of the forces demonstrate significant differences in frequency content between configurations.
- 4) Altering the structure by addition of a support yielded changes in the frequency content consistent with expectations.

Based on these observations, it is recommended that the force measurements be applied in relative terms for a given configuration. The system structural properties are different enough between configurations to make direct force comparison difficult without additional structural evaluation.

Measured Flows (No Check Valve Installed Cases)
Figure A-2

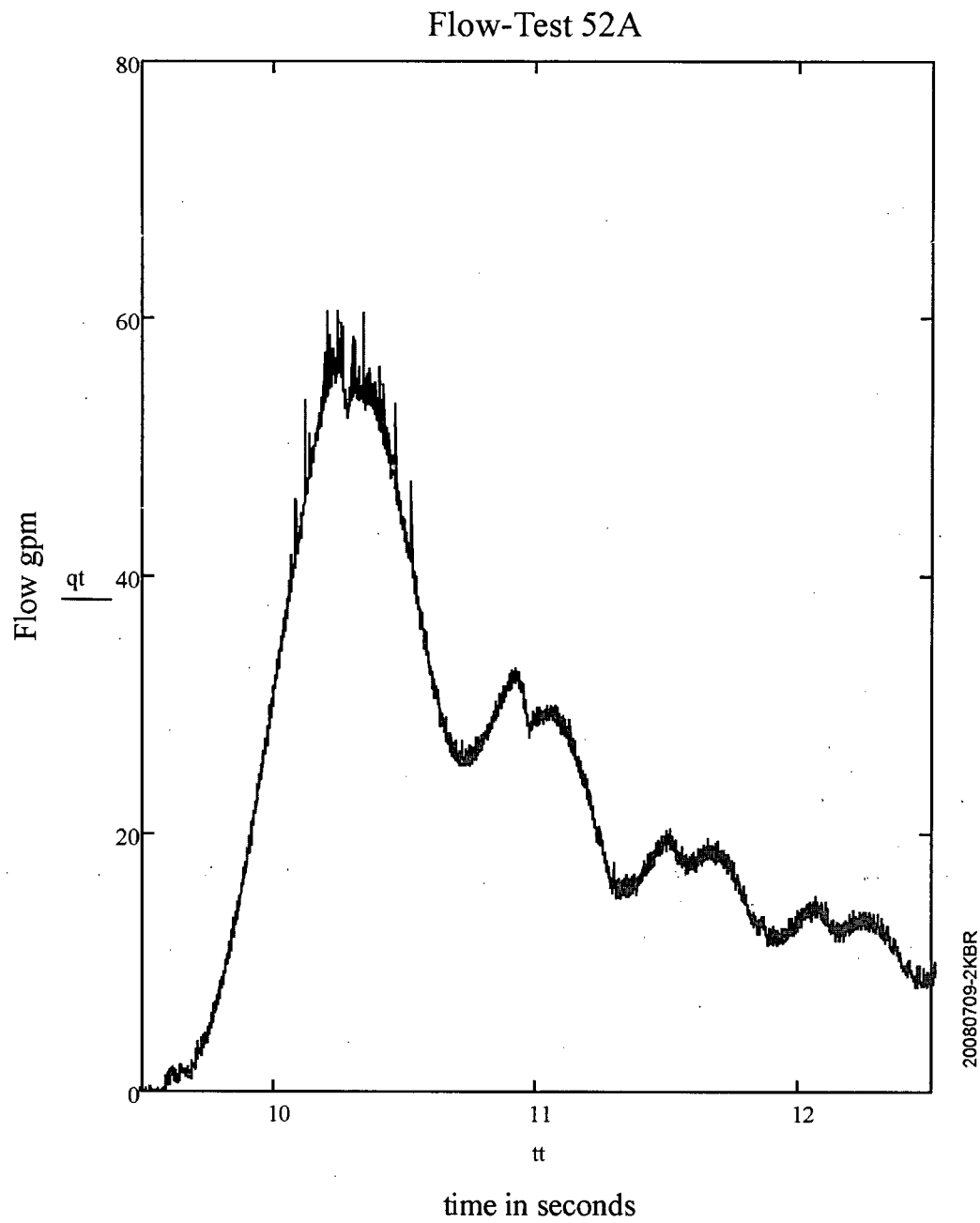


Figure A-3

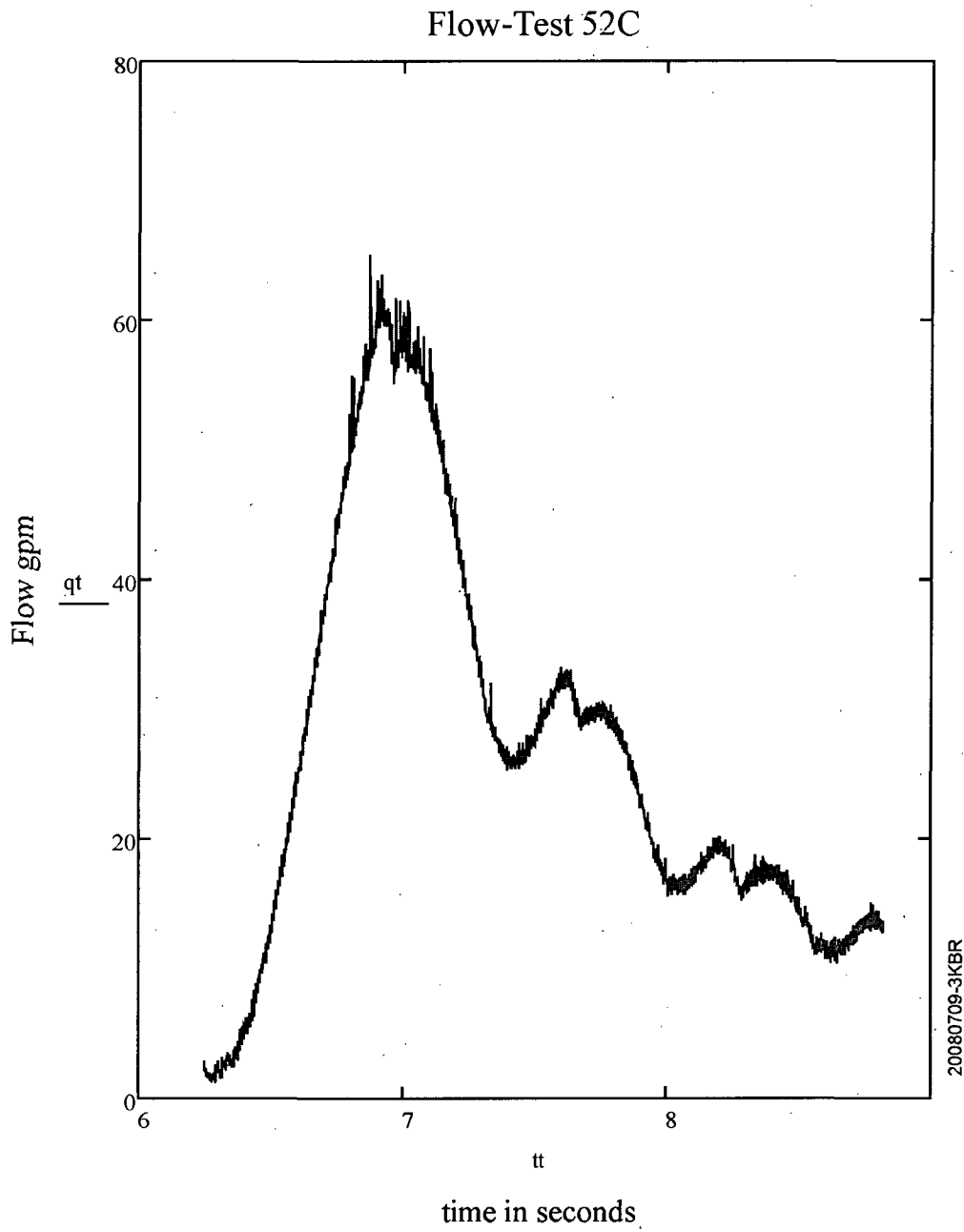
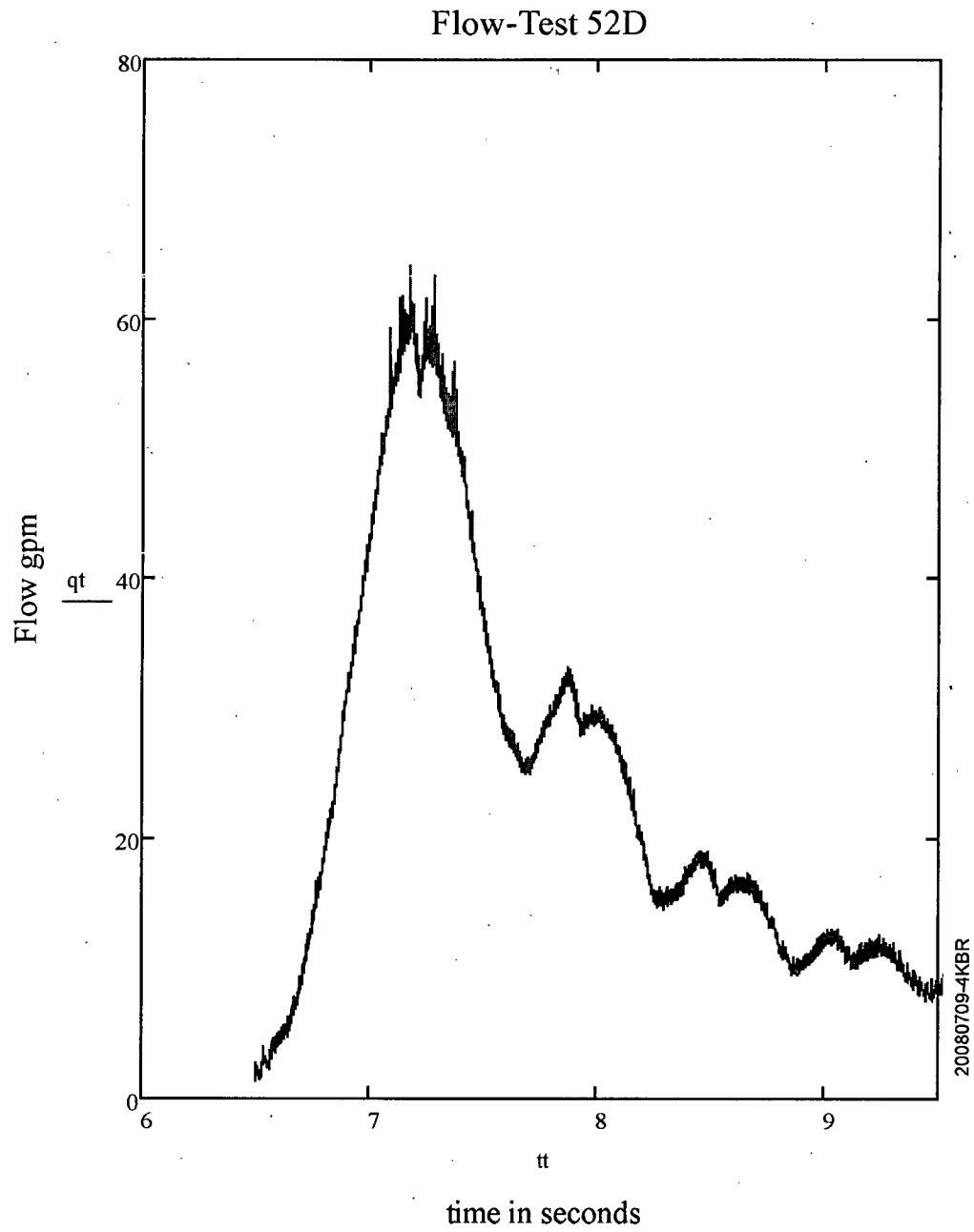


Figure A-4



Measured Flows (Check Valve Installed Cases)
Figure A-5

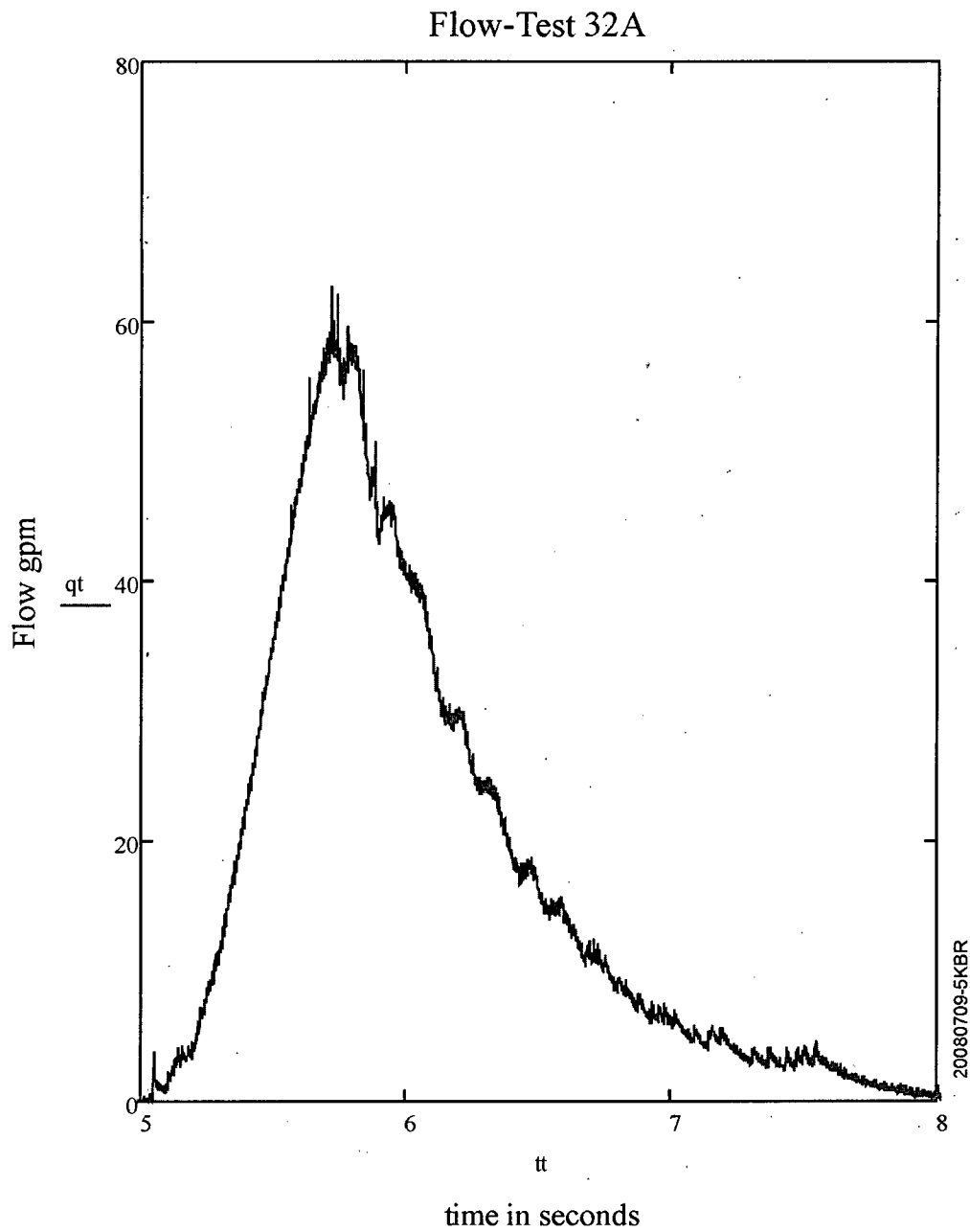


Figure A-6

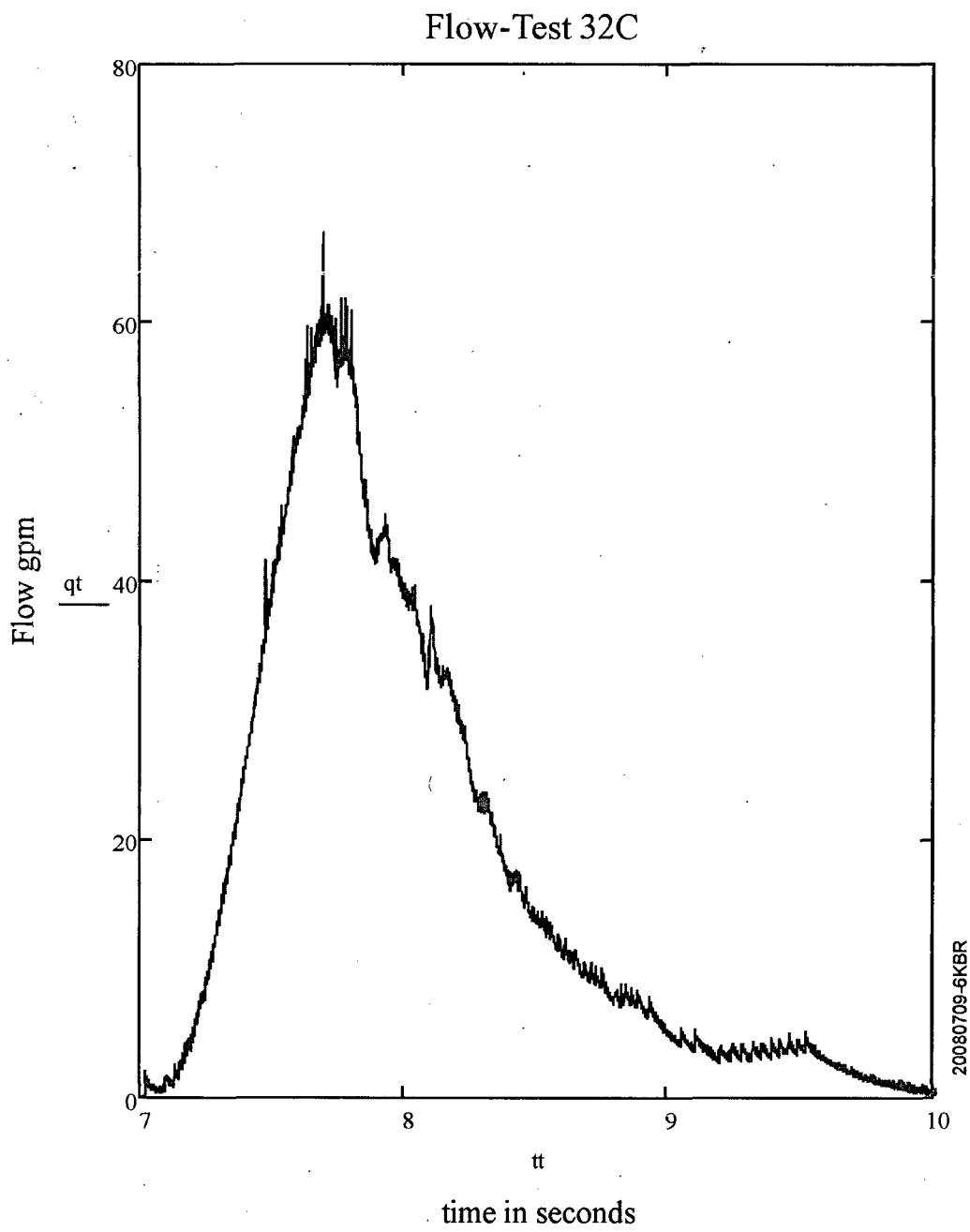
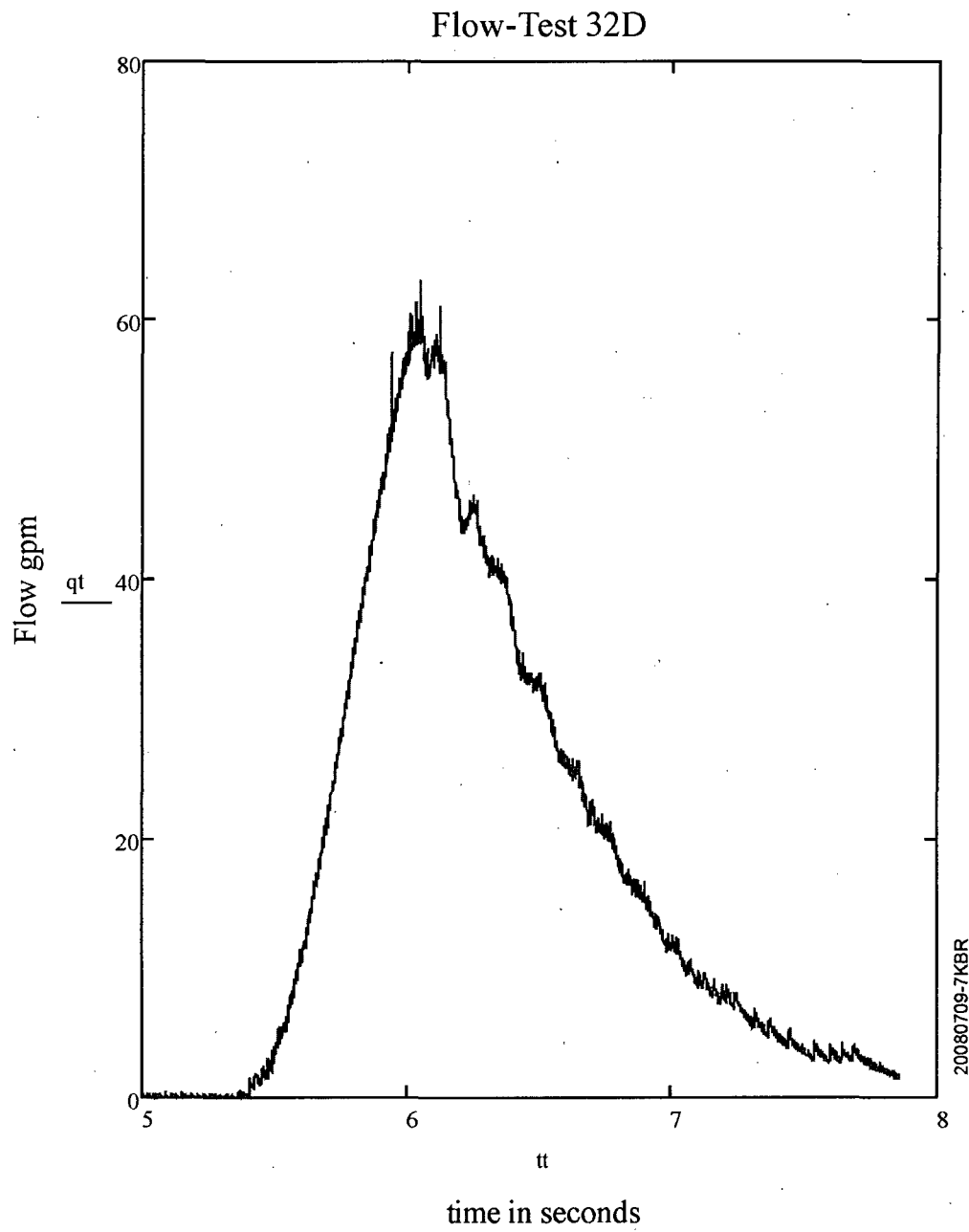


Figure A-7



Void Pressure Response (No check valve Installed)
Figure A-8

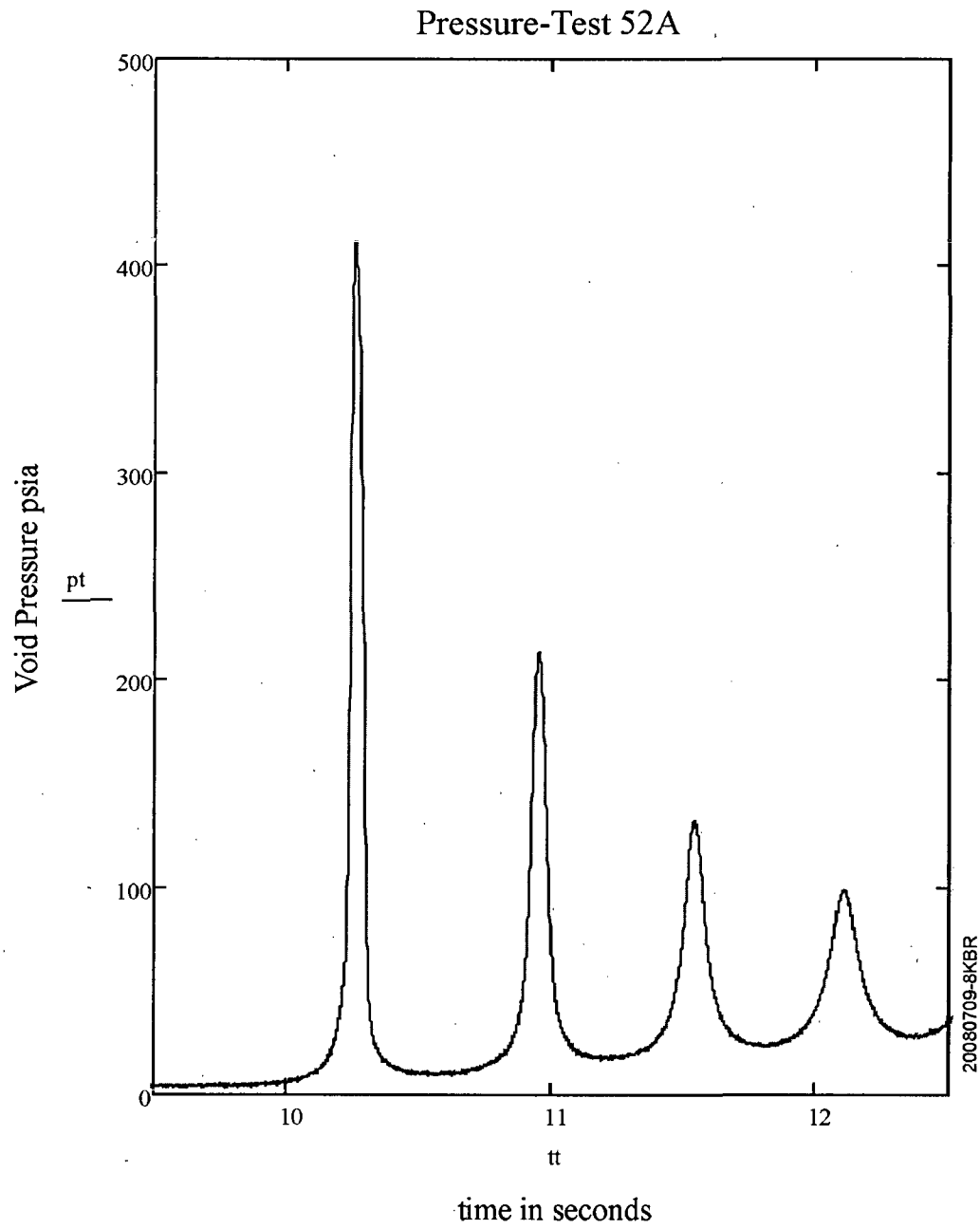


Figure A-9

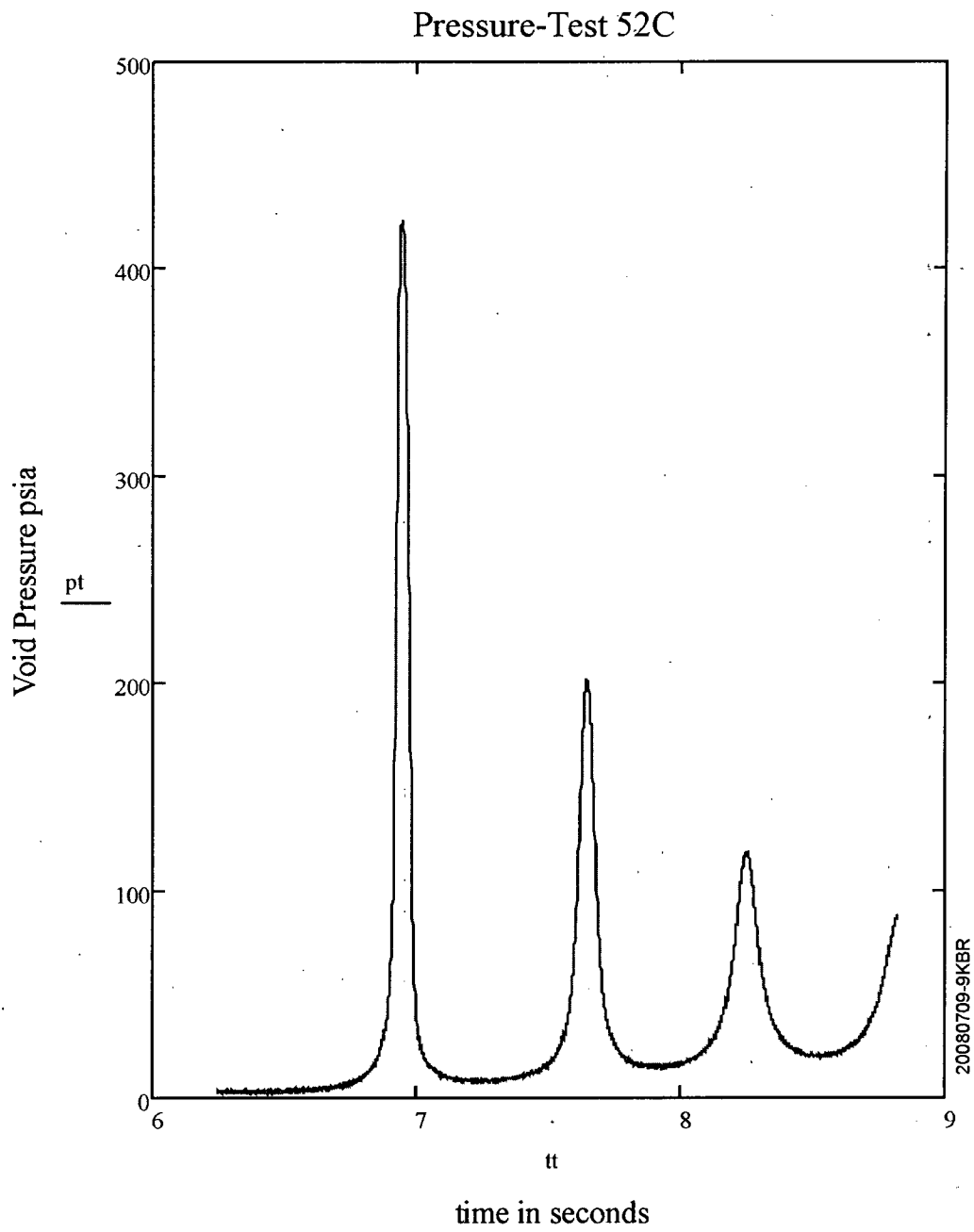
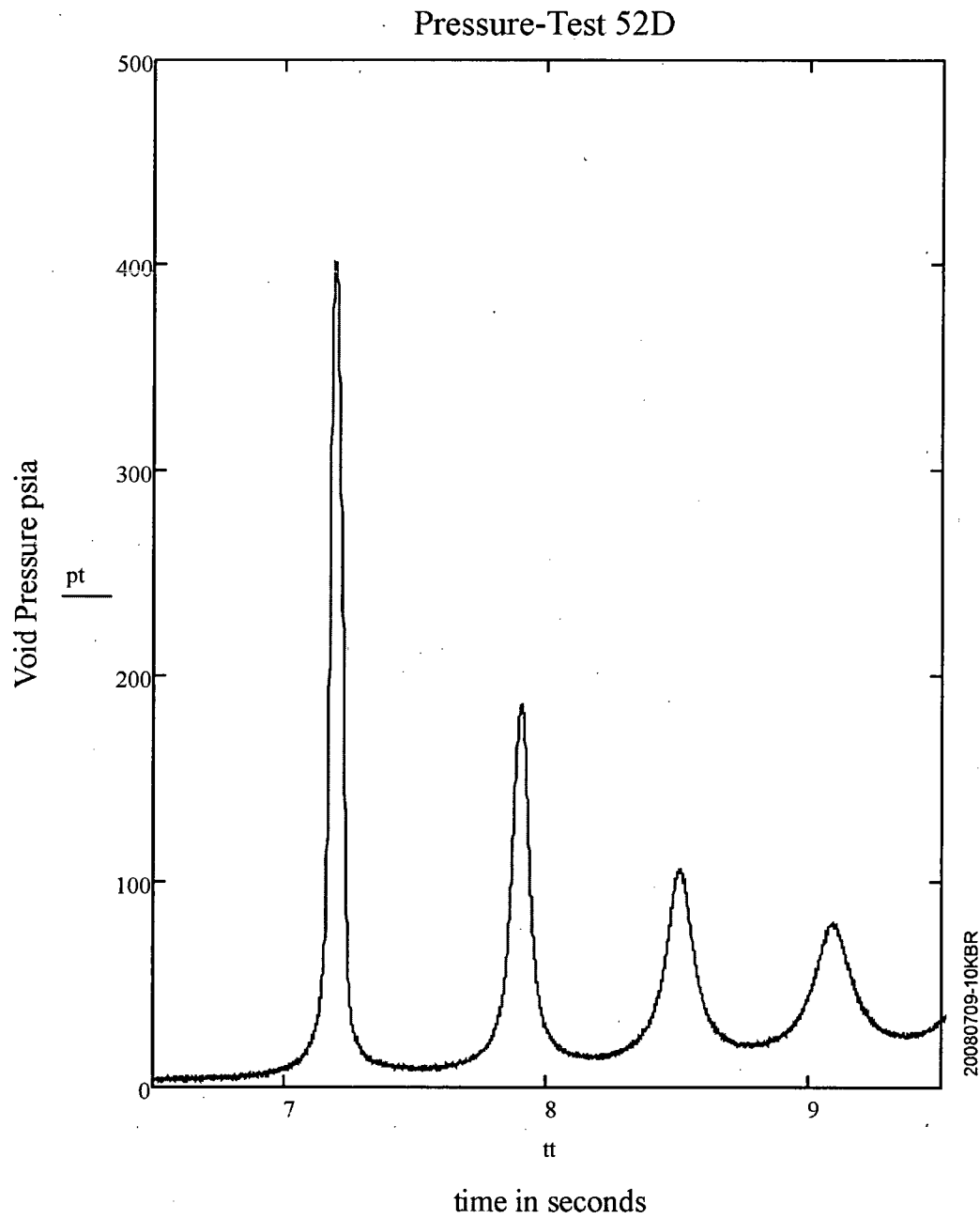


Figure A-10



Void Pressure Response (check valve Installed)
Figure A-11

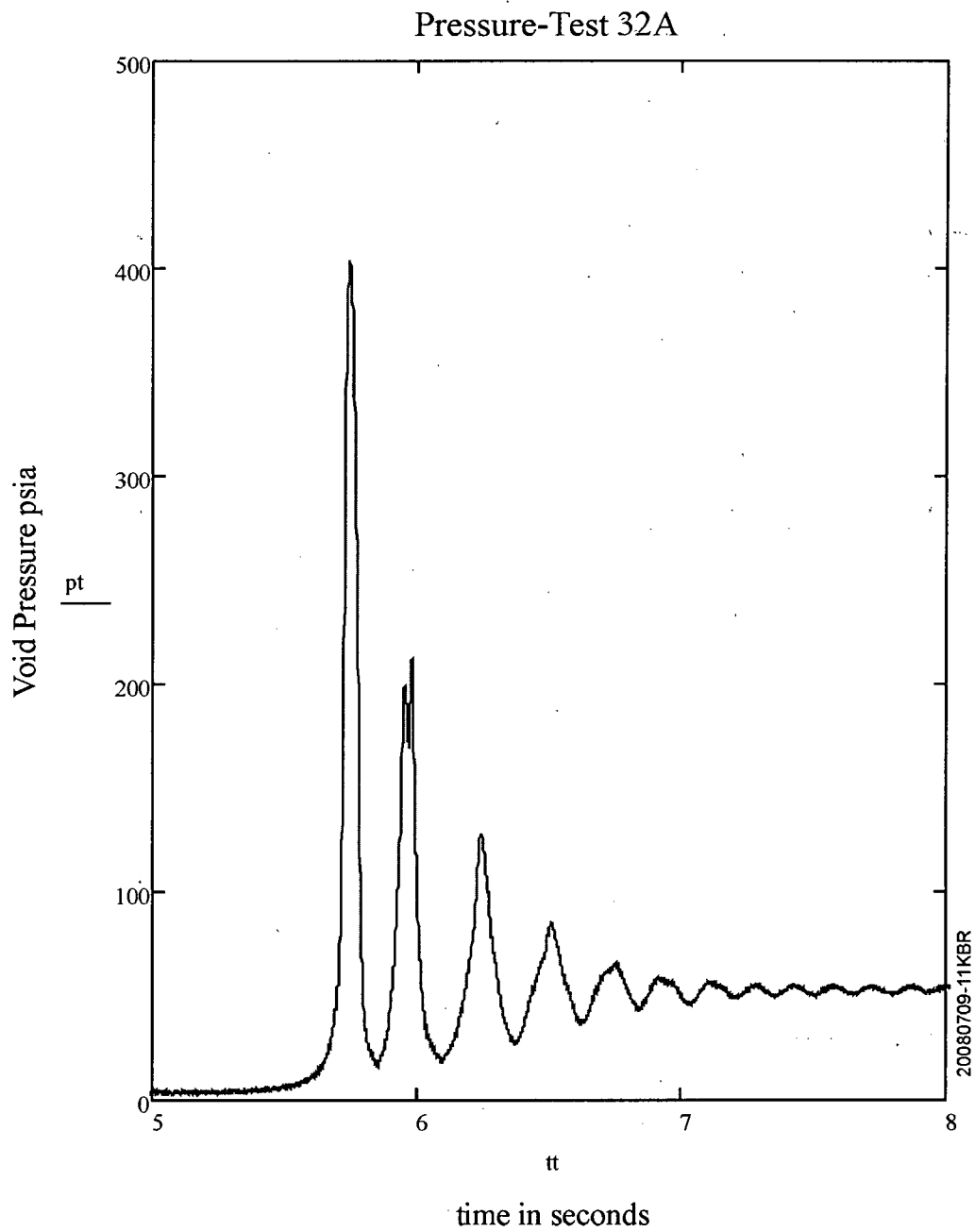


Figure A-12

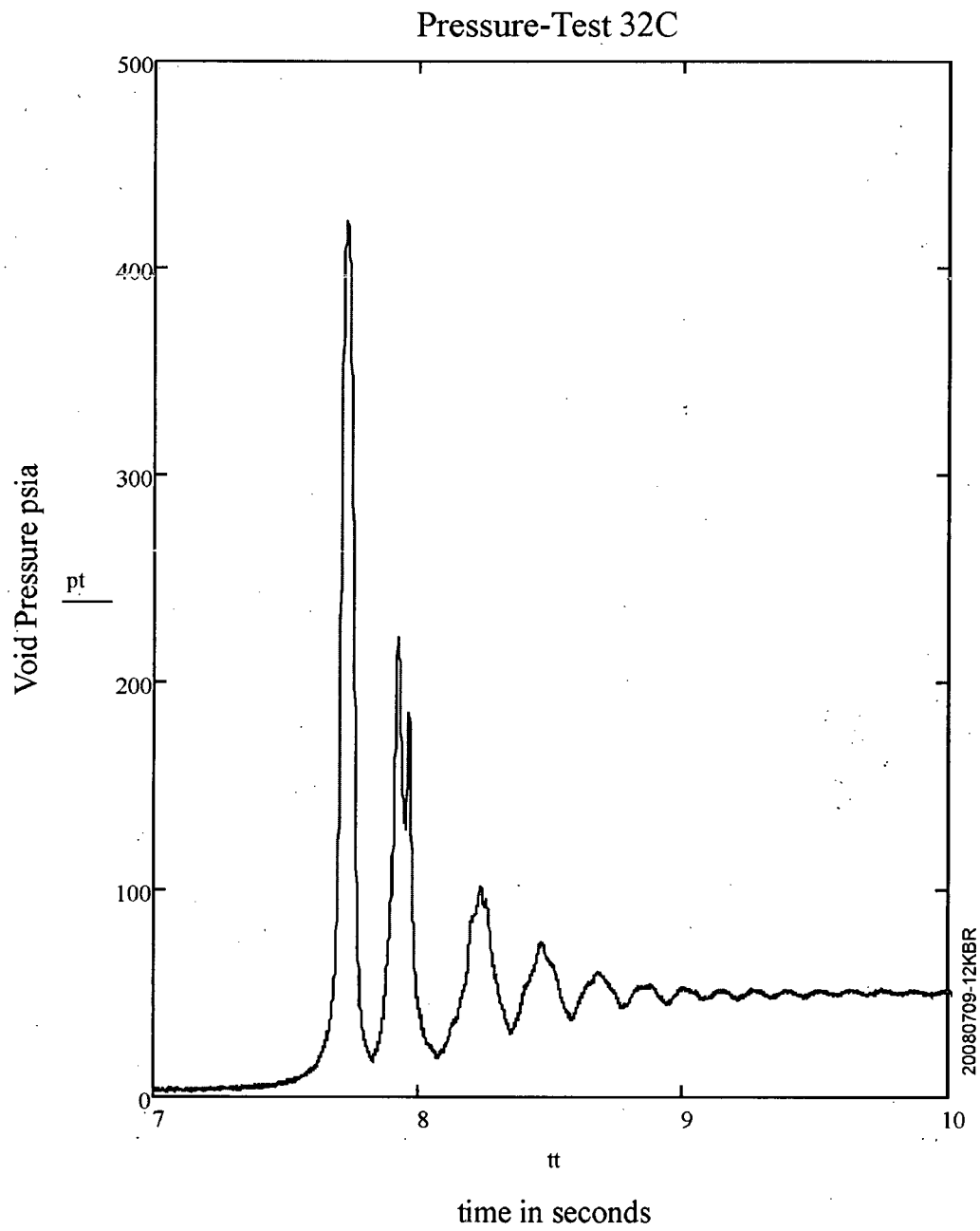
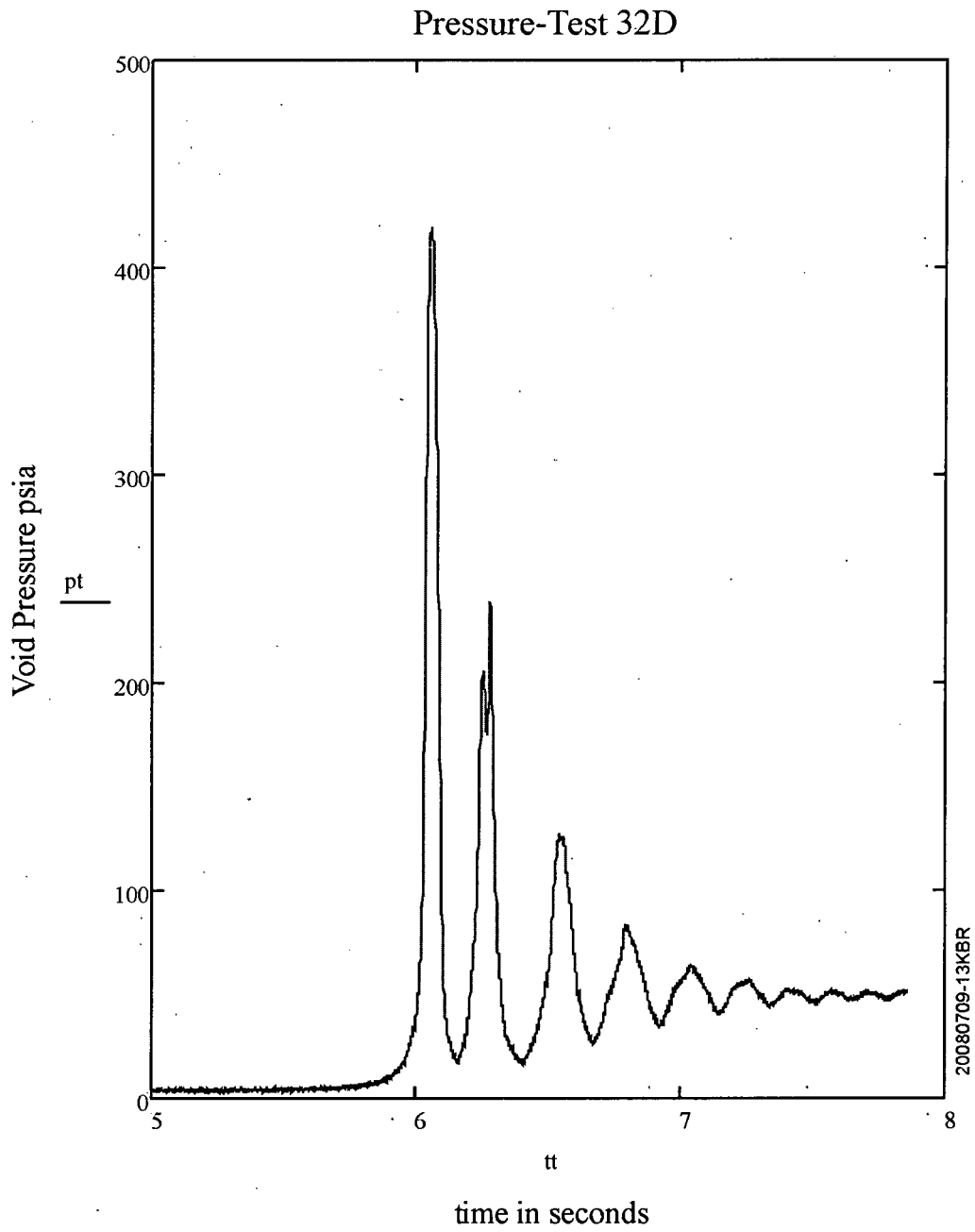


Figure A-13



Measured Force (Global-No Check Valve Installed)
Figure A-14

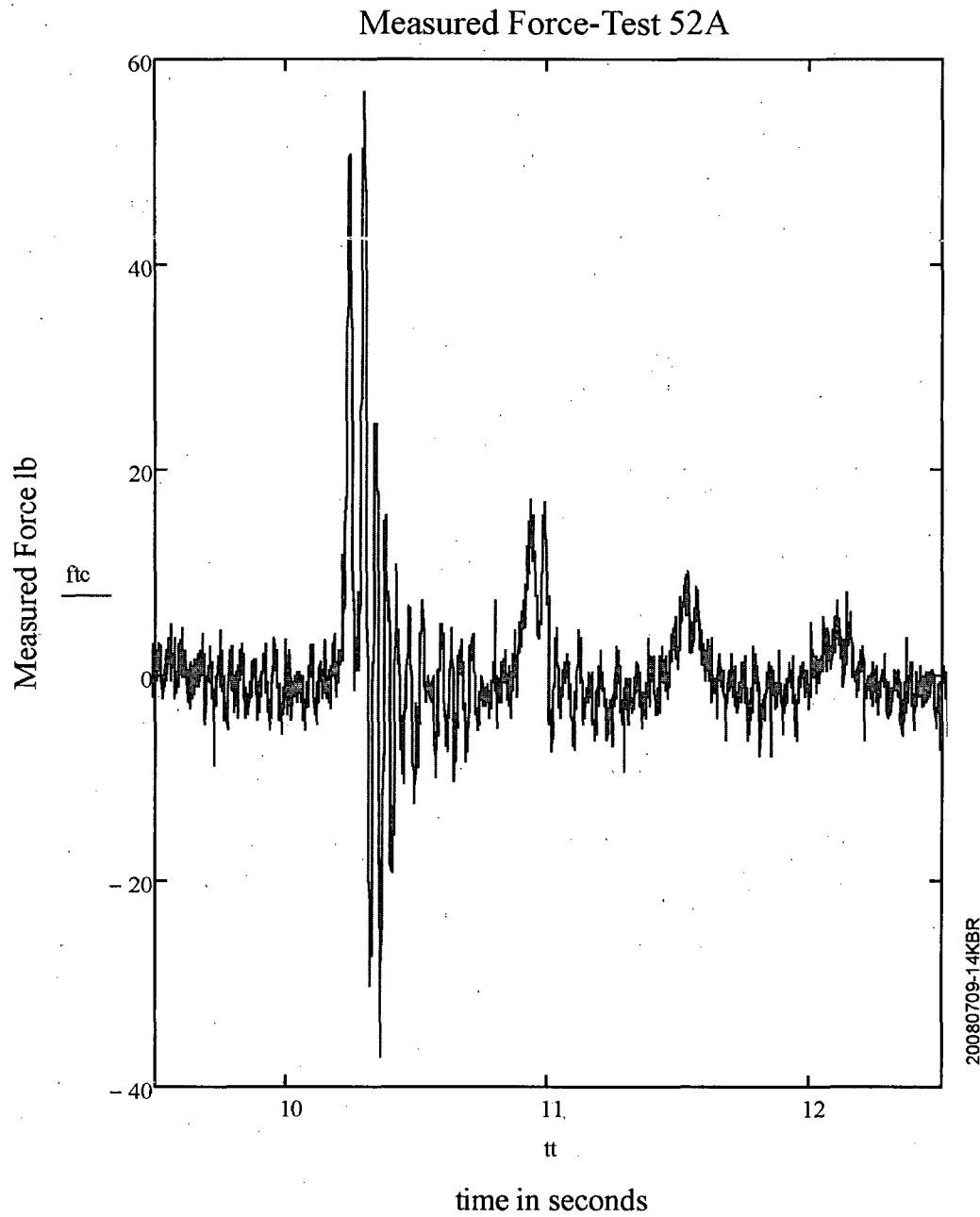


Figure A-15

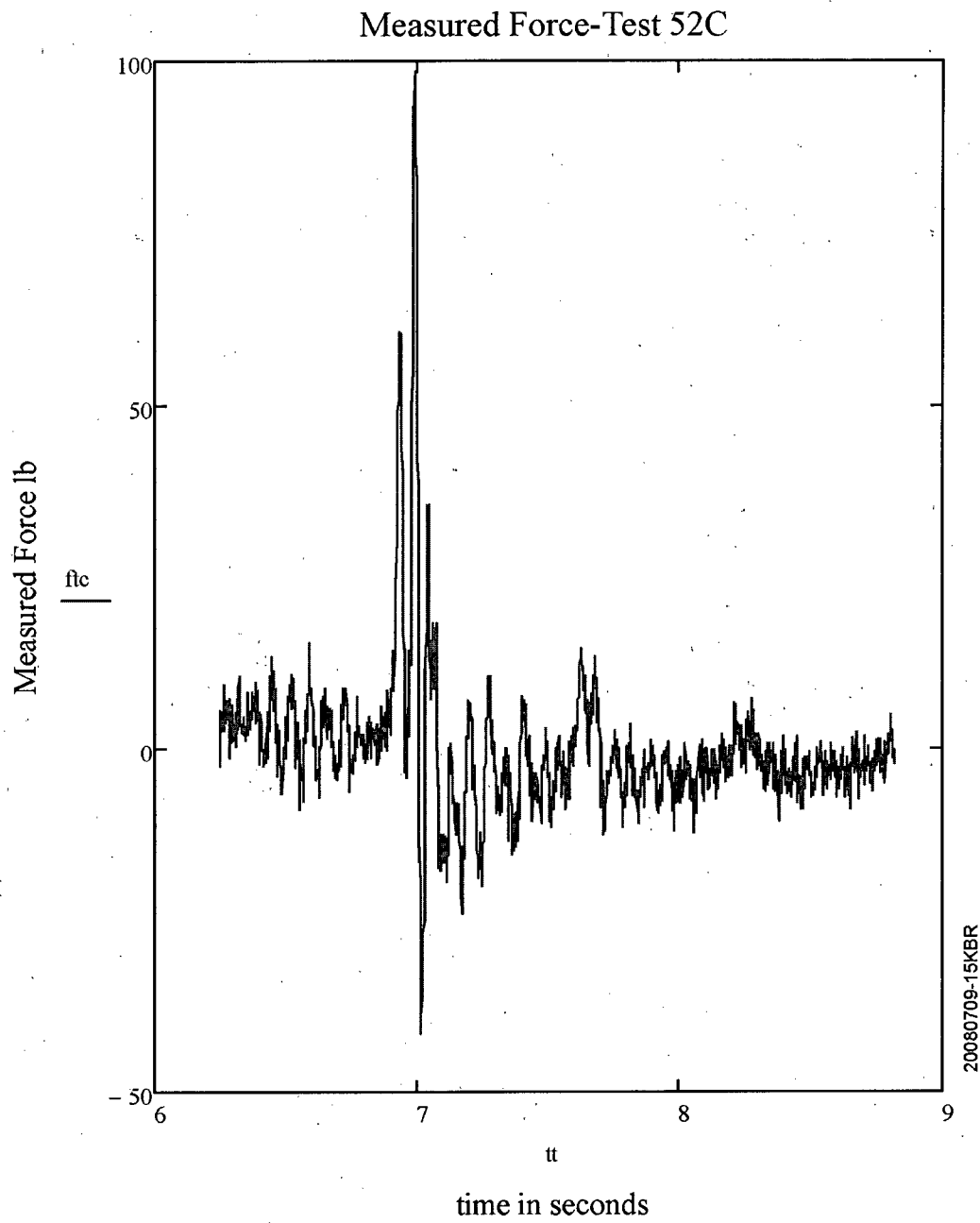
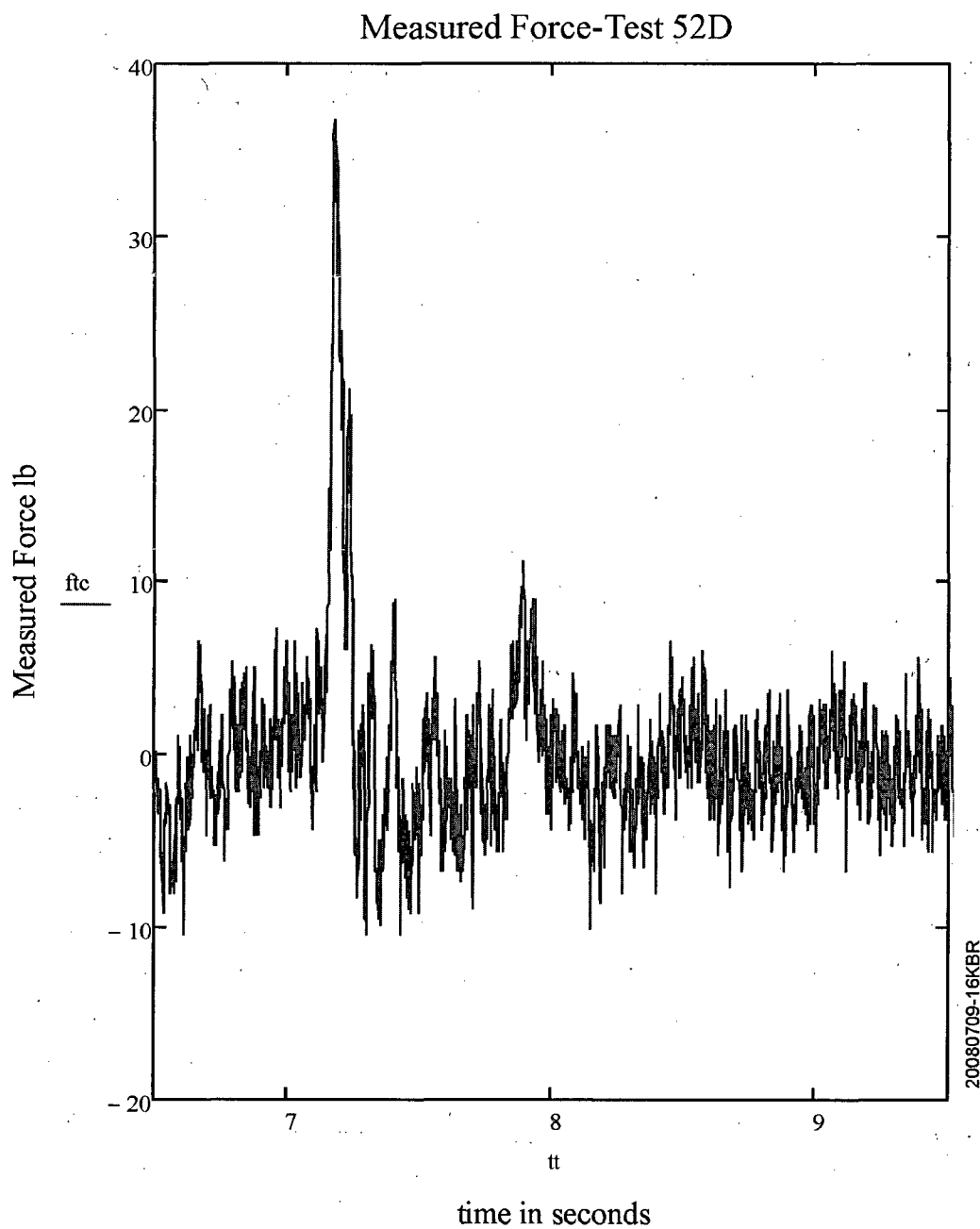


Figure A-16



Measured Force (Expanded Scale-No check valve Installed)
Figure A-17

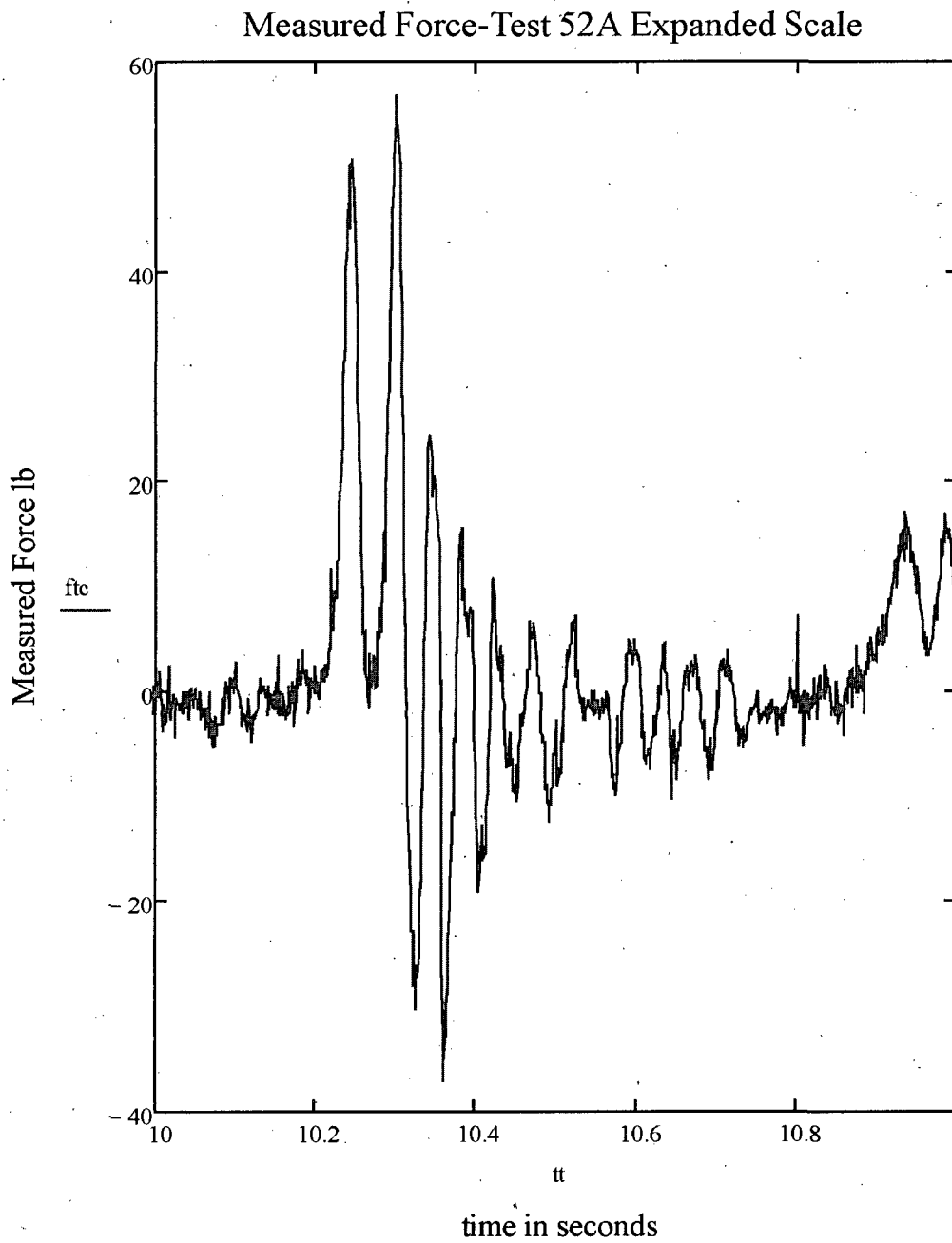


Figure A-18

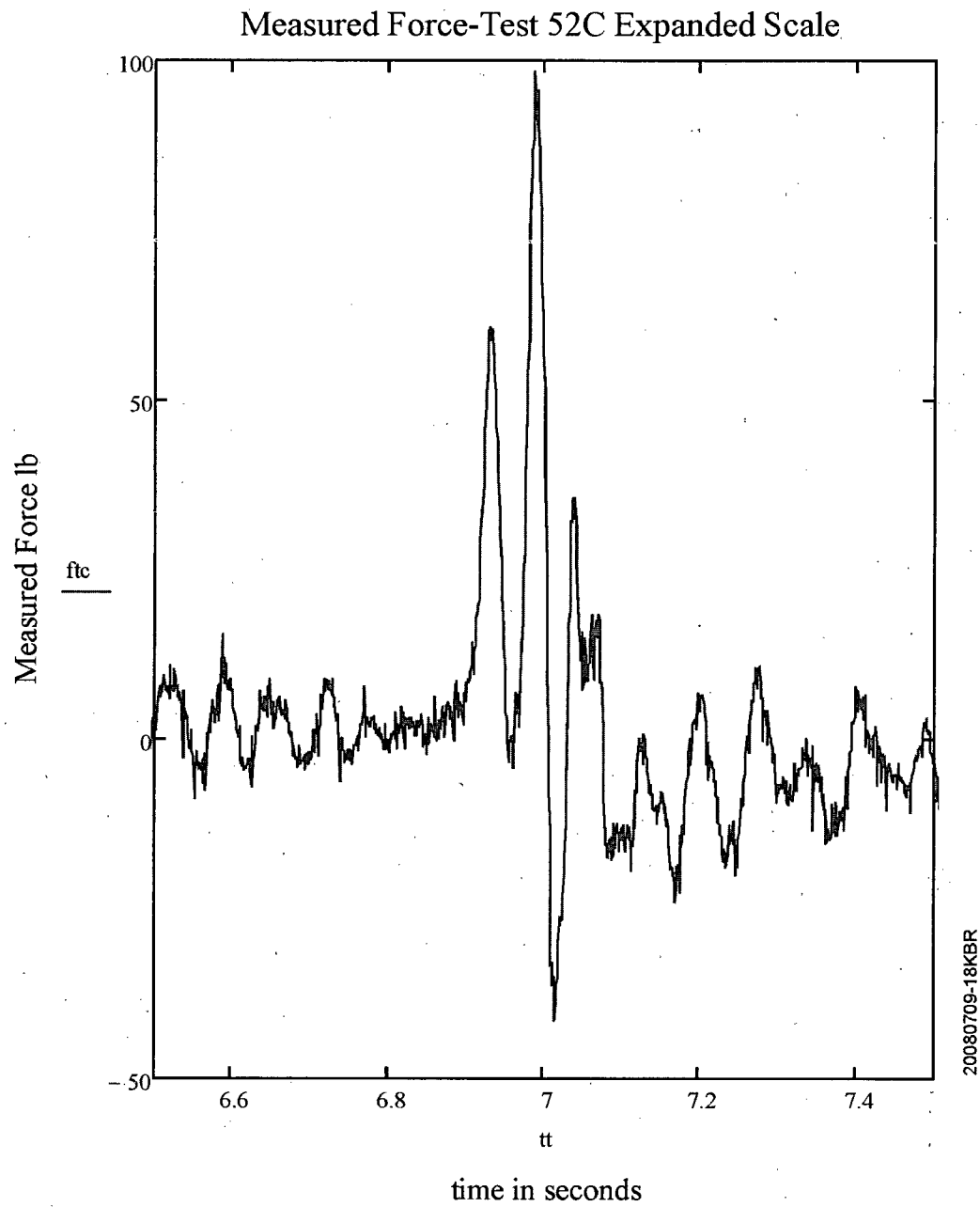
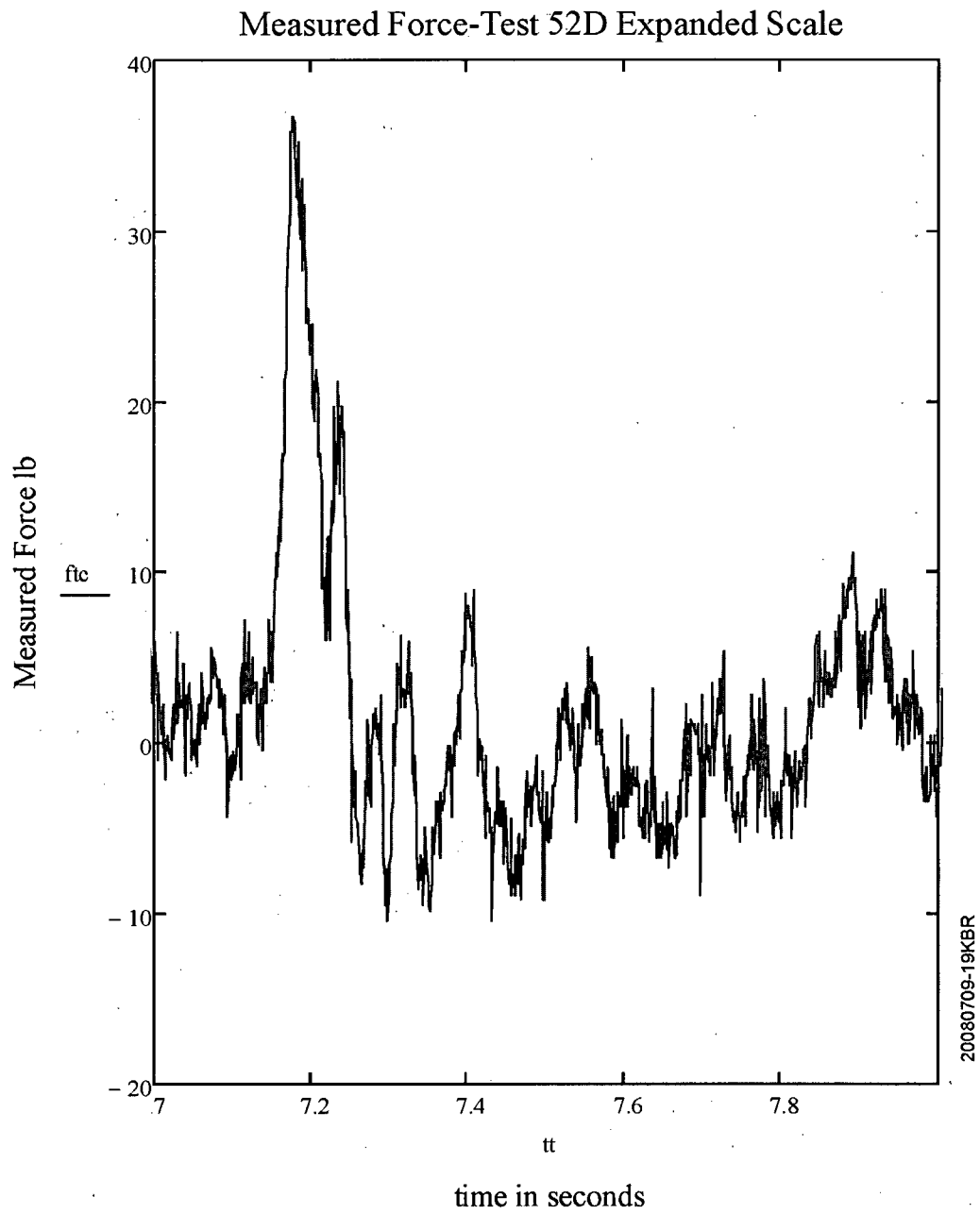


Figure A-19



Measured Force (Global-Check Valve Installed)
Figure A-20

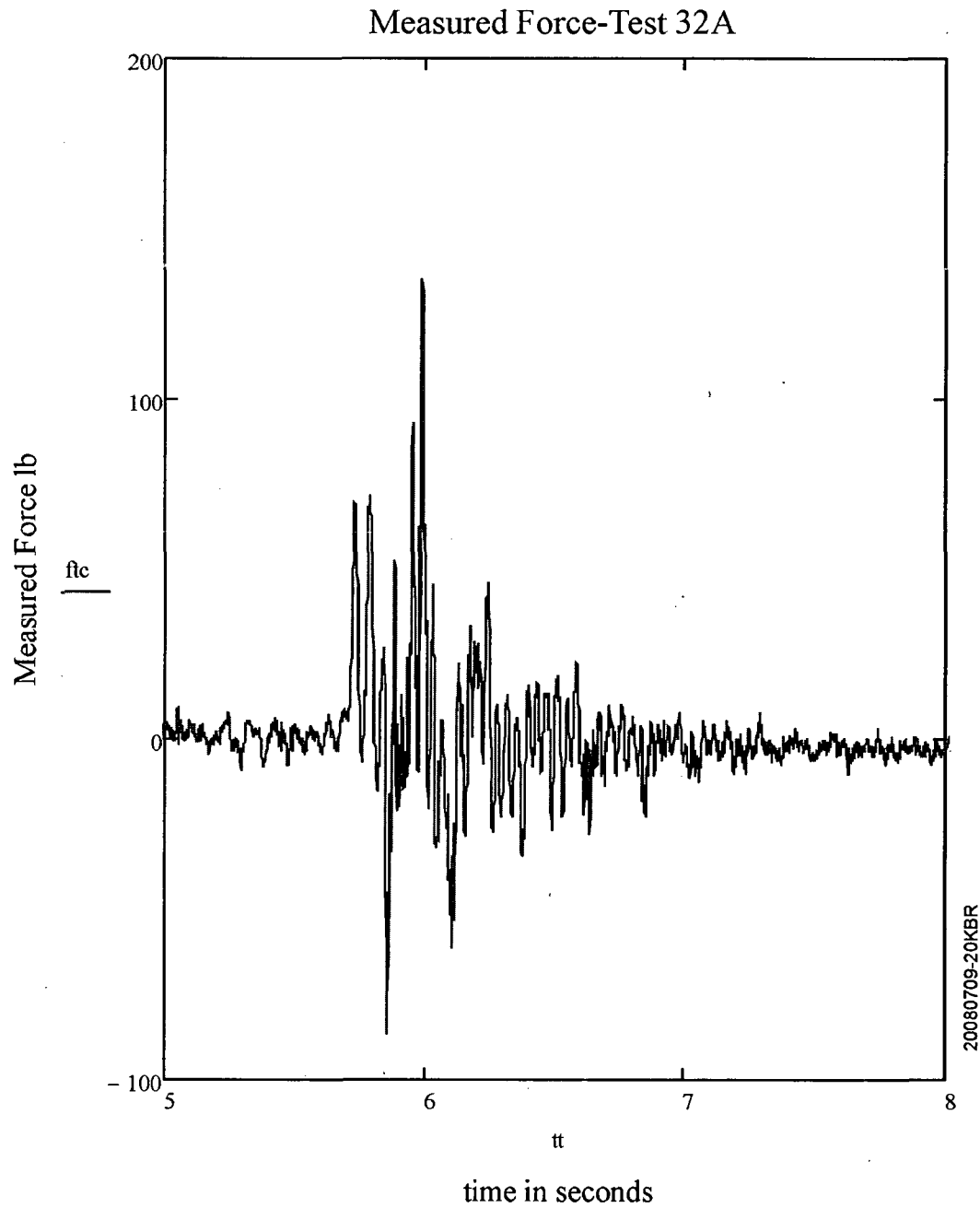


Figure A-21

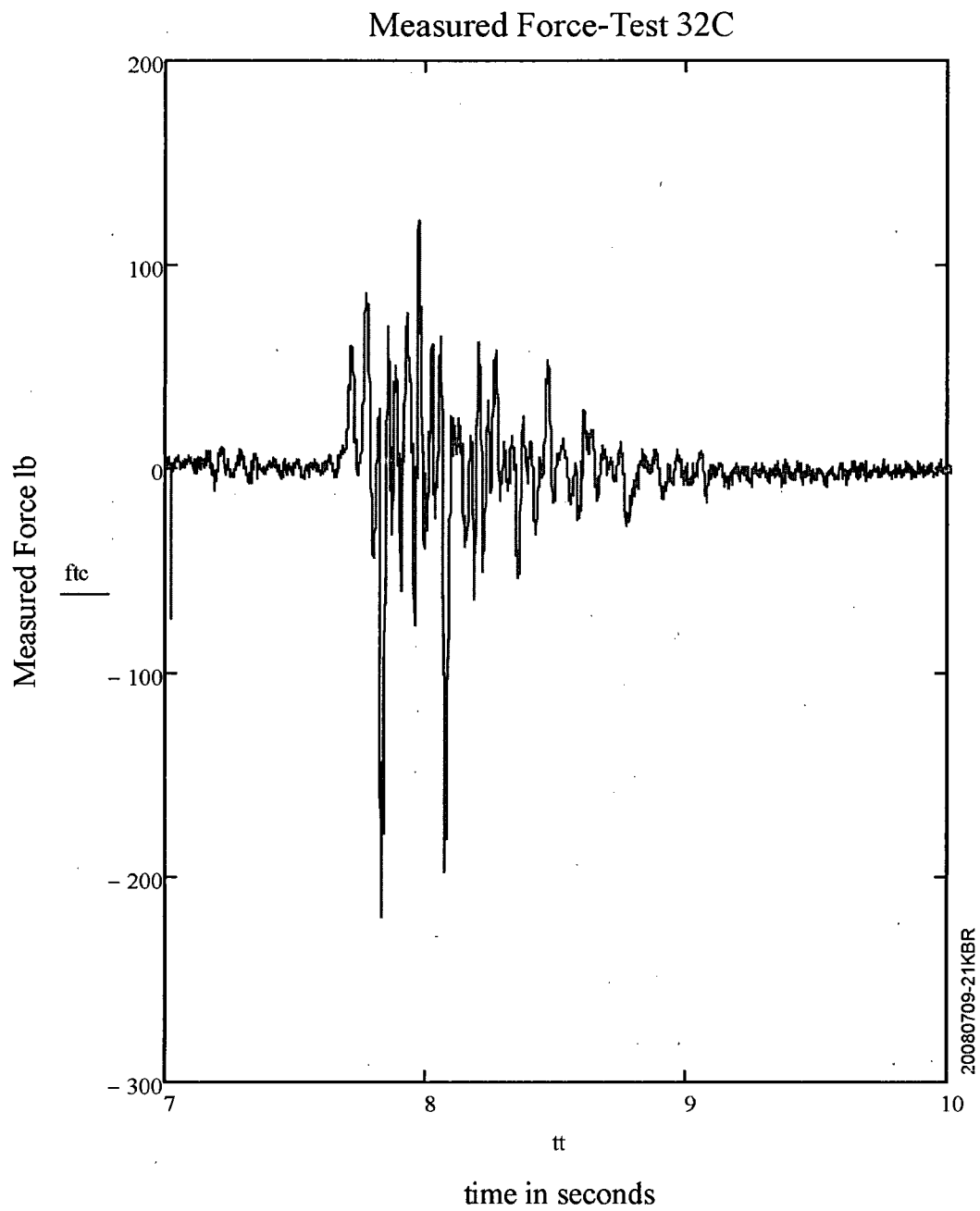
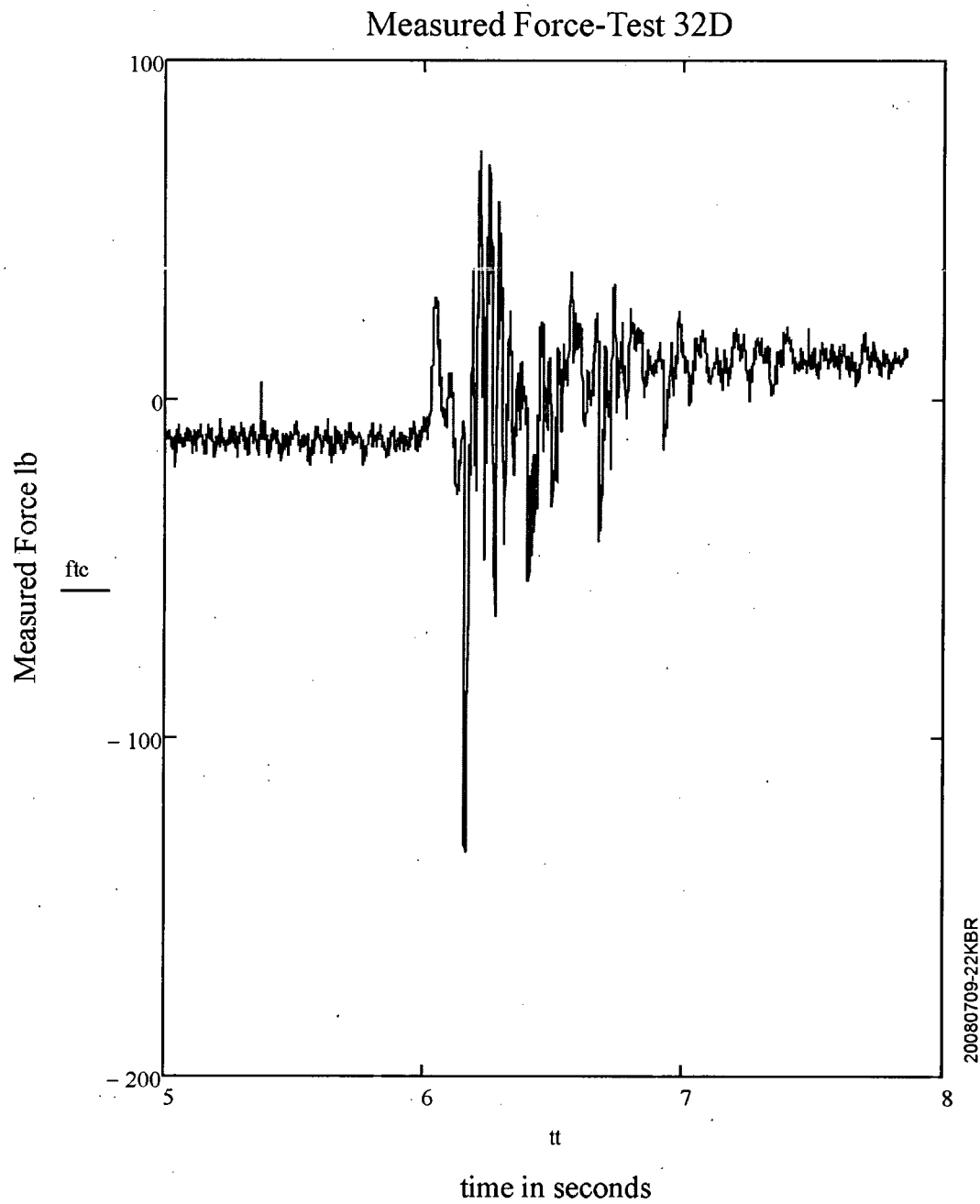


Figure A-22



Measured Force (Expanded Scale-Check Valve Installed)
Figure A-23

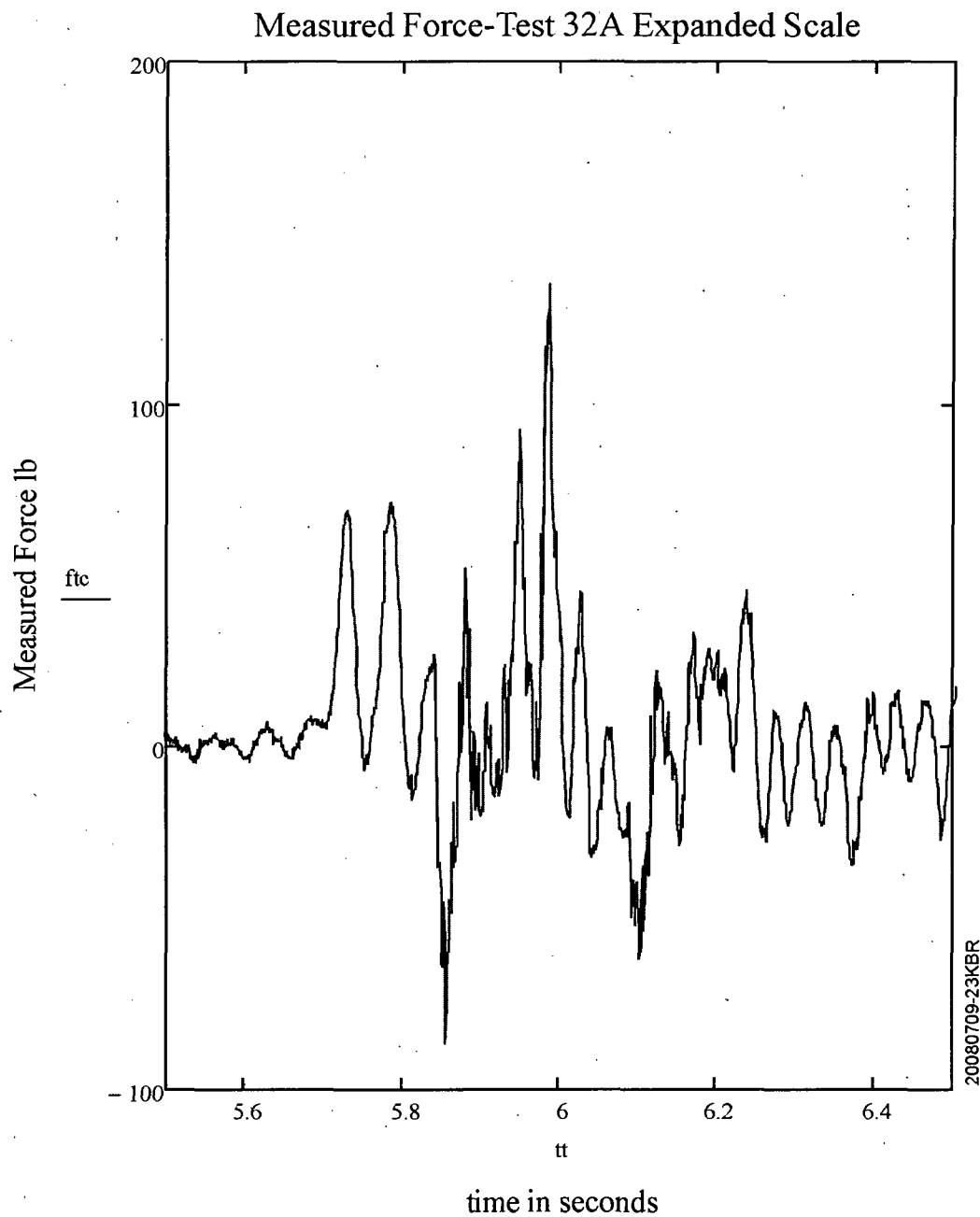


Figure A-24

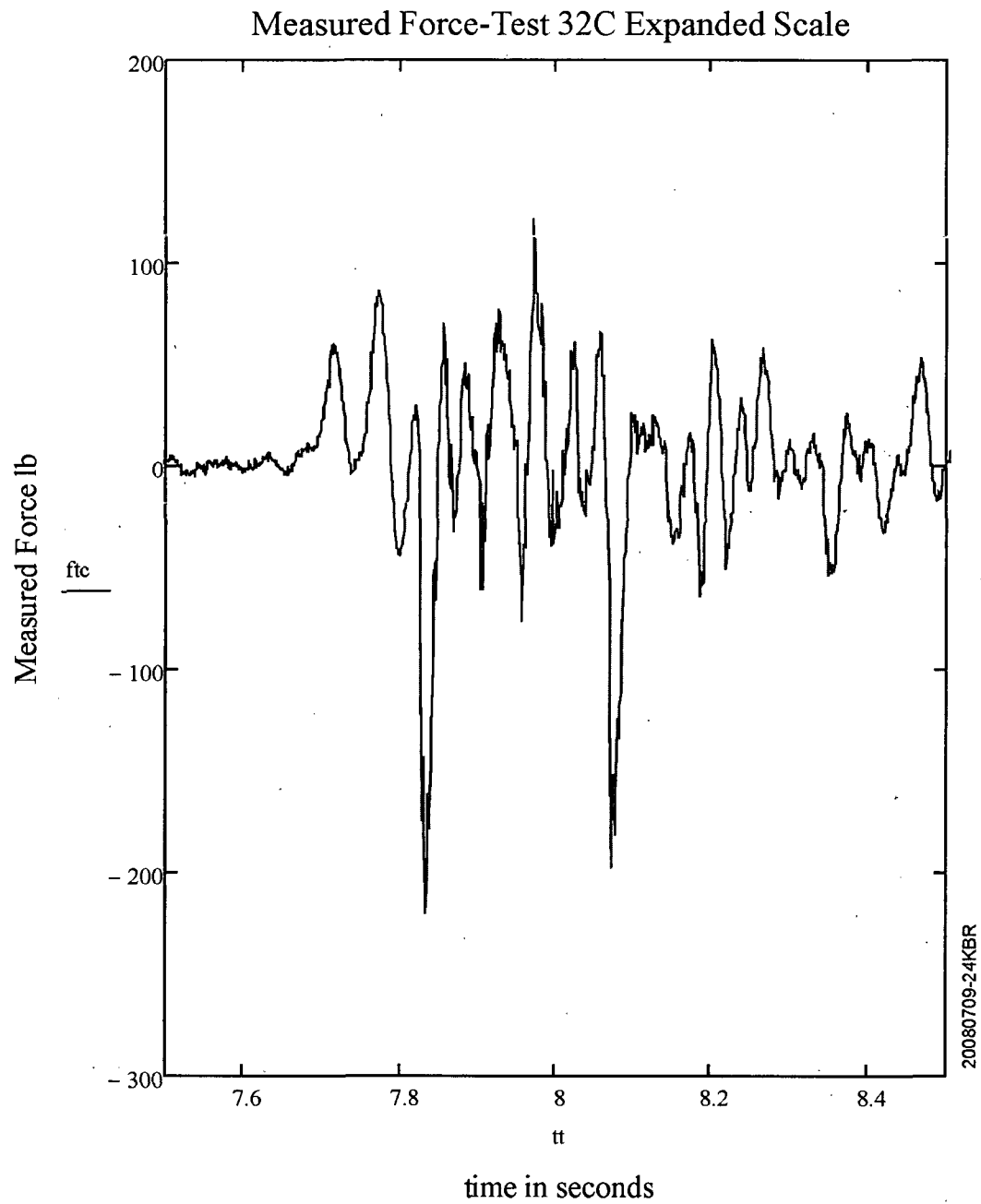
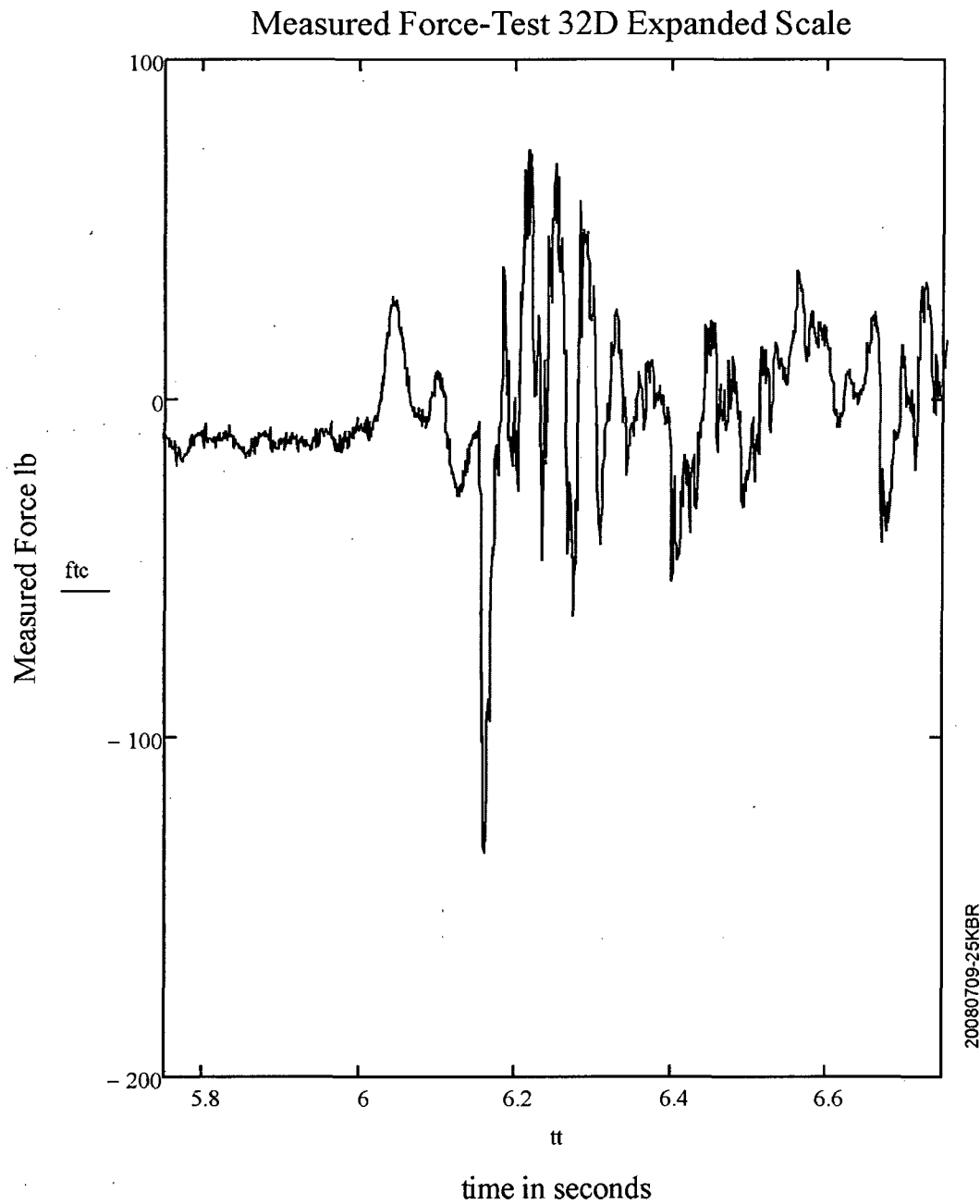


Figure A-25



Force Measurement Power Spectral Density- (No Check Valve Installed Cases)
Figure A-26

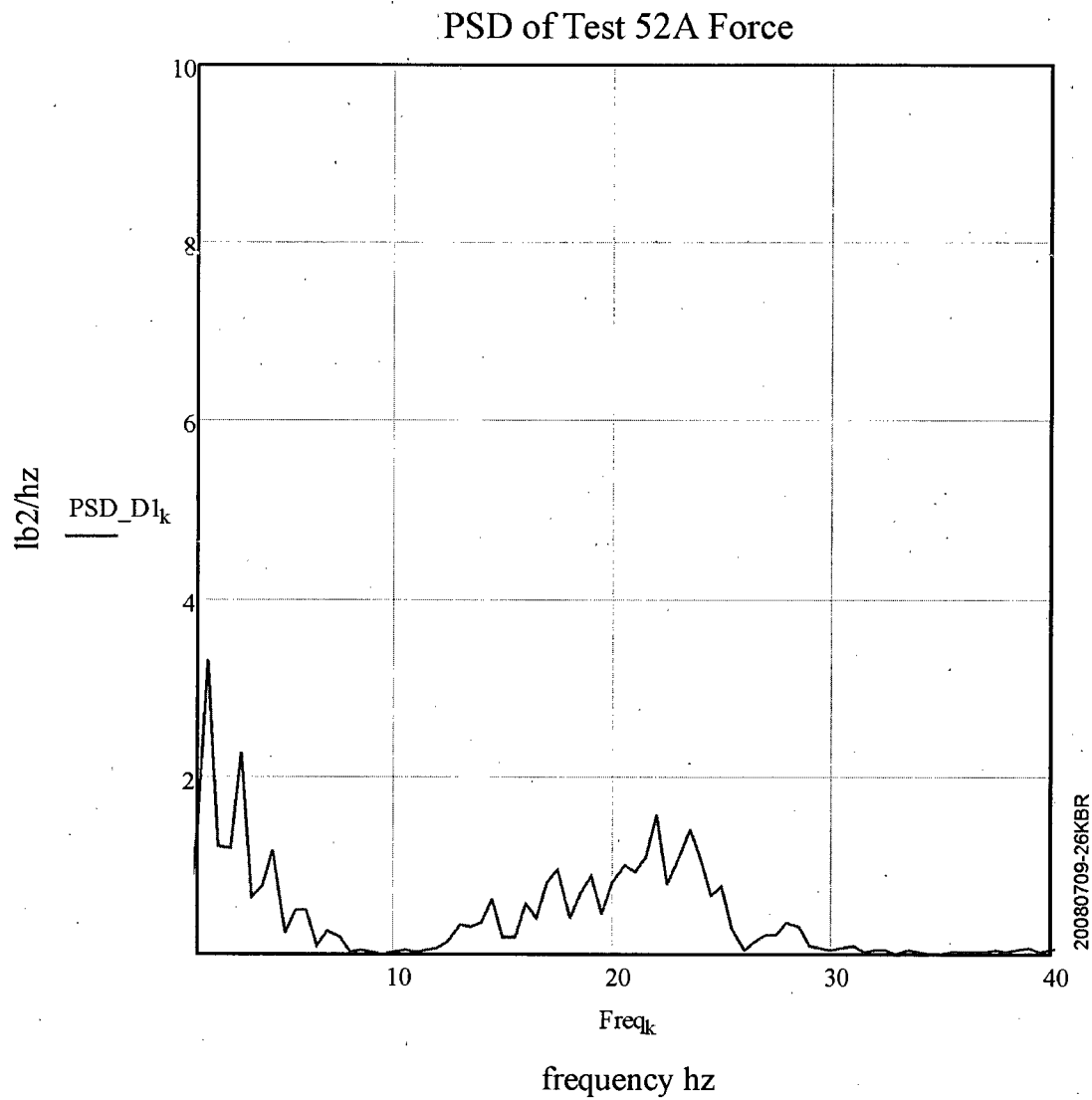


Figure A-27

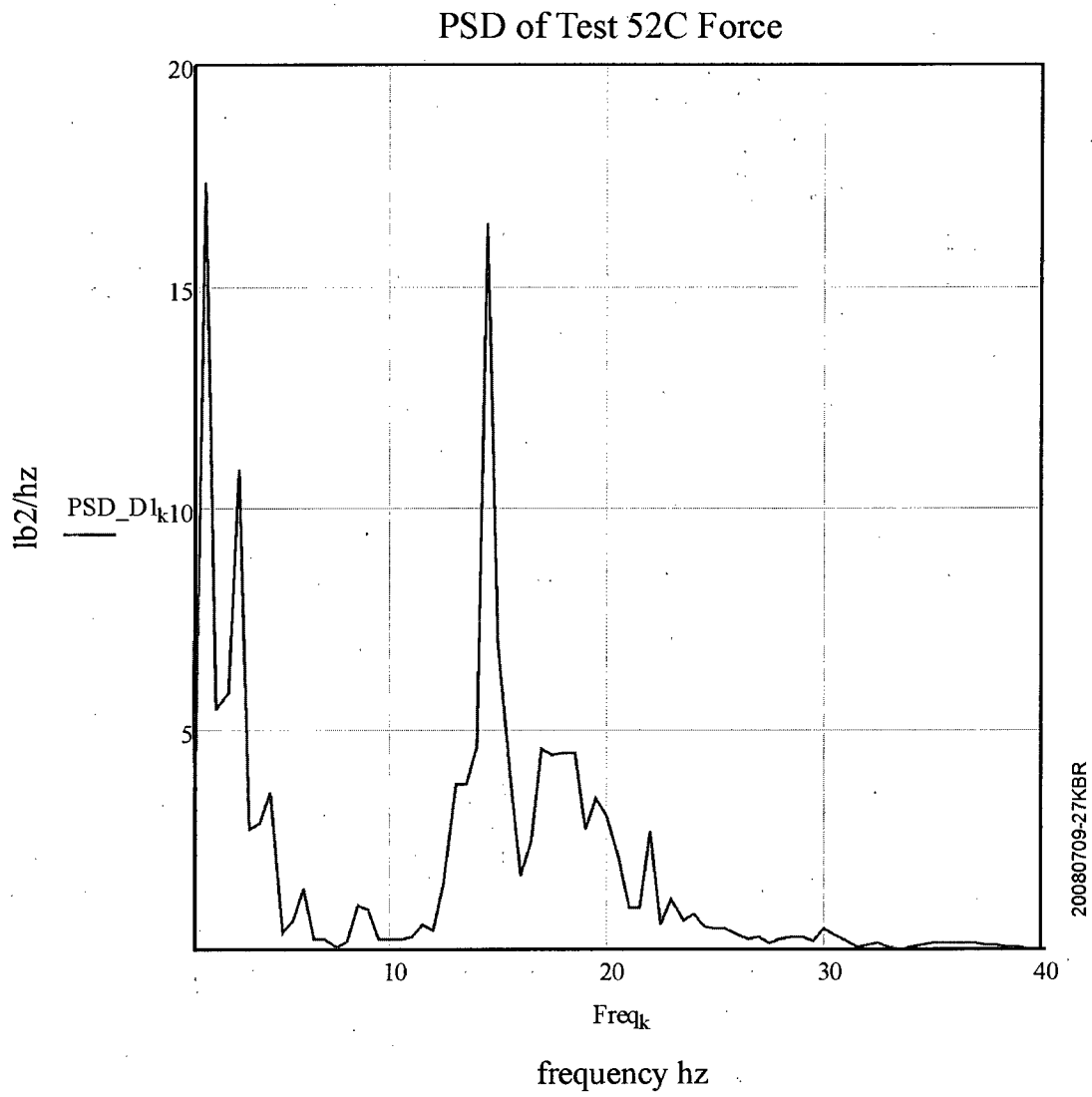
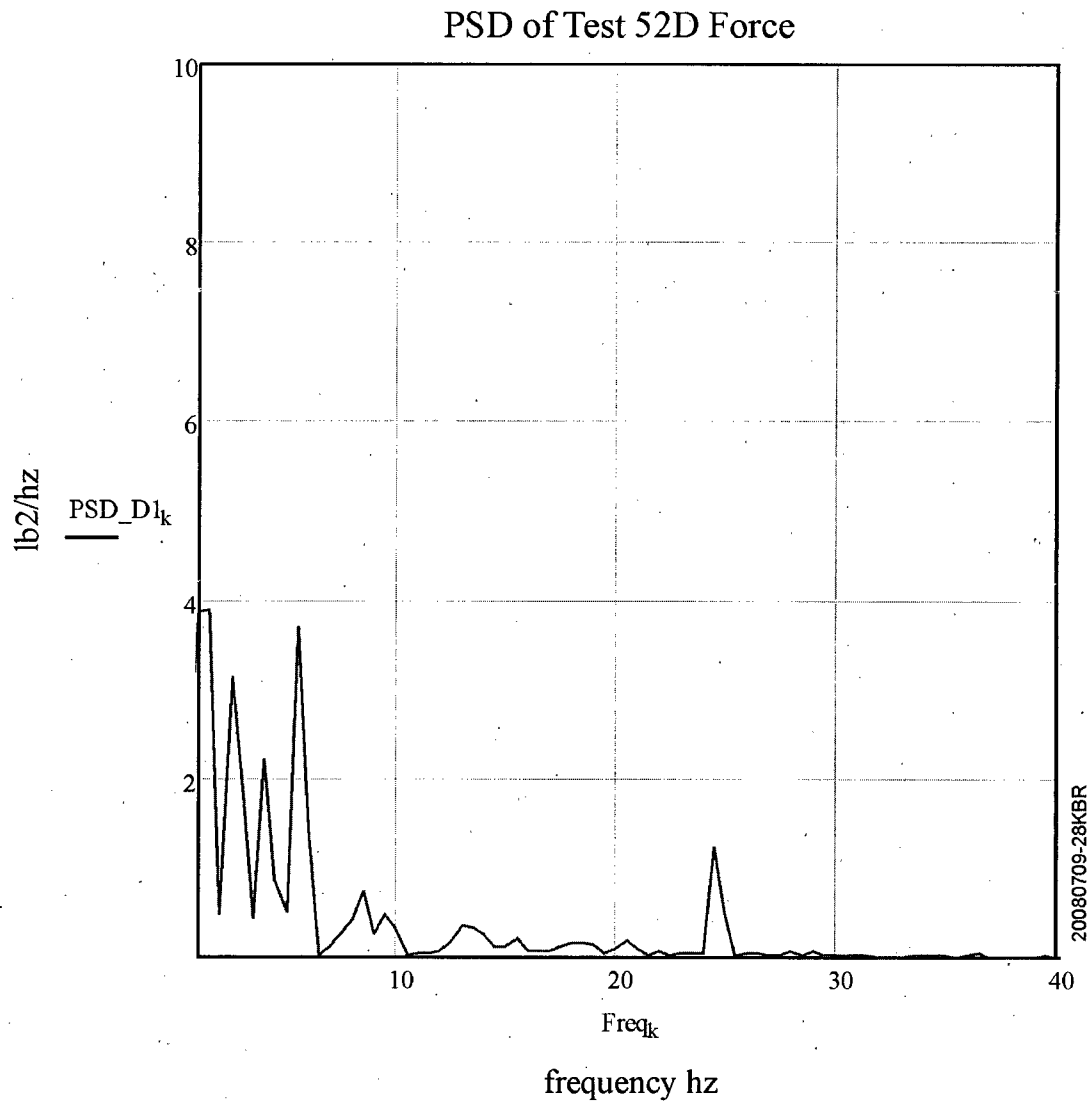


Figure A-28



Force Measurement Power Spectral Density (Check Valve Installed Cases)
Figure A-29

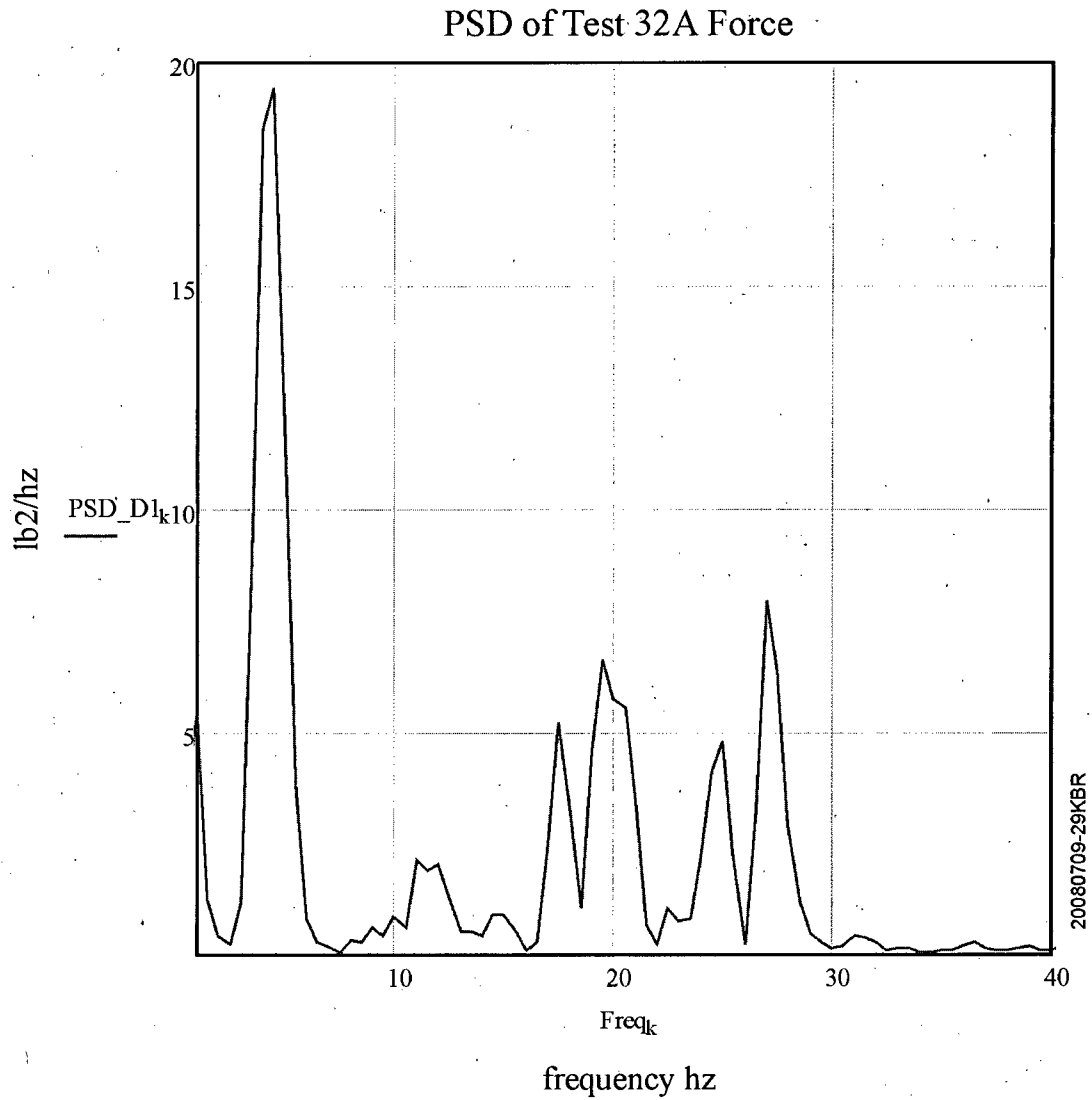


Figure A-30

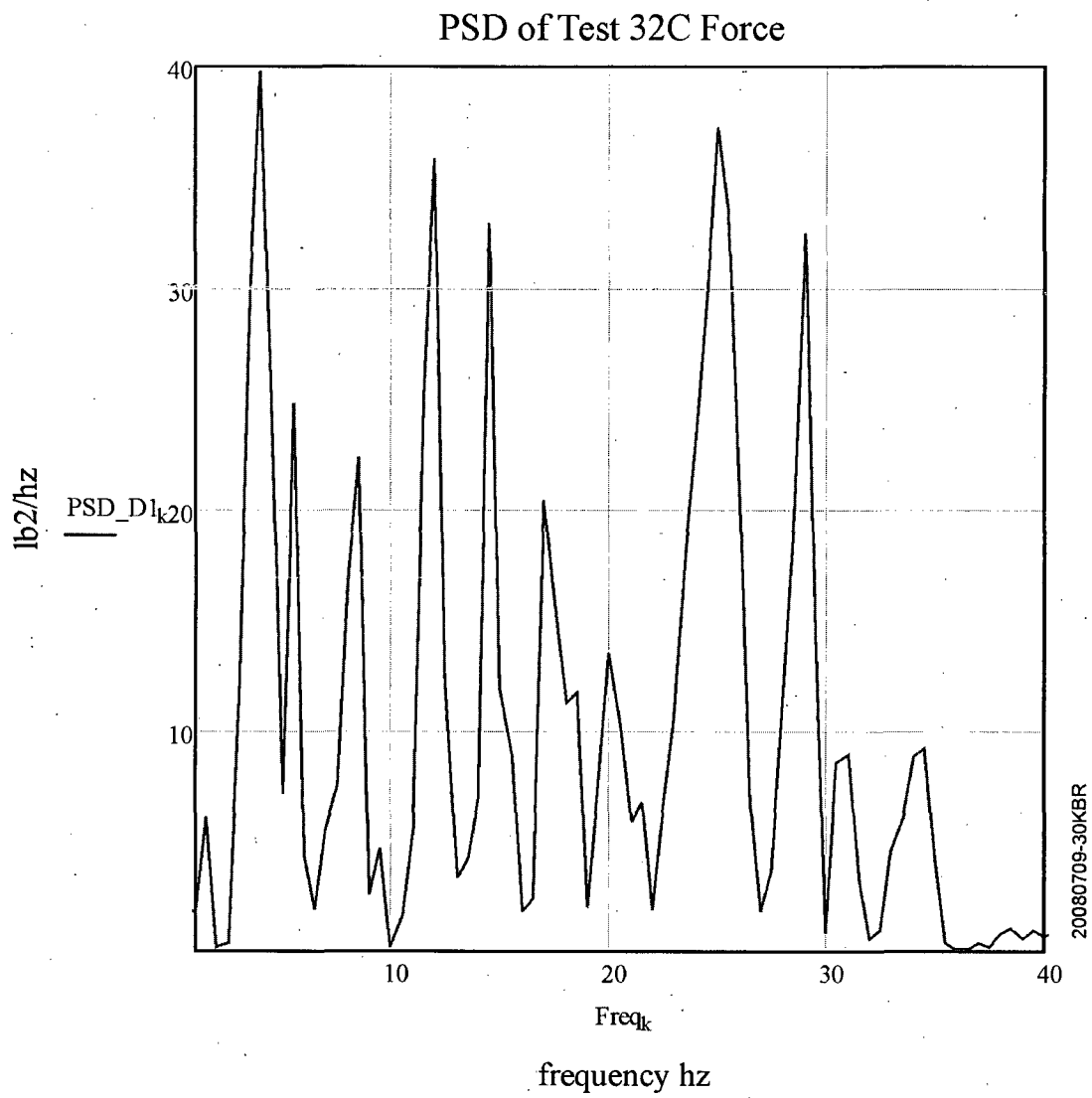


Figure A-31

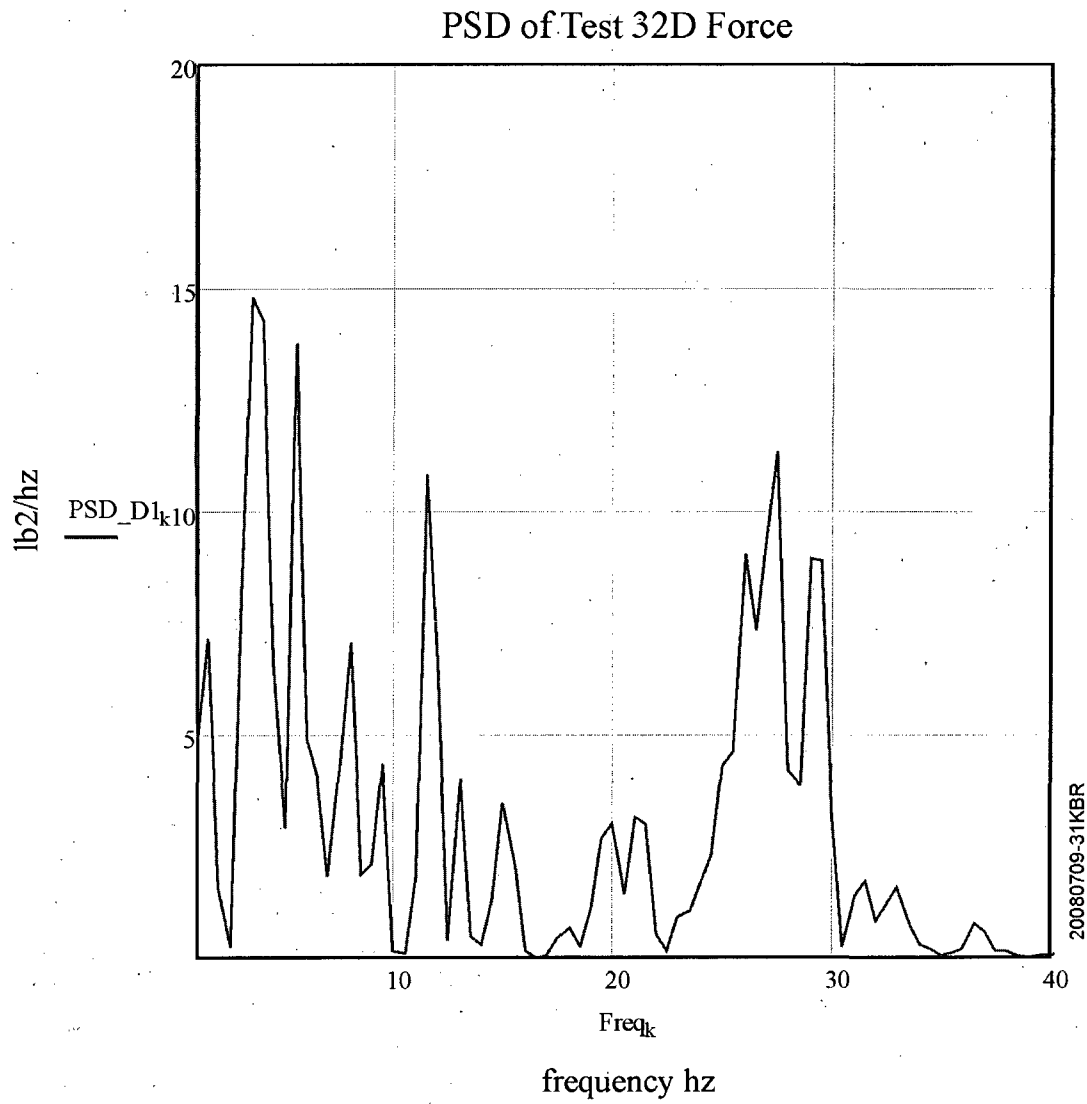


Figure A-32

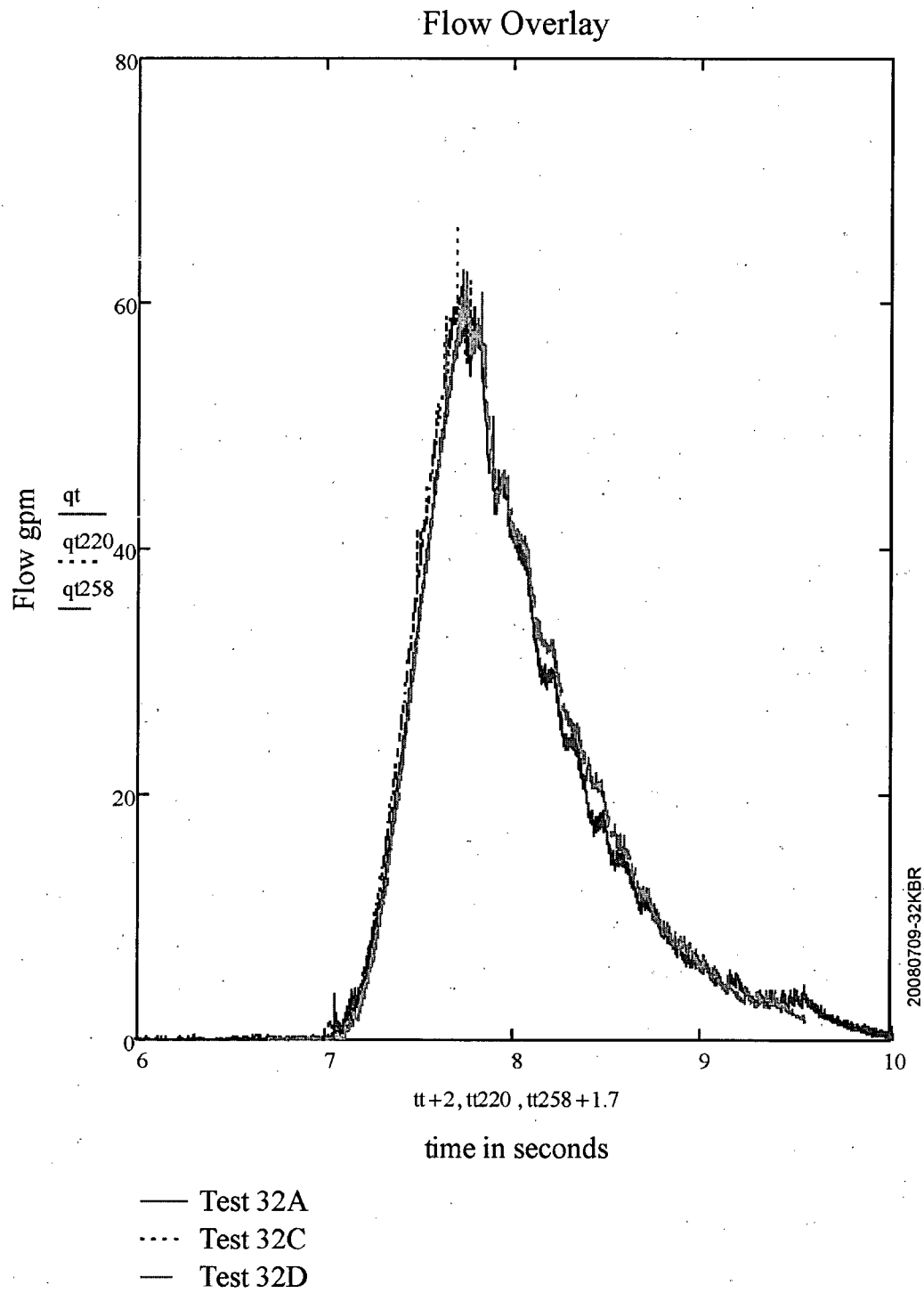


Figure A-33

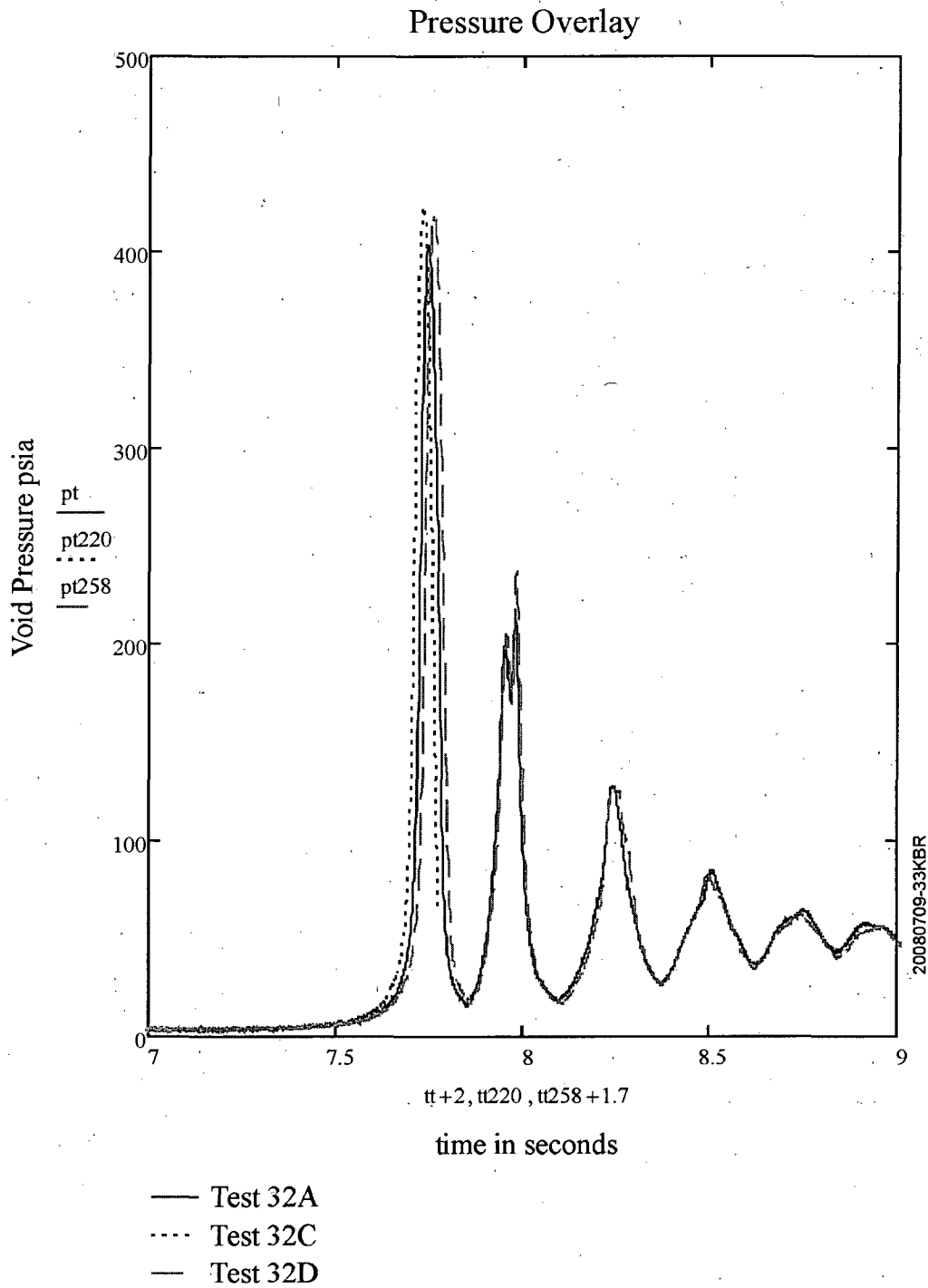
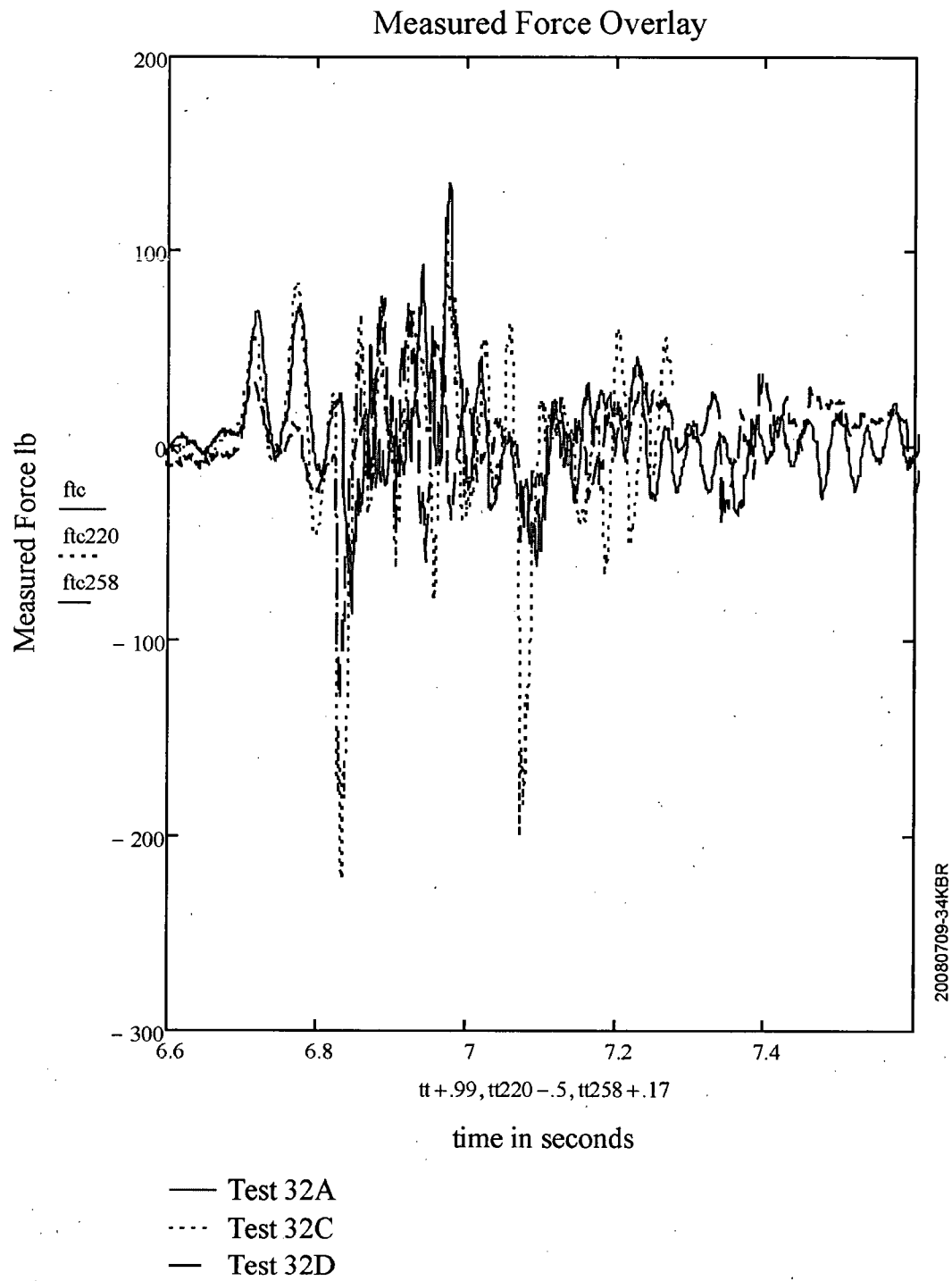


Figure A-34



APPENDIX B

Application of Analytical Considerations to the Air-Water Waterhammer Data

A simplified model for estimating the peak force loading on a highpoint is presented in section 2.0 of this report. This appendix applies the model to the air-water waterhammer data presented in this report, especially the interphase heat transfer (gas to water) that influences the thermodynamic path followed by the gas. As it was noted in section 2.0, some of the parameters within the model are semi-empirical, thus data is required to evaluate these parameters. In general, the gas compression early in the event follows the isentropic path described by $PV^\gamma = \text{constant}$. However, during the very rapid compression as the pressure wave ascends to its highest value, heat transfer between the gas and water decreases the exponent. To represent this behavior, another value of the polytropic exponent is used for this more rapid compression that occurs when the gas volume is very small.

The definition of the isentropic exponent for a single phase gas system is the ratio of the specific heat at constant pressure (c_{pg}) to that at constant volume (c_{vg}), i.e.

$$\gamma = c_{pg} / c_{vg} \quad (\text{B-1})$$

where $\gamma = 1.4$ for air, nitrogen and hydrogen. For a noncondensable gas-water mixture the ratio of the specific heats becomes

$$n1 = \frac{(1-x) c_{ws} + x c_{pg}}{(1-x) c_{ws} + x c_{vg}} \quad (\text{B-2})$$

where x (the mixture quality) is the mass fraction of gas in the mixture and c_{ws} is water specific heat. The ratio of the water mass (m_w) participating in the interphase heat transfer to the sum of the water and gas masses is given by:

$$1 - x = \frac{m_w}{m_w + m_g} = \frac{\rho_w \delta}{\rho_w \delta + \rho_{g0} x_0 L_{g0}} \quad (B-3)$$

or

$$1 - x = \frac{1}{1 + \alpha_0 \left(\frac{\rho_{g0}}{\rho_w} \right) \left(\frac{L_{g0}}{\delta} \right)} \quad (B-4)$$

The variables used in the above equations are defined as follows:

- $n1$ = coefficient of the polytropic process PV^{n1} ,
- ρ_{g0} = initial gas density (for these experiments it is air) prior to pump start,
- ρ_w = water density = 62.4 lbm/ft³ (1000 kg/m³),
- α_0 = initial gas void fraction prior to pump start calculated as the volume of gas at the highpoint divided by the highpoint volume (V_g/V_{HP}),
- δ = effective water depth (amount of water that participates in the interphase heat transfer during the rapid gas compression), set equal to 0.01 ft (0.003 m),
- L_{g0} = length of the gas void, which is equal to the high point length (L_{HP}), and
- γ = ratio of specific heats, $\gamma = 1.4$ for air, nitrogen and hydrogen.

The variable δ represents that small layer of water that could be entrained into the gas volume during the rapid deceleration of the water mass.

The above expression for $n1$ tends to a value of unity when x has a value that is much less than one and approaches γ as x approaches one. Furthermore, the dimensionless parameter in the denominator of equation B-4 is the ratio of the gas mass to that of the water that mixes with the gas during the final compression. In this equation the value of δ is an empirical value determined from the experimental results. The initial air density, ρ_{g0} , is calculated from the ideal gas law $P = \rho RT$, where P_{g0} is the initial pressure in the gas void. For the data presented below, the initial pressures considered are -24 in Hg, -20 in Hg, and -15 in Hg, which correspond to 2.7 psia, 4.7 psia and 7.1 psia. The ratio of the gas and water densities must use values in the same system of units. For

example, if the water is cold such that the density in British units is 62.4 lbm/ft³, the initial gas density is calculated by

$$\rho_{go} = \frac{144 (P_{go}) M_{wg}}{R (T_{go} + 460)} \quad (B-5)$$

where:

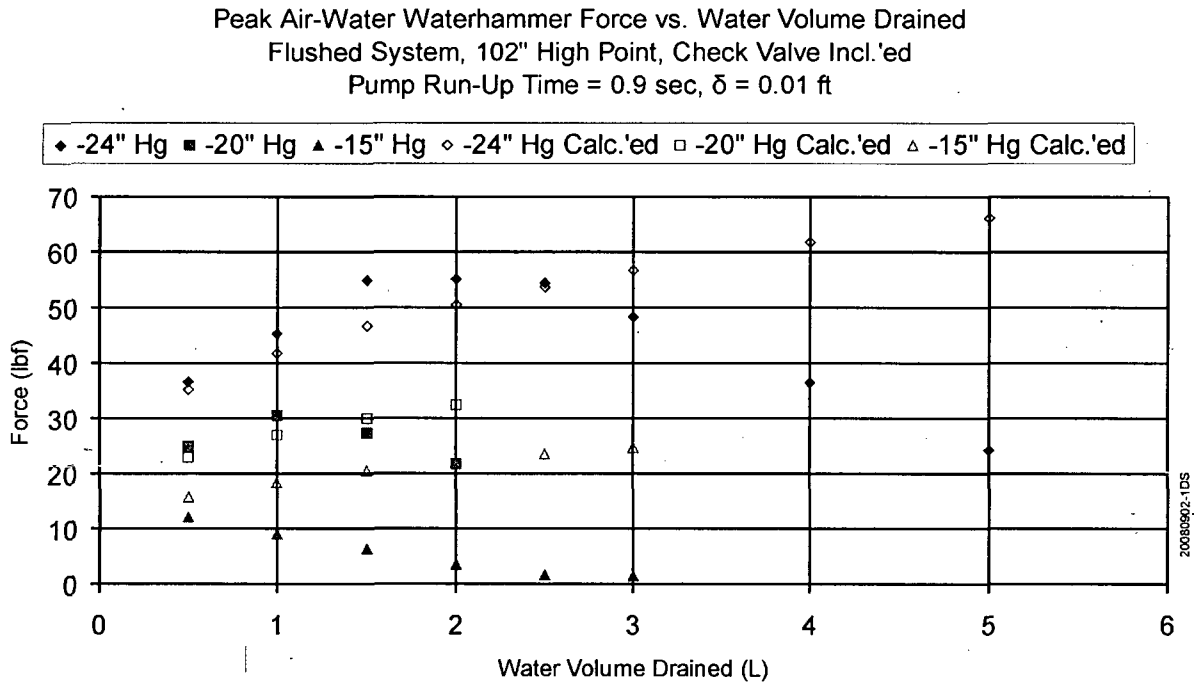
- P_{go} is the initial gas pressure in psia,
- M_{wg} is the molecular weight of the gas (28 for nitrogen, 29.2 for air and 2 for hydrogen),
- R is the universal gas constant (1545.35 ft lbf/(lbm moles °R) in British units), and
- T_{go} is the initial gas temperature in °F, which is usually the system temperature.

Similarly, the specific heats of the water and gas needs to have the values given in the same system of units. With cold water having a value of 1 BTU/lbm/°F, the corresponding values of nitrogen, air and hydrogen are 0.25, 0.24 and 3.8 BTUs/lbm/°F respectively.

Lastly, the ratio of the $\alpha_o L_{go}/\delta$ represents the relative lengths (volumes when both are multiplied by the pipe area) of the gas and water participating in the interphase heat transfer. Obviously, the initial void fraction and length of the gas void fraction are set by the initial conditions and the piping configuration. The value of δ is determined from the experimental measurements and is found to have a value of about 3 mm, or 0.01 ft. This illustrates that at small initial void fractions, it does not require much water entrainment to substantially influence the thermodynamic path.

Using the information presented above along with the methodology of section 2, the peak force was calculated for the waterhammer facility and the results were plotted as peak force versus water volume drained (Figure B-1). The calculations are presented as hollow symbols within the plot and the corresponding data is presented with the same, but filled in, symbol. As illustrated, the model represents the data for the smaller of void volumes of major interest. For very large void fractions, the model overstates the measured forces considerably.

Figure B-1: Peak Air-Water Waterhammer Force versus Water Volume Drained: Data and Calculations with Analytical Model.



APPENDIX C

Sample Problems for Estimating Air-Water Waterhammer Consequences

The following sample problems show how to implement the simplified methodology defined in Sections 2 and 6. The practitioner is encouraged to review the cautions and limitations provided in Section 6.1 before using these simplified approaches. Three flow transients are evaluated in this appendix, i.e. a pump start such as would occur during a surveillance test, a pump start as a result of a LOCA signal and a transient to RHR.

C.1 Pump Surveillance Test

For this sample problem, we consider a pump test with the following parameters:

- a nominal flow rate of 3000 gpm (6.68 cubic feet per second),
- a run-up interval of 2 seconds,
- a shutoff head at the elevation of the gas bubble of 200 psid,
- a gas (air) volume of 3 cubic feet,
- an initial gas pressure of 30 psia,
- an initial gas temperature of 70°F,
- the velocity of sound in water (C_w) is 4500 ft/sec,
- the discharge piping that is 8 inch schedule 40 (0.3474 ft² cross-sectional flow area, (Crane, 1976)),
- the pressure in suction side piping is 40 psia at the relief valve,
- the suction piping is 14 inch, schedule 10 (0.994 ft² cross-sectional area, (Crane, 1976)),
- the length of the piping highpoint (L_{HP}) where the waterhammer occurs is 40 ft. and
- the longest piping segment (L_L) in the system is 50 ft.

First we evaluate the gas volume compression to the pump shutoff pressure using the equation:

$$V_2 = V_1 (P_1 / P_2)^{(1/n)}$$

where:

- $V_1 = 3$ cubic feet,
- $P_1 = 30$ psia,
- $P_2 = 30 + 200 = 230$ psia and
- $n = 1.4$.

This results in $V_2 = 0.70$ cubic feet. Therefore, the volume of water added to compress the gas volume during this pressure increase is $3.0 - 0.70 = 2.3$ cubic feet.

Secondly, we evaluate the time required for the pump to run-up to the shutoff condition using the following equation:

$$t = [2 V_g t_{\text{run-up}} / Q]^{0.5}$$

where:

- $V_g = 2.3$ cubic feet,
- $t_{\text{run-up}} = 2$ seconds and
- $Q = 6.68$ cubic feet per second.

The calculated time for the pump to discharge sufficient water to pressurize the gas volume to the shutoff pressure is 1.17 seconds. From the linear pump run-up characteristic given by the equation:

$$Q_{\text{pump}}(t) = Q (t / t_{\text{run-up}})$$

we calculate the volumetric flow rate being pumped at this time as given by

$$Q_{\text{pump}}(t) = 6.68 (1.17/2) = 3.91 \text{ cubic feet per second}$$

For the specified pipe size and corresponding cross-sectional area, this volumetric flow rate would have a superficial velocity as calculated by:

$$U_s = Q_{\text{pump}}(t) / A_{\text{pipe}} = 3.91 / 0.3474 = 11.3 \text{ ft/sec}$$

Using this velocity, the gas-water waterhammer pressure that would result if this velocity were instantaneously stopped can be calculated from the Joukowsky-Frizell waterhammer equation that, in general, is written as:

$$\Delta P_{\text{WH}} = \rho C_w U_s$$

When the pressure increase is given in psi, the units for density are lbm/ft³ and the velocities are in ft/sec, the equation needs to be written as:

$$\Delta P_{\text{WH}} = \rho C_w U_s / (144 g_c) = 62.4 (4500) 11.3 / (144 \times 32.2) = 681 \text{ psi}$$

In this expression, g_c is the unit conversion constant and has a value of 32.2 lbm ft/(lbf sec²). For those practitioners that use SI units, the general equation can be used directly, i.e. no unit conversions are needed.

To assess the potential for lifting the relief valve in the discharge piping, the waterhammer pressure is added to the pump shutoff head pressure; i.e. final pressure is 230 + 681 = 911 psia. Generally, this would be a sufficient pressure to lift the relief valve in the discharge piping. While this is clearly a conservative estimate of the pressure that could be developed, if this is judged to be too conservative, a detailed model of the fluid response in the piping system should be used.

If a gas-water waterhammer were to occur, the compression waves would propagate upstream through the pump and also potentially pressurize the suction side sufficiently for the suction piping relief valve to lift. Typically, these relief valves have lift pressures of about 450 psig, or 464.7 psia. Given the stagnation of a volumetric flow of 3.91 ft³/sec, this corresponds to a velocity of 3.93 ft/sec

in the larger suction piping. As with the discharge side piping, the pressure required to stagnate this velocity is calculated from the waterhammer equation, i.e.:

$$\Delta P_{WH} = \rho C_w U_s / (144 g_c) = 62.4 (4500) 3.93 / (144 \times 32.2) = 238 \text{ psi}$$

This pressure increase is added to the static pressure of 40 psia to give a peak waterhammer pressure of 278 psia. In general, this pressure increase during a pump surveillance transient would not result in lifting the suction side relief valve.

To estimate the maximum force imbalance on the discharge piping highpoint where the waterhammer occurs, we first calculate the gas volume that would exist at half of the waterhammer pressure increase and at the full pressure increase. At half of the pressure increase the gas volume pressure at this intermediate point (PI) would be:

$$PI = 230 + 681/2 = 571 \text{ psia}$$

and the gas volume (VI) at this intermediate pressure can be calculated by:

$$VI = V_1 (P_1/PI)^{1/n} = 3 (30/571)^{0.714} = 0.37 \text{ cubic feet}$$

and the water velocity at this intermediate pressure would be reduced to one-half of the maximum value by the ongoing waterhammer event, i.e. $(11.2/2 = 5.6 \text{ ft/sec})$.

To calculate the gas volume (VM) at the maximum pressure of 911 psia, the two-phase exponent n_1 must be evaluated. With the initial parameters defined, the initial gas void fraction is given by:

$$\alpha_o = \frac{V_g}{A_{\text{pipe}} L_{HP}} = \frac{3}{0.3474(40)} = 0.22$$

and the initial gas density is calculated as

$$\rho_{go} = \frac{144 (P_{go}) M_{wg}}{R (T_{go} + 460)} = \frac{144 (30) 29.2}{1545.35 (70 + 460)} = 0.154 \frac{\text{lbm}}{\text{ft}^3}$$

Using the equation for the mixture quality (x) participating in the interphase heat transfer given in Appendix B results in

$$1 - x = \frac{1}{1 + \alpha_o \left(\frac{\rho_{go}}{\rho_w} \right) \left(\frac{L_{go}}{\delta} \right)} = \frac{1}{1 + 0.22 \left(\frac{0.154}{62.4} \right) \left(\frac{40}{0.01} \right)} = 0.315 ; x = 0.685$$

and the two-phase exponent is:

$$n1 = \frac{(1 - x) c_{ws} + x c_{pg}}{(1 - x) c_{ws} + x c_{vg}} = \frac{(1 - 0.685)(1) + 0.685 (0.24)}{(1 - 0.685)(1) + 0.685 (0.17)}$$

$$n1 = \frac{0.479}{0.431} = 1.11$$

(The specific heat at constant volume for air is $c_{vg} = c_{pg}/\gamma = 0.24/1.4 = 0.17$.)

With this exponent evaluated, the gas volume at the maximum pressure, including the influence of heat transfer is then calculated by:

$$VM = V_i (P_i / P_{max})^{1/n1} = 3 (30/911)^{1/1.11} = 0.139 \text{ ft}^3$$

which gives a volume change between these two pressures of 0.231 cubic feet. Dividing this by the pipe flow area results in a length of 0.665 feet and dividing this length by the water velocity of 5.6

ft/sec results in a time of 0.119 seconds. With this as the interval and the pressure difference of $681/2 = 340.5$ psi, we can conservatively calculate the reference pressurization rate as:

$$dP/dt)_R = 340.5/0.119 = 2861 \text{ psi/sec}$$

With this the maximum force imbalance acting on the piping highpoint can be calculated as follows:

$$F_{HP} = A dP/dt)_R (L_{HP}/C_w) = 0.3474 (2861) 144 (40/4500) = 1272 \text{ lbf}$$

Since the pressure wave is propagating through water filled system of constant diameter, the force imbalance on the longest pipe can be assessed as;

$$F_L = F_{HP} (L_L/L_{HP}) = 1272 (50/40) = 1590 \text{ lbf}$$

Piping systems also have changing pipe diameters which cause the velocity to decrease and the area on which the pressure acts to increase. Conservatively neglecting any loss coefficients in the piping, these effects cancel one and another. Hence, the maximum imbalance can be simply propagated through the system based on the length of the piping segment alone. This simplified approach can be used to estimate the maximum force imbalances but should not be used to develop detailed force-time histories as inputs to a detailed model of the piping system and the supports/restraints.

C.2 Pump Start due to a LOCA Signal

Given the conditions that could produce a LOCA signal, the ECCS pumps would be started to ensure injection to the Reactor Coolant System (RCS) with the water source being the RWST, RWT or BWST depending on the reactor design. If a gas volume is accumulated in the injection piping, a gas-water waterhammer could occur should the pump start(s) compress the gas with the downstream flow path completely shutoff by a closed, or slowly opening injection valve or a check valve that is held closed by an elevated RCS pressure. Given one or more of these situations, the gas

volume would be compressed in essentially the same manner as considered for the pump surveillance test except that two pumps could be started simultaneously and thus accelerate the compression. This can be evaluated using the same approach for the possible consequences of lifting the relief valves as well as for estimating the maximum force imbalances.

Using the same approach, the pump shutoff head would be identical to that evaluated for the pump surveillance test, i.e. 230 psia, and the volume at this pressure would also be 0.70 ft³. As was calculated above, the decrease in the gas volume is 2.3 ft³. The difference begins with the nominal pump flow rate considered being 6000 gpm (13.37 ft³/sec) instead of 3000 gpm and the time to run-up to the shutoff head being given by

$$t = [2(2.3)/13.37]^{0.5} = 0.830 \text{ secs}$$

At this time the pumped flow rate is calculated to be

$$Q_{\text{pump}}(t) = Q(t/t_{\text{run-up}}) = 13.37 \left(\frac{0.83}{2} \right) = 5.55 \text{ ft}^3/\text{sec}$$

and the water superficial velocity is:

$$U_s = Q_{\text{pump}}(t)/A_{\text{pipe}} = 5.55/0.3474 = 16.0 \text{ ft/sec}$$

with the waterhammer pressure increase being

$$\begin{aligned} \Delta P_{\text{WH}} &= \rho c_w U_s / (144 g_c) = 62.4 (4500) 16.0 / (144 \times 32.2) \\ &= 969 \text{ psi} \end{aligned}$$

and the total (maximum) pressure is

$$P_{\max} = 30 + 200 + 969 = 1199 \text{ psia}$$

Propagation of the pressurization upstream through the pumps and into the suction piping would occur through two suction pipes since two pumps are operating. With two 14 inch schedule 10 suction pipes, the total cross-sectional area for flow is 1.988 ft² and the water superficial velocity in these pipes would be:

$$U_{ss} = 5.55 / 1.988 = 2.8 \text{ ft/sec}$$

with the waterhammer pressure increase needed to stagnate this velocity being given by

$$\Delta P_{\text{wHS}} = \frac{\rho c_w U_{\text{ww}}}{144 g_c} = \frac{62.4 (4500) 2.8}{144 (32.2)} = 170 \text{ psi}$$

Therefore, the maximum pressure in the suction piping is:

$$P_{\max,s} = 40 + 170 = 210 \text{ psia}$$

In general, this is considerably less than the relief valve setpoints in the suction piping.

As calculated for the pump surveillance test, the maximum force imbalance is evaluated by assessing the rate of rise for the intermediate pressure of one-half of the waterhammer pressure increase to the maximum pressure. This intermediate pressure is

$$PI = 30 + 200 + (969 / 2) = 714.5 \text{ psia}$$

and the intermediate volume is

$$VI = V_i (P_i / PI)^{1/n} = 3 (30 / 714.5)^{0.714} = 0.31 \text{ ft}^3$$

At this intermediate condition, the water velocity is reduced to one-half of the initial value, or 8 ft/sec.

Since the conditions of the initial void fraction, the initial-gas pressure, etc. are the same as those in the pump surveillance calculation, the value of n_1 is the same, i.e. 1.11. Therefore, the gas volume at the maximum pressure is calculated as:

$$VM = V_i (P_i/P_{\max})^{1/n_1} = 3 (30/1199)^{0.9} = 0.109 \text{ ft}^3$$

such that the volume decrease between these two conditions is 0.201 ft^3 , or an effective length (volume/area) of 0.58 ft with a "time of flight" of $0.58/8 = 0.072$ secs. With this, the pressurization rate becomes

$$\left. \frac{dP}{dt} \right|_R = \frac{969}{2 (0.072)} = 6729 \text{ psi/sec}$$

with the force on the high point being:

$$F_{HP} = A \left. \frac{dP}{dt} \right|_R \left(\frac{L_{HP}}{c_w} \right) = 0.3474 (144) (6729) \frac{40}{4500} = 2992 \text{ lbf}$$

Also, the force on the longest pipe is calculated to be:

$$F_L = F_{HP} (L_L/L_{HP}) = 2992 \left(\frac{50}{40} \right) = 3740 \text{ lbf}$$

C.3 Transition to RHR/SDC Cooling

Another hydraulic transient that could lead to a gas-water waterhammer is the transition to Residual Heat Removal (RHR) or ShutDown Cooling (SDC) with a low pressure noncondensable gas volume in the connected piping. To initiate this function, the RCS would be depressurized substantially to about 350 psig. While the specific procedures for implementing this transfer vary between plants, for this example we assume that the valve for the pump suction is opened first and this begins to pressurize the piping system to the RCS pressure. In this example we are again considering an initial gas volume of 3 cubic feet with a valve opening interval of 10 seconds.

As noted in Section 6, if the opening of a valve initiates the transient, the flow development time is considered to be a small fraction of the valve opening interval. This is expressed as:

$$Q_f = 2 V_1 / (K t_o) = 2 (3) / (0.2 \times 10) = 3 \text{ ft}^3/\text{sec}$$

With this maximum flow rate, the water superficial velocity is given by:

$$U_s = Q_f / A_{\text{pipe}} = 3 / 0.3474 = 8.6 \text{ ft/sec}$$

and the waterhammer pressure is calculated by

$$\begin{aligned} \Delta P_{\text{WH}} &= \rho_w c_w U_s / (144 g_c) \\ &= 62.4 (4500) 8.6 / (144 \times 32.2) = 521 \text{ psi} \end{aligned}$$

With this pressure increase, the maximum pressure would be

$$P_{\text{max}} = 14.7 + 350 + 521 = 885.7 \text{ psia}$$

This is the pressure that is used to assess whether a relief valve would lift as the gas volume is exposed to the RCS pressure.

The evaluation for the maximum force on the highpoint and on the longest piping sequence is performed in the same manner as the above examples once the volumetric flow rate and waterhammer pressure increases are known. Specifically, the intermediate volume is calculated as

$$VI = V_1 (P_1/PI)^{1/\gamma} = 3 \left[30 / (14.7 + 350 + (521/2)) \right]^{1/1.4}$$

$$VI = 3 (30/625.2)^{0.714} = 0.34 \text{ ft}^3$$

with the water superficial velocity being one-half of 8.6 ft/sec, or 4.3 ft/sec. Similarly, the gas volume at the maximum pressure is given by

$$VM = V_1 (P_1/P_{\max})^{1/n1} = 3 (30/885.7)^{0.9} = 0.14 \text{ ft}^3$$

with the volume difference between these being 0.20 ft^3 and an effective length of 0.58 ft. This "time of flight" for closing to the final volume is

$$\Delta t = 0.58/4.3 = 0.13 \text{ secs}$$

and the reference pressurization rate is:

$$\left(\frac{dP}{dt} \right)_R = \frac{521}{2 (0.13)} = 2004 \text{ psi/sec}$$

With this, the force imbalance on the highpoint is

$$F_{HP} = A \left(\frac{dP}{dt} \right)_R \frac{L_{HP}}{c_w} = 0.3474 (2004) 144 (40) / 4500$$

$$F_{HP} = 891 \text{ lbf}$$

For the longest pipe the force imbalance is calculated as:

$$F_L = F_{HP} (50/40) = 1114 \text{ lbf}$$